METHOD AND APPARATUS FOR THERMOACOUSTIC ANALYSIS (TAA)

A Thesis

Submitted to the College of Graduate Studies and Research

in Partial Fulfilment of the Requirements

for the Degree of

Master of Science

in the

Department of Electrical Engineering

University of Saskatchewan

by

Vinod Ramchand Mirchandani

Saskatoon, Saskatchewan

January 1991

Dedicated to

My

Beloved Parents and Grandmother

COPYRIGHT

ACKNOWLEDGEMENTS

I would like to express my sincere gratitude and indebtedness to my supervisor Dr. S.O. Kasap for his valuable guidance and incessant encouragement. I would also like to extend special thanks to Dr. S. Yannacopoulos for providing the composite samples for Thermoacoustic analysis, for permitting to use equipments in the Metallurgical laboratories during the course of numerous experiments in the research and for many valuable discussions and suggestions.

Mr. I. Wacker's part in performing measurements on polymers by using Differential Scanning Calorimetry and Thermomicrohardness measurements is appreciated. Thanks are also due to Mr. B. Gerard from Engineering shops for fabrication of some of the mechanical items, Mr. R. Elvin for glass work and Mr. B. Polischuk for writing a mutually applicable software for the temperature controller.

Financial assistance from the University of Saskatchewan in the form of a Graduate Scholarship is gratefully acknowledged.

Last but not the least, I would like to thank my Professors, parents, brother, sister-in-law, relatives and friends for their consistent encouragement in academic endeavours.

University of Saskatchewan

Electrical Engineering Abstract #91A339

Method and Apparatus for Thermoacoustic Analysis (TAA)

Student:V.R.Mirchandani Supervisor:Dr. S.O.Kasap

M.Sc. Thesis Submitted to the
College of Graduate Studies and Research
January 1991

ABSTRACT

A prototype of an apparatus for Thermoacoustic Analysis (TAA) was designed and implemented which allows thermal analysis of solid materials by a non-destructive technique using ultrasonic waves. Longitudinal ultrasonic waves are generated by a high voltage RF pulse excitation of an X-cut quartz transducer at its resonant frequency of 4 MHz. The waves are coupled to and from the material by two identical buffer glass rods while the material temperature is ramped accurately by a PID temperature controller. The changes in the transit time of the acoustic waves and their relative attenuation, are monitored with sample temperature. Transit time measurements have been carried out by noting the time difference between the reflected and the transmitted waves. Relative attenuation measurements are done by taking the peak-to-peak voltage of the received signal at various sample temperatures with respect to the peak-to-peak voltage of the received signal at room temperature. The apparatus can be used at room temperature as well as from room temperature to 250°C at a maximum heating rate of about 10°C/min and with a resolution of around 10 ns in transit time measurement. The accuracy of the transit time measurement is thus around 10 ns or better and that of the peak-to-peak received signal voltage is around 1 mV.

The apparatus was applied at room temperature to determine the mechanical properties of amorphous polymers and thermally cycled composites. A correlation between normalised velocity, relative attenuation and flexural strength with number of thermal cycles is obtained for three types of composites. Furthermore, the usefulness of the apparatus has been demonstrated by carrying out ultrasonic measurements as a function of temperature at different heating rates for polycarbonate (PC). An excellent correlation between TAA, viscosity, and the conventional thermal analysis techniques viz. Differential Scanning Calorimetry (DSC), Thermo-microhardness (TμH) for polycarbonate (PC) has been found. The TAA technique developed herein has been also applied to Poly(methyl methacrylate) (PMMA), Polyphenylenesulphide (PPS) and a near-stoichiometric amorphous arsenic triselenide alloy.

TABLE OF CONTENTS

LIST OF FIGURES

LIST OF TABLES

1. INTRODUCTION

1.1 ULTRASONICS

Unlike electromagnetic waves, sound waves propagate by means of vibration of the material medium. Sound waves with a frequency of vibration less than 20 Hz are called *infrasonics*. Waves audible by a normal human ear are in the range of frequencies 20 Hz - 15 kHz and those which have frequencies above 20 kHz are called *ultrasonics*. The spectrum of acoustic vibrations is illustrated in Fig. 1.1. Acoustic waves in the frequency range 500 MHz to 1000 GHz as shown in Fig. 1.1, are referred to as *microsound*. The acoustic frequency which has been used in this research work falls in the ultrasonic range, which has been shown shaded in Fig. 1.1.

The acoustic waves may fall under two categories, one dealing with low amplitude vibrations and the other with high energies. In low amplitude vibrations, it is of interest to find out the effect of the medium on the waves since permanent changes do not take place in the medium. Whereas, in high energy acoustic wave propagation it is of interest to find out the changes brought about by the waves in the medium.

One of the first applications of ultrasonics was in 1883[1] when Galton devised a high frequency whistle for measuring upper frequency limit of the human ear. The first important use of ultrasonics was made by Langevin[1] during the 1914-1918 war for underwater soundings. It was not until after

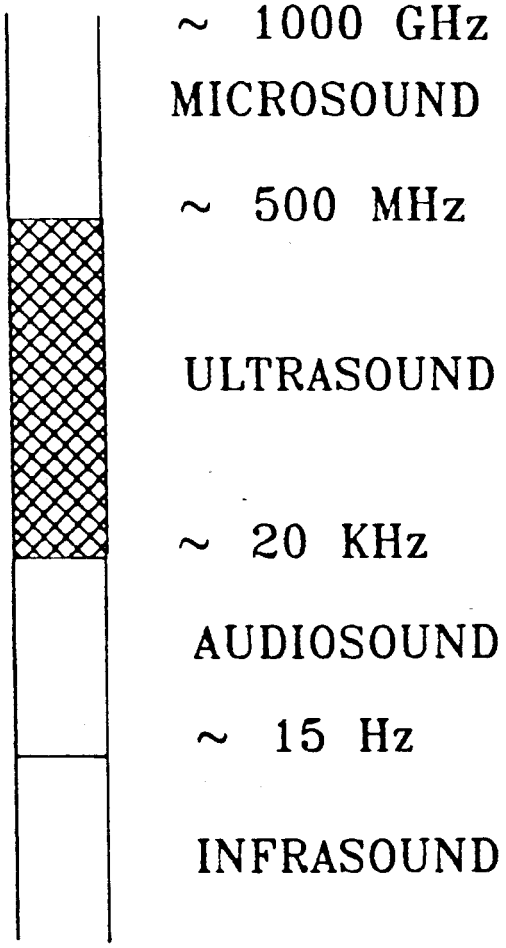

Fig. 1.1 Acoustic frequency scale[2].

the 1939-1945 war that any major advances were made in the field of ultrasonics. Currently there are numerous scientific applications of ultrasonics such as[2]:

(a) Determination of elastic moduli of materials.
(b) Determination of absorption coefficients of materials.
(c) Determination of sound velocity in materials.
(d) Non-invasive methods for determination of blood flow.
(e) Non-destructive evaluation of defects in materials.
(f) Catalysis of chemical reactions.
(g) Thickness measurements.
(h) Ultrasonic medical imaging.
(i) Ultrasonic cleaning, drilling.
(j) Intrusion detection.

The principal reasons for using ultrasonic frequencies instead of the audio frequencies are the following[1]:

(a) Since ultrasonics include high frequencies, which imply shorter wavelengths, plane wave conditions are more easily realised. This is especially important for small size specimens.

(b) Absorption coefficients are usually much higher and thus more easily measurable at high frequencies.

(c) Another major advantage of using high frequencies is that they are more easily focused.

1.2 THERMAL ANALYSIS

The terminology of *thermal analysis* currently in usage has been defined by Mackenzie[3], and the International Confederation for Thermal Analysis (ICTA). It is defined as "a group of techniques in which a physical property of a substance and/or its reaction products is measured as a function of temperature whilst the substance is subjected to a controlled temperature program".

For this definition to be applicable three criteria must be satisfied[3]:

(a) A physical property should be measured.
(b) The measurement should be expressed (directly or indirectly) as a function of temperature.
(c) The measurement should be made under a controlled temperature program; temperature-time profile of the sample should be well defined.

The various physical properties which can be measured by thermal analysis include mass, enthalpy, dimension e.g. thickness, electrical characteristics, optical characteristics.

Some of the thermal analysis techniques which are based on changes in thermal properties are *Differential Scanning Calorimetry (DSC)*, and *Thermomechanical Analysis (TMA)*. From the DSC technique, one can measure enthalpy changes, glass transition temperatures, rates of reaction, melting temperatures etc. Whereas from TMA one can measure mechanical deformations such as contraction or expansion of materials as a function of temperature.

In TMA, measurements are normally made under an applied stress, thus changes in shape or size may result. TMA response is a combination of expansion behaviour and *viscoelastic effect*. It is widely used to study the properties of polymers and other materials under various experimental conditions.

In DSC, a sample and a *thermally inert* reference material are both subjected to a controlled temperature-time profile which is usually a temperature ramp. In the event of a transition in the sample due to phase changes, however,

thermal energy is added to or subtracted from the sample with respect to the inert reference material so as to maintain both sample and reference at the same temperature. This balancing energy which maintains a zero temperature differential between the sample and the reference is a direct calorimetric measurement of the transition energy. Further details of DSC and TMA techniques are given in Section 3.2 and 3.3 respectively.

1.3 SIGNIFICANCE OF MATERIAL STRUCTURE

As seen from Fig. 1.2 the structure of the material plays an important role in determining its major properties viz. mechanical, electronic, thermal, optical. Any variation in the structure of the material due to environmental interaction e.g. temperature, pressure, or due to defects, impurities results in variation of the properties of the material.

The mechanical properties are reflected by parameters such as microhardness (H_V), elastic moduli (E), viscosity (η) etc. The mechanical properties influence the deformation and fracture behaviour as well as the wear characteristics of the material. For example, structural variation could result in limiting the mechanical life-time of the material. Similarly, the electrical properties are reflected by parameters such as conductivity (σ), mobility (μ), charge carrier relaxation time (τ). The electrical properties, for instance, influence the electrical resistance of a material used in electronic applications. The optical properties of a material are

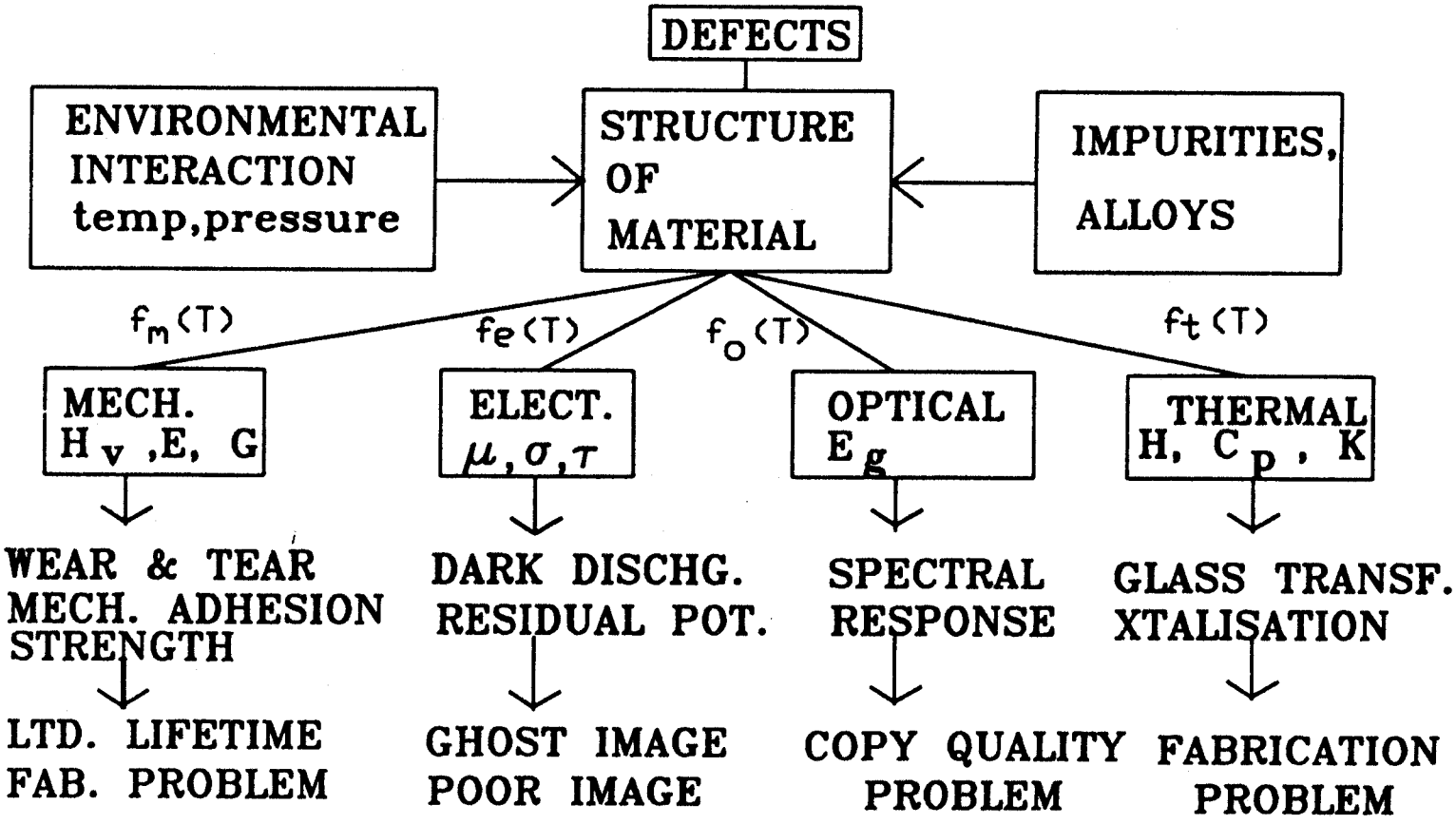

Fig. 1.2 Thermoacoustic measurements in materials - Perspective view.

characterised largely by its bandgap E_g which influences the spectral response of the material. The thermal properties are characterised by parameters such as enthalpy (H), thermal conductivity (K) and specific heat at constant pressure (C_p). Structural changes in the material result in changes in the thermal properties which may affect the suitability of the material for an engineering application.

Thus one can realise from the above discussion the relative importance of the structure of the material and the possible effects its variation can have on its properties. The particular example chosen in Fig. 1.2 is that of amorphous selenium (a-Se) alloys used in xerographic photoreceptors. The figure summarizes how changes in structure affect the mechanical, electrical, optical and thermal properties and thus influence the use of the material in an engineering application.

1.3.1 RESEARCH OBJECTIVES

One of the prime objectives of this research work was to develop the prototype of an apparatus for Thermoacoustic analysis of solid amorphous materials. The working of the electronics and thermal subsystems of the apparatus was then to be determined by applying the TAA apparatus on various engineering materials at room temperature as well as under different controlled heating rates in the range of 0.2°C/min-10°C/min.

The TAA technique was then to be confirmed by correlating

it with conventional thermal analysis techniques viz. Thermal Microhardness (TμH), Differential Scanning Calorimetry (DSC) applied to different engineering materials under controlled heating rates upto a maximum temperature of 250°C.

The thermoacoustic analysis apparatus can measure the absolute as well as relative changes in longitudinal ultrasonic velocity and attenuation in materials when the material is heated at a programmed rate. The TAA apparatus can also be used isothermally. One important use of the data obtained by TAA apparatus is in determing the glass transition temperature of a glassy material at a particular heating rate.

Furthermore, the resourcefulness of the TAA apparatus was to be established by non-destructively obtaining the Young's modulus of thermally cycled composite engineering materials. From TAA, Young's modulus of a material can be obtained at any temperature provided the density and Poisson's ratio of the material at that temperature are known.

1.4 THESIS OUTLINE

The thesis has been divided into six Chapters. This first Chapter gives a brief overview of ultrasonics and thermal analysis. The contents of the second Chapter will help in understanding some of the underlying principles applied in experimentation. The second Chapter is divided into three main Sections describing in brief the different types of ultrasonic waves, methods of generation and detection of ultrasonic waves and basic principal electronic methods for measuring sound

velocity in solids. The third Chapter gives concise descriptions of some of the present methods for studying the variation in the structure of the material by using thermal analysis techniques. It also gives a brief preview of the TAA technique in relation to the Differential Scanning Calorimetry (DSC) and Thermomechanical Analysis techniques.

The description of the TAA apparatus designed and implemented, experimental and electronic design details, are covered in the fourth Chapter. In addition to the electronic subsystem, thermal and mechanical subsystems of the apparatus are also described. Results and their interpretation are discussed in Chapter five. The final Chapter outlines the major conclusions of the present work and mentions suggestions for future work.

2. ULTRASONIC TECHNIQUES

2.1 INTRODUCTION

Non-destructive evaluation of any solid material can be done by using various types of ultrasonic waves e.g. surface waves, shear waves and longitudinal waves. The choice for the use of a particular type of ultrasonic wave is usually based on the region of investigation in the material e.g. bulk or surface. The waves are generated and detected in the medium by using acoustic transducers. The choice for the use of a particular type of transducer is based on the frequency of the ultrasonic wave desired.

The elastic properties of a solid can be determined from the sound velocity of ultrasonic waves in the medium. Different techniques have been developed for sound velocity measurements in solids depending on the accuracy and elastic modulus desired.

2.2 TYPES OF ULTRASONIC WAVES

There are several types of ultrasonic waves, namely, longitudinal, transverse (shear), and surface. The transmission of ultrasonic energy depends on particle vibrations. The particles of the medium are displaced as the wave travels through the medium.

2.2.1 LONGITUDINAL WAVES

Longitudinal waves exist when the motion of the particles in the medium is parallel to the direction of wave

propagation[4,5]. This wave can travel in solids and liquids as well as gases. This type of wave mode is illustrated in Fig. 2.1.

For a solid in the form of a rod, where the cross-sectional dimensions are small compared to the wavelength, the velocity, c_L, of the longitudinal waves in the axial direction is given by[7]

$$c_L = \sqrt{\frac{Y}{\rho}} \qquad (2.1),$$

where

Y = Young's modulus,

ρ = density of the material.

The bulk velocity of longitudinal waves, i.e. velocity in a medium whose dimensions are much greater than the wavelength, is given by[7]

$$c_L = \sqrt{\frac{Y(1 - \nu)}{\rho(1 + \nu)(1 - 2\nu)}} \qquad (2.2),$$

where

ν = Poisson's ratio for the material.

Experiments have indicated that the velocity may vary with the intensity of the applied vibration; velocities varying by as much as a factor of three have been reported[8]. It is known that under high intensities the elastic properties undergo a change in value due to the extreme stresses experienced and this conceivably alters the velocity.

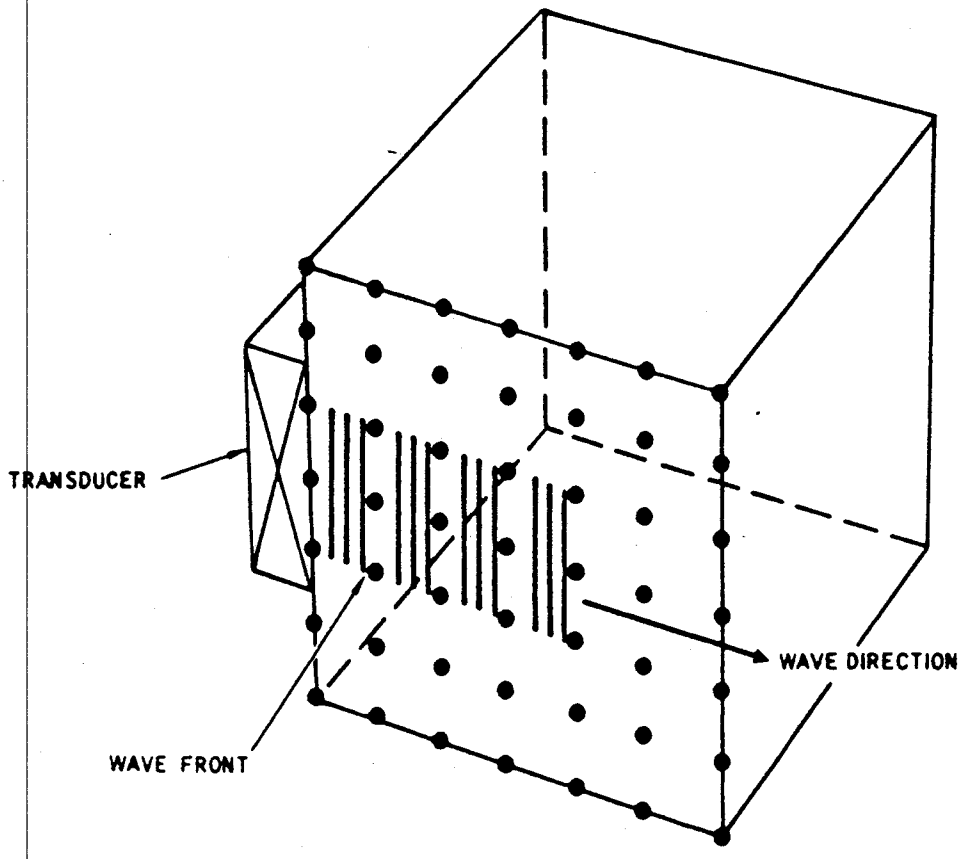

Fig. 2.1 Longitudinal wave propagation[6].

When shear waves are used, the movement of the particles in the medium is at right angles to the direction of wave propagation. If the wave propagation is in the x direction, the particle displacement is in the yz plane. Fig 2.2(a) illustrates the particle motion in a shear wave. These waves may exist in a limited area or entirely throughout a body.

The shear wave velocity is about 48 % of that of a longitudinal wave in the same material. The shear velocity is given by[4]

$$c_S = \sqrt{\frac{G}{\rho}} \qquad (2.3),$$

where

G = the modulus of rigidity of the material.

The shorter wavelength waves are more sensitive to small inclusions, and hence are more easily scattered within a material. Unlike longitudinal waves, shear waves do not travel in liquids or gases.

2.2.3 SURFACE WAVES

Surface waves can be divided into four classes, namely, Rayleigh waves, Lamb waves, Love waves, Stoneley waves.

(A) RAYLEIGH WAVES

Rayleigh waves are somewhat analogous to water waves[9] in which the motion of particles is both transverse and longitudinal in a plane containing the direction of propagation and the normal to surface. In Rayleigh waves the

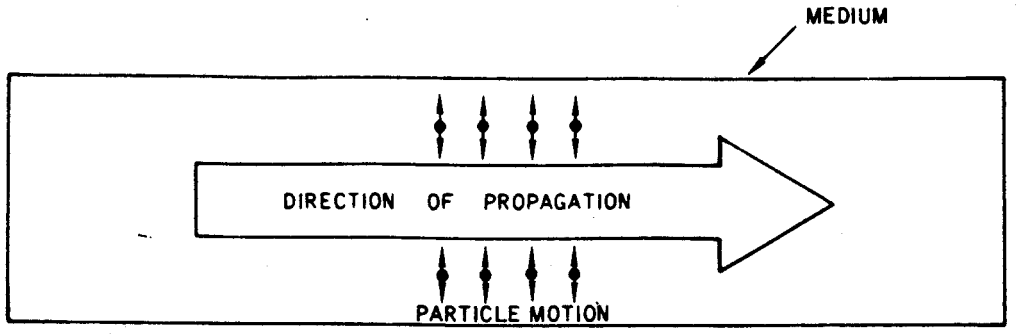

(a)

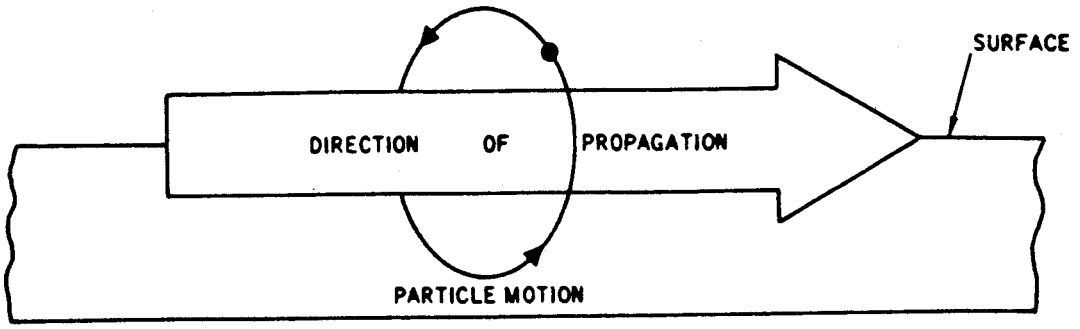

(b)

Fig. 2.2 (a) Transverse wave propagation[6]. (b) Rayleigh wave propagation[6].

particle movement is elliptical and such waves exist only in the surface layer of large solids. The major axis of the ellipse is normal to the surface along which the wave is travelling. The minor axis is parallel to the direction of propagation. At greater depths than one wavelength below the surface the particle motion is practically zero. A representation of Rayleigh wave propagation is given in Fig. 2.2(b). The surface velocity is usually about ~ 0.9[4]times the transverse wave velocity in most solids.

(B) LAMB WAVES

Lamb waves are produced when ultrasonic waves travel along a test specimen with a thickness comparable to the wavelength[6]. A thin plate is capable of transmitting an infinite number of Lamb waves. There are two main types of Lamb waves; symmetrical or antisymmetrical. The type is determined by whether the particle motion is symmetrical or antisymmetrical with respect to the medial plane of the specimen. Both types of Lamb waves are shown in Fig. 2.3. The wave velocity depends on the plate thickness, frequency and the test material.

(C) LOVE WAVES

Love waves travel on the surface without any vertical component. They are basically transverse waves with the direction of oscillation parallel to the surface. Such waves require that a thin layer of some material of different density be present on the bulk material. Love waves propagate

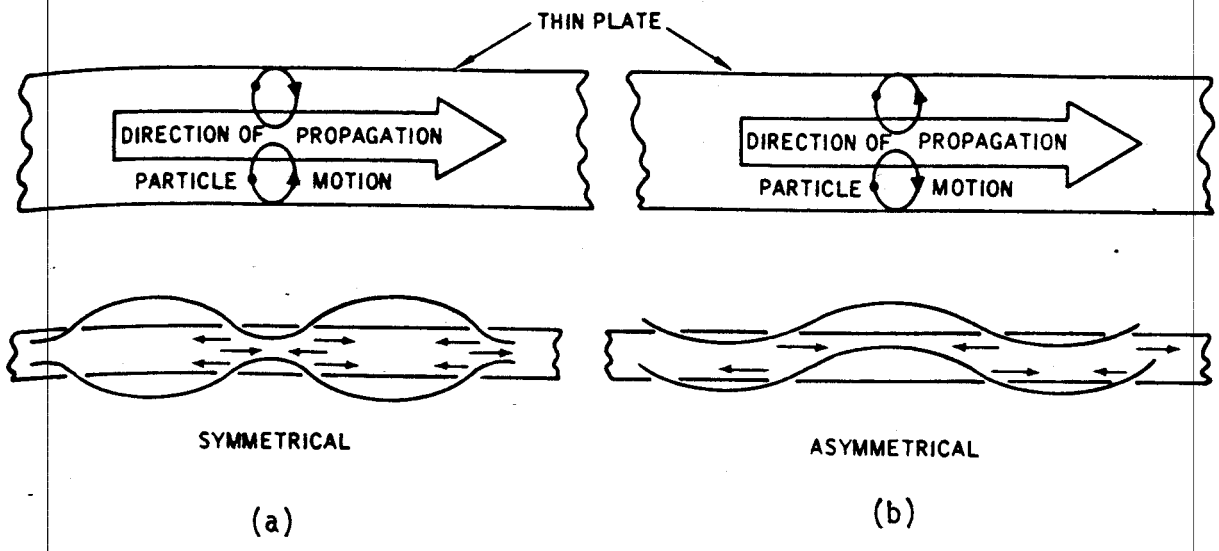

Fig. 2.3 (a) Lamb wave symmetrical. (b) Lamb wave unsymmetrical[6].

with velocities which are dependent on the frequency; in general the velocity decreases with increasing frequency[5].

(D) STONELEY WAVES

These are basically leaky Rayleigh waves which are produced when there is a surface wave at a liquid/solid interface, and there is some transfer of ultrasonic energy back into the liquid medium[9].

2.3 BEAM SPREADING

An ultrasonic beam travels through matter with very little divergence or spreading. As the wavelength becomes shorter, the beam shape approaches that of an almost rectilinear propagation. The region in which the waves are propagated is called the *ultrasonic field*, the configuration of which depends on the diameter (d) of the transducer and also the wavelength (λ). This field is divided into two regions; namely *far field* and the *near field*. Fraunhofer diffraction causes the beam to spread at $d^2/4\lambda$ distance from the face of the transducer. At this distance, the beam spreads outward to appear to originate from the centre of the radiating face of the transducer (Fig. 2.4(a)). This spread is a function of λ/d. The angle of divergence of the beam is given by[6]

$$\sin\theta = 1.2\,\frac{\lambda}{d} \qquad (2.3),$$

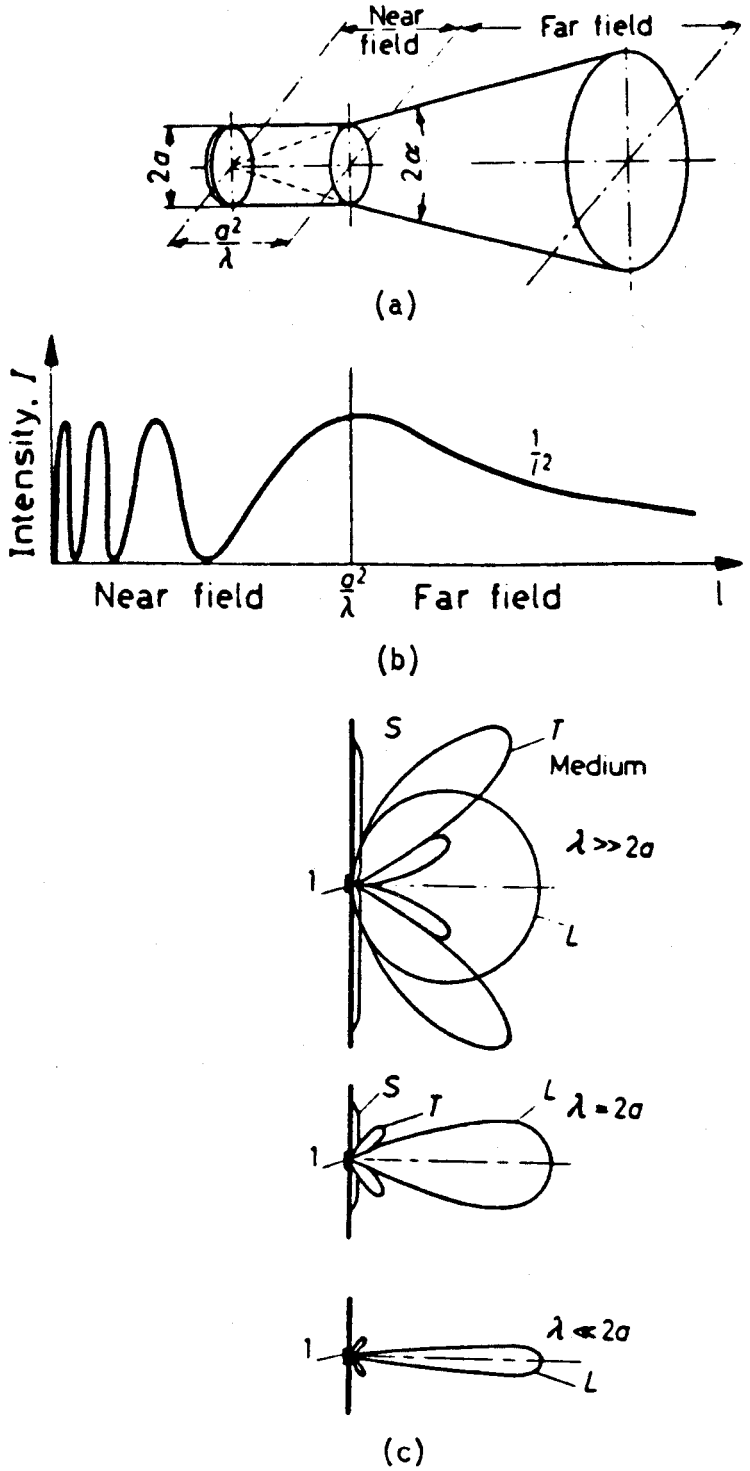

Fig. 2.4 (a) Spreading of longitudinal ultrasonic waves. (b) Intensity distribution along axis of the transducer. (c) Directional characteristics of a longitudinal wave transducer 1, of diameter 2a[7].

where

θ = Angle of divergence of the beam.

The directional characteristics of a longitudinal wave transducer at different wavelengths is presented in Fig. 2.4(b). The variation of intensity with axial distance from the transducer is shown in Fig. 2.4(c).

2.4 GENERATION AND DETECTION OF ULTRASONIC WAVES

Ultrasonic waves are generated and received by *a transducer* which basically converts energy from one form to another. Reversible acoustic transducers are used to convert the acoustical energy to or from such forms of energy as electrical, mechanical and thermal. An acoustic transducer is equivalent to an electrical transformer in which the electrical components, i.e. the true electrical resistances and reactances appear in the primary circuit and the mechanical components appear in the secondary circuit.

Transducers used for generating ultrasonic waves are piezoelectric, magnetostrictive, electromagnetic, and mechanical devices. Transducers most often used for receiving or detecting ultrasonic energy are piezoelectric and magnetostrictive devices. Some of the transducers, other than the piezoelectric type, are described in Appendix A.

2.4.1 CRYSTAL OSCILLATORS

Basically two types of crystals may be used for generating ultrasonic waves, one which displays the *piezoelectric effect* and the other *electrostrictive effect*.

Some of the crystals which show piezoelectric effect are quartz, tourmaline, Rochelle salt, lithium sulphate and artificially grown crystals such as ammonium dihydrogen phosphate (ADP), potassium dihydrogen phosphate (KDP), ethylene diamine tartrate (EDT)[1]. Crystals which show electrostrictive effect are barium titanate, lead meta-niobate and lead zirconate titanate (PZT)[1].

Vigoureux and Booth[1] have recommended the following requirements for an ultrasonic transducer:

(a) It should have satisfactory piezoelectric characteristics for the required modes of vibration.
(b) Variations of its properties with temperature should be small.
(c) It should be chemically and physically stable.
(d) It should be capable of matching electric circuit and medium of propagation.
(e) The generation of parasitic frequencies which may arise from unsatisfactory mounting should be minimal.

(A) PIEZOELECTRIC EFFECT

The piezoelectric effect occurs in crystals in which there is an absence of centre of symmetry[1]. If a slab or disc of such a crystal is cut with its parallel surfaces lying normal to a polar axis, then on subjecting this slab to a mechanical stress, equal and opposite electric charges appear on the parallel surfaces. Provided the crystal is not strained beyond its elastic limit, the magnitude of the charge density (or dielectric polarisation) is directly proportional to the applied stress.

Conversely, when an electric field is applied in the direction of a polar axis the slab is mechanically strained, the amount of strain being proportional to the intensity of the applied field. The direct and inverse piezoelectric effects are equal and opposite[1]. The microscopic origin of piezoelectricity lies in the displacement of ionic charges within the crystal. In the absence of strain, the distribution of charges at the lattice site is symmetric, so the internal field is zero. When the crystal is strained, the charges are displaced. If the charge distribution is no longer symmetric, then a net polarisation, and a concomitant electric field develops. This is the field which operates in piezoelectric effect. Fig. 2.5(a) illustrates that if there is a centre of inversion even after distortion then the polarisation remains zero. However, as it can be seen from Fig. 2.5(b), in the case of quartz, in which there is no centre of inversion, distortion produces polarisation. The lack of inversion centre is not however a sufficient condition to guarantee piezoelectricity[10].

Quartz, which is very commonly used for ultrasonic propagation, belongs to the trigonal system and a typical quartz transducer with different cuts is illustrated in Fig. 2.5(c). It can be seen from this diagram that the Z-axis, the optic axis, is non-polar and that a section through the main body of the crystal, normal to the Z-axis, is hexagonal in shape. The three axes joining opposite edges are known as the

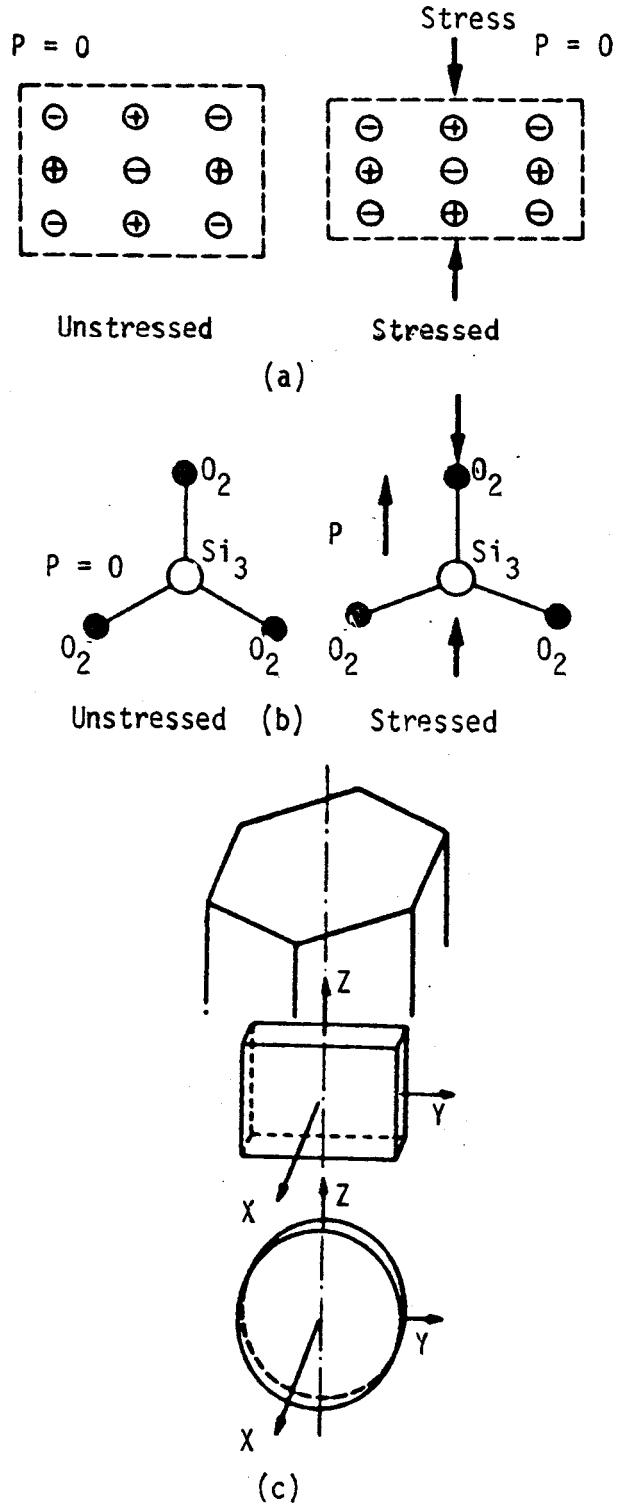

Fig. 2.5 (a) Crystal with centre of inversion exhibits no piezoelectric effect. (b) Origin of piezoelectric effect in quartz. (c) X-cut rectangular and circular plates from a quartz crystal[11].

X-axis and the corresponding axes perpendicular to these i.e. joining opposite faces, are called the Y-axes. These are polar axes, and slabs cut with their faces perpendicular to them display the piezoelectric effect[1]. Crystals cut with their faces normal to an X- or Y-axis are called X- or Y-cuts, respectively. X-cut crystals are normally used for the propagation of compression/longitudinal waves and Y-cut crystals are often used for the generation of shear waves[1].

Consider an X-cut crystal in the shape of the rectangular prism as shown in Fig. 2.5(c). An electric field applied along the X-axis of the crystal in a given direction produces compression in that direction, and simultaneously, an expansion takes place along the Y direction of the crystal. By reversing the direction of field the compression and expansion take place along Y and X direction respectively. It is emphasised here that there is no change along the Z axis.

Electrodes may be formed by coating the surface normal to the X or Y axis by means of a conducting material. The fundamental frequency of the crystal is dependent on its thickness (Section 4.3.1). Apart from exciting the crystal at its fundamental frequency, it can also be excited at its harmonic frequencies to generate higher frequency ultrasonic waves.

Quartz possesses most of the desirable properties of a transducer. It remains piezoelectric at temperatures upto 573 °C and is very stable both chemically and physically except at

Table 2.1: Principal Piezoelectric Properties of some of the More Common Transducer Materials[1].

SUBSTANCE	DIELECTRIC CONSTANT	d* (coulomb newton^{-1}x 10^{12}	k_c** %	Upper Curie Temp. °C
Quartz (X-cut)	4.5	2.3	11	550
Barium titanate	400 to 1700	60 to 190	20 to 50	120 to 140
Lead zirconate titanate	900 to 1500	80 to 320	23 to 76	350 to 490
Lead meta-niobate	225	85	42	550
Rochelle salt (45° Y-cut)	9.4	27	29	45
Rochelle salt (45° X-cut)	450	430	78	45
Ammonium dihydrogen phosphate (ADP) (45° Z-cut)	15	24	29	120

very high temperatures and pressures where it becomes partially soluble in water[1]. Internal losses are small and if mounted properly it has a Q factor of 25,000[1].

Quartz is easily worked and specimens as thin as 0.1 mm thick may be cut. Comparison of the salient properties of quartz with other major crystal transducers is given in Table 2.1.

---

*Piezoelectric strain constant.

**Electro-mechanical coupling factor.

For a piezoelectric transducer following relations hold good within the elastic limit[1].

$$S = Ts + Ed' \qquad (2.4),$$

$$D = Td + \varepsilon E \qquad (2.5),$$

where

T, E = Tensile stress and Electric strength respectively,

S = Resultant mechanical strain,

D = Electric displacement,

s = Elastic constant,

ε = Electric permittivity,

d, d′ = Piezoelectric strain constant.

(B) ELECTROSTRICTIVE EFFECT

Certain dielectrics called *ferroelectrics* exhibit a strong electrostrictive effect. The application of an electric field in a given direction produces a mechanical strain, the magnitude of which is proportional to the square of the applied field strength and is thus independent of the direction of the field. Consequently, a positive strain may occur for both positive and negative values of the exciting field. To obtain a sinusoidal variation in strain one must polarise the transducer[1]. This is usually done by heating it to a temperature above the Curie point, and then allowing it to cool down slowly in a strong direct field oriented in the direction in which it is intended to apply the exciting field.

Provided that the exciting field is small compared with the initial polarising field, the strain will vary sinusoidally at the frequency of the exciting field[1].

A polarised ferroelectric transducer appears to display the same effect as a piezoelectric transducer. For the construction of this type of transducer, many small crystallites of the ferroelectric material, together with suitable additives, are bonded together to form a ceramic of the required shape. Various shapes of these transducers can thus be obtained.

These electrostrictive transducers have high internal damping[1]. This makes them suitable for generation of short pulses. However, some of the ferroelectric transducers such as barium titanate have low Curie temperatures of around 115°C[12]whereas others such as lead zirconate titanate have a Curie temperature of 490 °C[1].

The equivalent circuit for a barium titanate transducer is the same as that for quartz transducer. However, because of much higher dielectric constant, the static capacitance is considerably higher for barium titanate. Barium titanate has a lower dynamic impedance in comparison to quartz. Thus for the same power output from a barium titanate transducer as from a quartz transducer, a large current must be used[7].

2.5 EQUIVALENT CIRCUITS

The equivalent circuit of the transducer is useful for predicting its efficiency, transformation factor, Q value, and

for analyzing the performance of the transducer after it is constructed. An equivalent circuit is based on the assumption that the transducer operates in a linear manner and, therefore all circuit values are constants[13].

In the case of quartz, the piezoelectric element is an electric condenser of capacitance C_o by virtue of the dielectric nature of the transducer material and the electroded surfaces. The electrical resistance of this condenser is negligible. The capacitance C_o appears in parallel with a series branch that includes the converted mechanical impedances. These mechanical impedances consist of (1) a resistance R_1 corresponding to the losses in the transducer, (2) a load resistance or radiation impedance Z_R; (3) an inductance L due to the mass of the transducer; and (4) a capacitance, C, due to the compliance 1/K of the transducer[13].

For an air backed transducer, the circuit elements are given by[13]

$$R_R = \frac{Z_R}{4\alpha^2}, \quad L = \frac{M}{4\alpha^2}, \quad C = \frac{4\alpha^2}{K} \qquad (2.6),$$

where

α = is the transformation factor.

However, there are losses in the piezoelectric element in the form of dielectric losses and internal losses due to strain. Inserting these losses, a simple equivalent circuit for an air-backed quartz at resonance is illustrated in Fig.

2.6. From the equivalent circuit the efficiency η of the piezoelectric transducer becomes[13]

$$\eta = \frac{R_D\left(\frac{\rho_o c_o S}{4\alpha^2}\right)}{\left(R_f + \frac{\rho_o c_o S}{4\alpha^2}\right)\left(R_f + R_D + \frac{\rho_o c_o S}{4\alpha^2}\right)} \qquad (2.7),$$

where

$\rho_o c_o$ = is the characteristic acoustic impedance of the load,

α = the transformation factor,

S = is the area of radiating surface,

R_D = corresponds to resistance due to dielectric losses,

R_f = corresponds to internal losses due to strain.

The efficiency of the transducer when there is maximum power transfer from the generator to load is given by[13]

$$\eta = \frac{R_D}{2(R_D + 2R_R)} \qquad (2.8),$$

This occurs when the transducer is matched to the generator and the radiation impedance is equal in magnitude to the internal loss resistance of the transducer.

The transformation factor kc is basically the ratio of the mechanical energy stored in the transducer to the electrical energy supplied to it[1]. It is another way of indicating the efficiency of the transducer.

The Q of the transducer is the ratio of the energy stored in its reactive components to the energy dissipated in its resistive components, which include the radiation resistance.

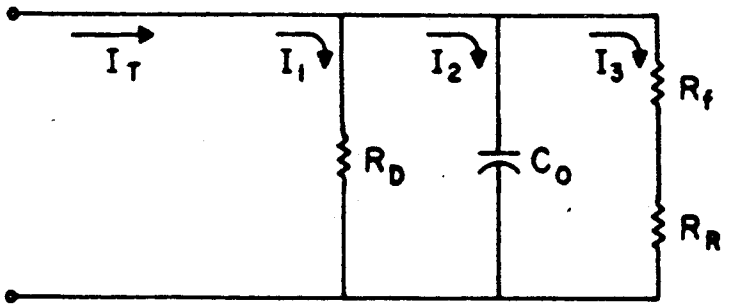

R_D = Resistance due to dielectric losses.

C_o = Capacitance due to electrodes.

R_f = Resistance due to internal strain losses.

R_R = Radiation resistance.

Fig. 2.6 Equivalent circuit of a simple air-backed, resonant piezoelectric transducer with losses[13].

The operating frequency bandwidth of the transducer is a function of the Q.

2.6 ULTRASONIC VELOCITY MEASUREMENT TECHNIQUES IN SOLIDS

There are quite a few techniques for measuring the velocity of sound in solids. The electronic techniques are listed below:

1) Pulse echo technique
2) Sing-around technique
3) Pulse superposition technique
4) Pulse echo overlap technique (PEO).
5) Superposed pulse echo overlap method (SPEO).

In all these techniques the solid sample in which the ultrasonic velocity is to be determined should have parallel surfaces. The piezoelectric transducer is mounted on the specimen such that the coupling produced by the bonding medium is tight, producing satisfactory acoustic impedance matching. Also the sample thickness should be measured accurately and the transducer should be excited at its resonant frequency.

2.6.1 PULSE ECHO TECHNIQUE

Firestone[11] in 1940 was first to recognise the importance of the pulse echo method for non-destructive testing, in particular for the location of flaws.

Fig. 2.7 shows a simplified block diagram for a pulse echo instrument. A trigger circuit initiates the time base generator which provides a sweep for the X-plates of the oscilloscope besides acting as a triggering for the pulse

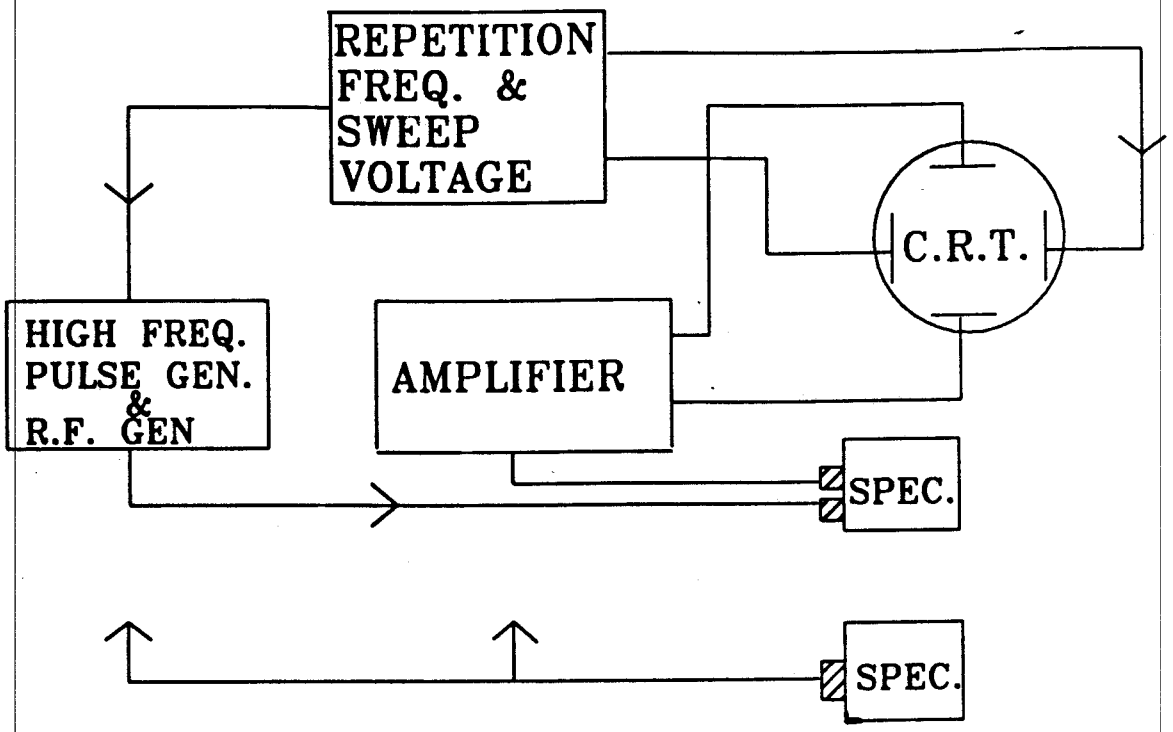

Fig 2.7 Pulse echo technique[11].

generator. The pulse generator in turn triggers the RF generator for the specified duration of the pulse width. RF generator is tuned to the resonant frequency of the crystal. RF generation is thus synchronised with the sweep generation. The generated RF is applied to the transmitting crystal which is excited at its resonant frequency and thus sends ultrasonic waves through the sample. The ultrasonic echoes are either received by another transducer or the same transducer can also act as the receiver. The RF signal generated by the receiving transducer is fed to an amplifier and rectified thereafter. The rectified echoes are then fed to the Y-plates of the oscilloscope. As the acoustic signal within the sample is reflected back and forth several times, the received electrical signal represents a typical exponentially decaying waveform. Care should be taken in this method of controlling the means of trigger and the repetition rate of the RF train so that the next RF train is applied after the echo train resulting from the preceding RF train has completely died down. In practice, the next RF train is applied after ~ 60^{11}times the echo duration. Since the time base frequency is synchronised with the pulse repetition frequency the echoes appear stationary on the oscilloscope. Since thickness of the sample has already been determined the velocity of sound in the sample can be readily resolved.

2.6.2 SING-AROUND TECHNIQUE

This technique was invented by Holbrook[1] and Hieldmann et al.[11] have used it for determining the velocity of sound. The block diagram of this method is shown in Fig. 2.8. Two X-cut transducers are mounted exactly opposite to each other on the specimen as shown. A RF pulse excites the transmitting transducer generating longitudinal ultrasonic waves. These waves after transit through the specimen are detected by the receiving transducer. The feedback circuit essentially acts as a control for triggering the RF pulse generator as soon as the pulse has reached the receiving transducer. The time of travel through the specimen is obtained from the pulse repetition rate found from the frequency counter. The relation between velocity and pulse repetition rate (P.R.R.) is given by[13]

$$c_L \approx L \times P.R.R. \qquad (2.9),$$

where

L = is the thickness of the material.

This equation holds good if the correction factor for delays in coupling between transducers and the specimen and in the electrical components is neglected. The received signal can be viewed on the CRO if required.

2.6.3 PULSE SUPERPOSITION TECHNIQUE

This method was devised by H.J. McSkimin[14]. The advantage of this method is that it overcomes the error produced by coupling. Consider a short duration RF pulse produced by the methods described above. This will give rise to echoes V_1, V_2,

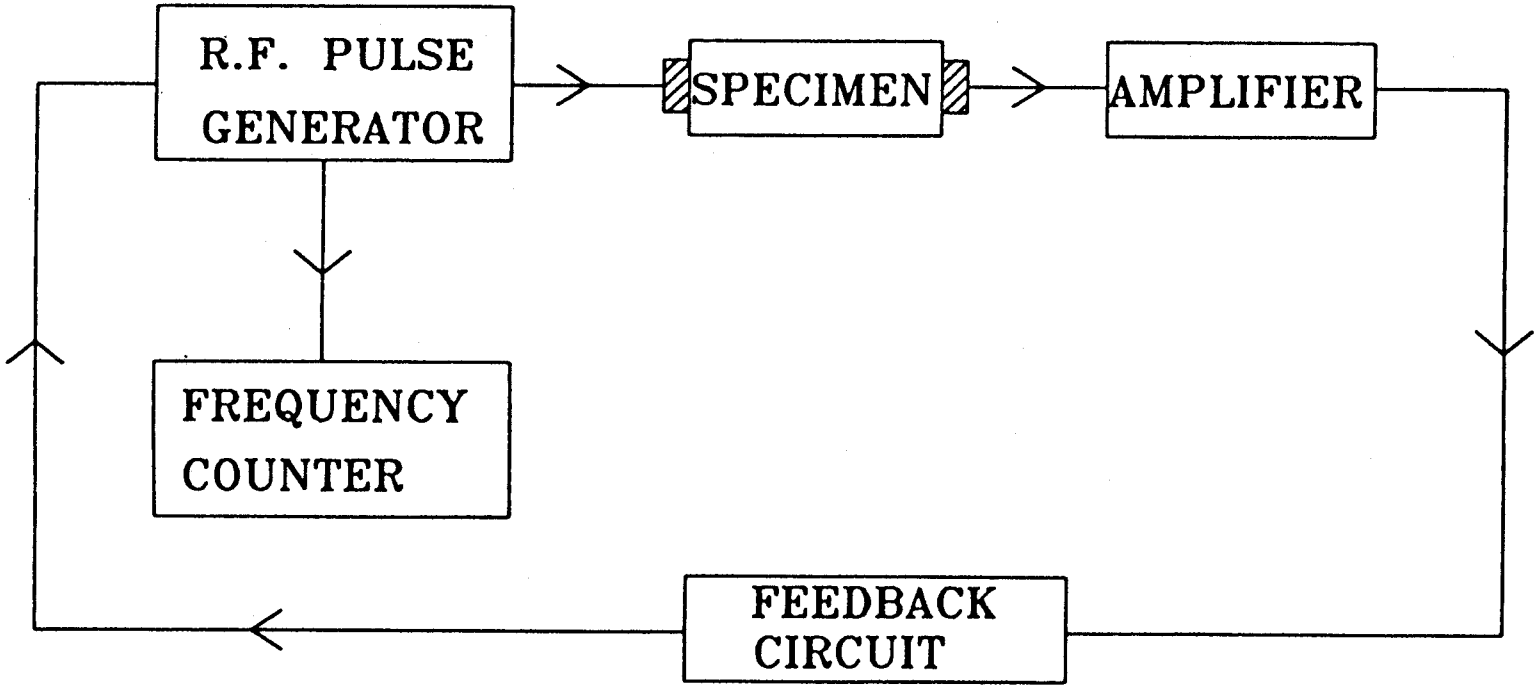

Fig. 2.8 Sing-around technique[1].

V_3 as shown in Fig. 2.9. This RF pulse train is produced every T seconds where T is approximately equal to some multiple p of the round time delay in the specimen. It can be seen from Fig.2.9 that this results in odd numbered echoes appearing in the same time slot, net result of which is superposition. By adjusting T, the superposition is done such that when this in-phase condition of echoes is achieved, T is equivalent to the time between echo pulses as seen in the Fig. 2.9. In general the equation which holds good for T is[14]

$$T = p\delta - \left(\frac{p\gamma}{360f}\right) + \frac{n}{f} \qquad (2.11)$$

where

γ = is the phase angle associated with the reflection of waves at transducer,

f = is the RF frequency of pulse,

n = is the number of cycles of mismatch,

δ = is the round trip delay time.

Thus, by finding T from the CRO the round trip delay time δ can be found from the above equation. As the thickness of the specimen is known the velocity of sound in the specimen can be determined.

2.6.4 PULSE ECHO OVERLAP TECHNIQUE (PEO)

This technique was originated by May[15], and was later extended to pulse-echo phase delay measurements by E.P. Papadakis[15]. The PEO method is a very versatile and highly

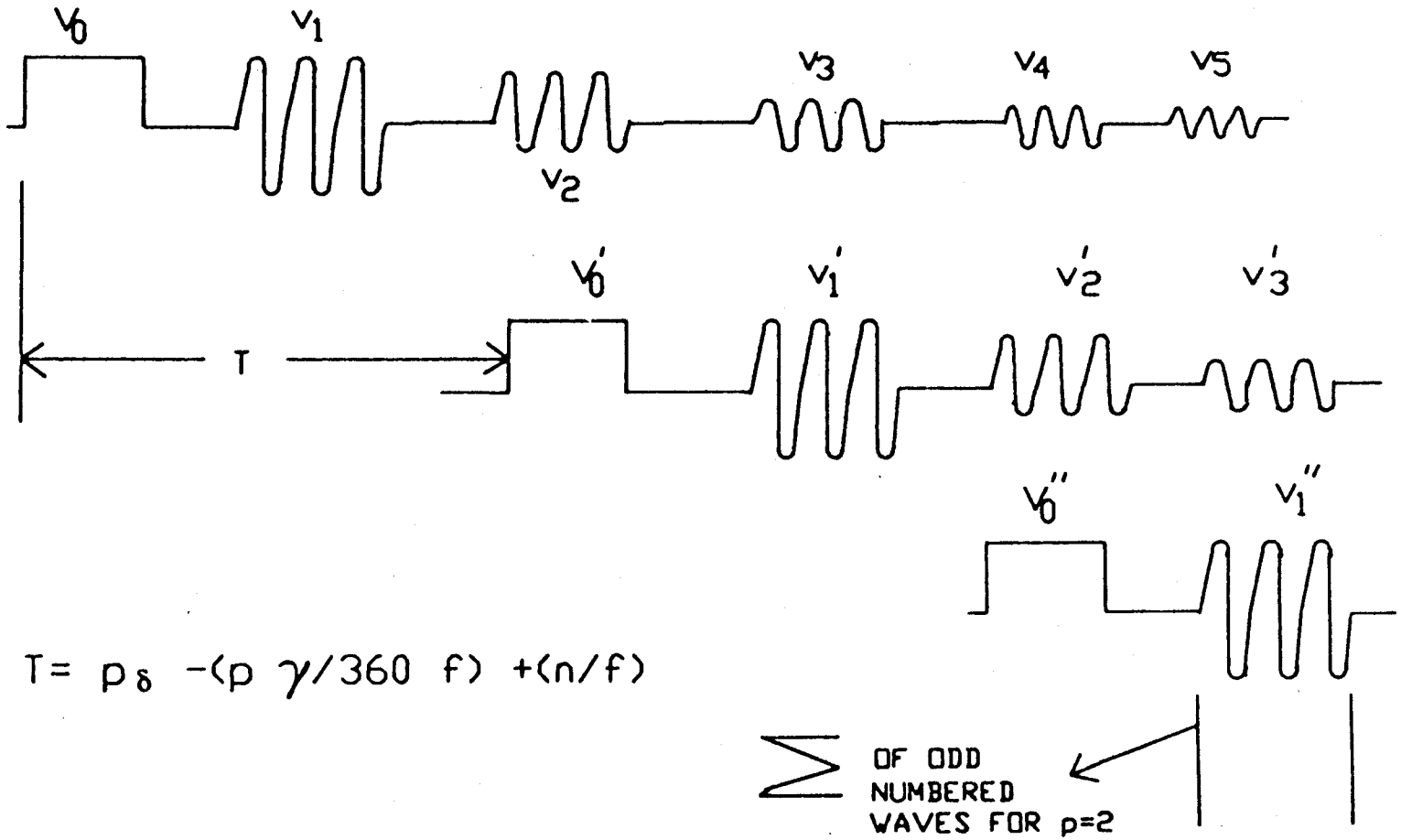

Fig. 2.9 Pulse superposition technique[14].

accurate process for measuring the velocity of ultrasonic waves in material and structures.

In this method echoes are observed on the oscilloscope, which is triggered externally by a continuous wave (CW) sinusoidal signal approximately equal in period to the travel time between the echoes or an integer fraction thereof. The proper adjustment of CW frequency produces alignment of the cycles of the RF in the echoes so that CW period corresponds to the travel time for the phase velocity of the ultrasonic waves. The block diagram of apparatus is shown in Fig. 2.10. The audio generator produces sweep for the oscilloscope, besides triggering the time delay generators and the pulsed RF generator. The RF pulse excites the transducer at the resonant frequency. The hybridge allows only the received echoes to go to the amplifiers but blocks the output RF pulse. The echoes are then received by the CRO. The intensity gate attached to the Z-axis of the CRO is actuated by time delay generators producing intensified trace of the overlapping echoes. First the oscilloscope is operated with a linear sweep in order to observe several echoes. But then it is put in the X-Y operation and the scope intensity is reduced so that the intensified overlapped echoes are visible.

The two echoes which overlap are matched up cycle for cycle by adjusting the period of the audio-sweep signal to be equal to the time delay between echoes. When the audio signal period τ_o becomes equal to the delay T between the echoes and

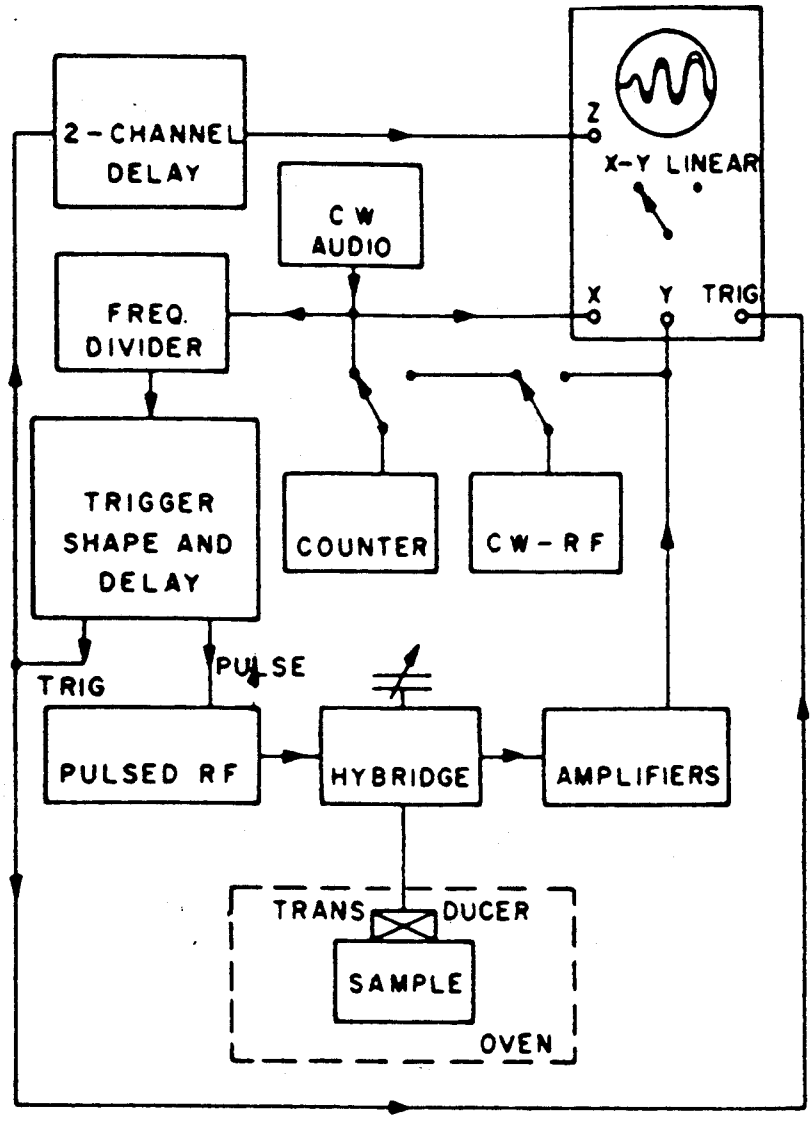

Fig. 2.10 Block diagram of the circuitry for ultrasonic pulse-echo overlap (PEO) method for velocity measurements[15].

the corresponding frequency is f_o, then matching of echoes occurs at audio frequencies mf_o (m=1,2,3....). The audio frequency is read by the counter when the echoes are aligned. It is advantageous to use large m numbers and then average the result so as to decrease the error due to the counter.

However, the main disadvantages of this method are that a quick measurement is difficult, and an extension to an automatic measurement system is not possible.

2.6.5 SUPERPOSED PULSE ECHO OVERLAP METHOD (SPEO)

SPEO has only been recently formulated by Negita and Takao[16]. This method basically incorporates the advantages of McSkimins pulse superposition technique and pulse echo overlap technique.

The method is explained by the illustration in Fig. 2.11. The pulse echo methods generate a series of echoes after a RF pulse excites the transducer. The velocity is determined by measuring the round-trip time (t_r) of the echoes. In PEO, echoes are overlapped by adjusting period of trigger pulse t_o (Fig. 2.11(c)) for the sweep of the oscilloscope to t_r, with the interval of exciting pulse (Fig. 2.11(b)), t_i being integral multiple of t_o; $t_i=nt_o$. In SPEO however more than two successive trigger pulses are used for the RF generation, with a pulse interval t_s as shown in Fig. 2.11(d) equal to t_r, echoes are superposed after the last exciting pulse. The echoes can be overlapped on the oscilloscope to satisfy the condition $t_s=t_r=t_o$ and $t_i=nt_o$ where n is an integer. From this

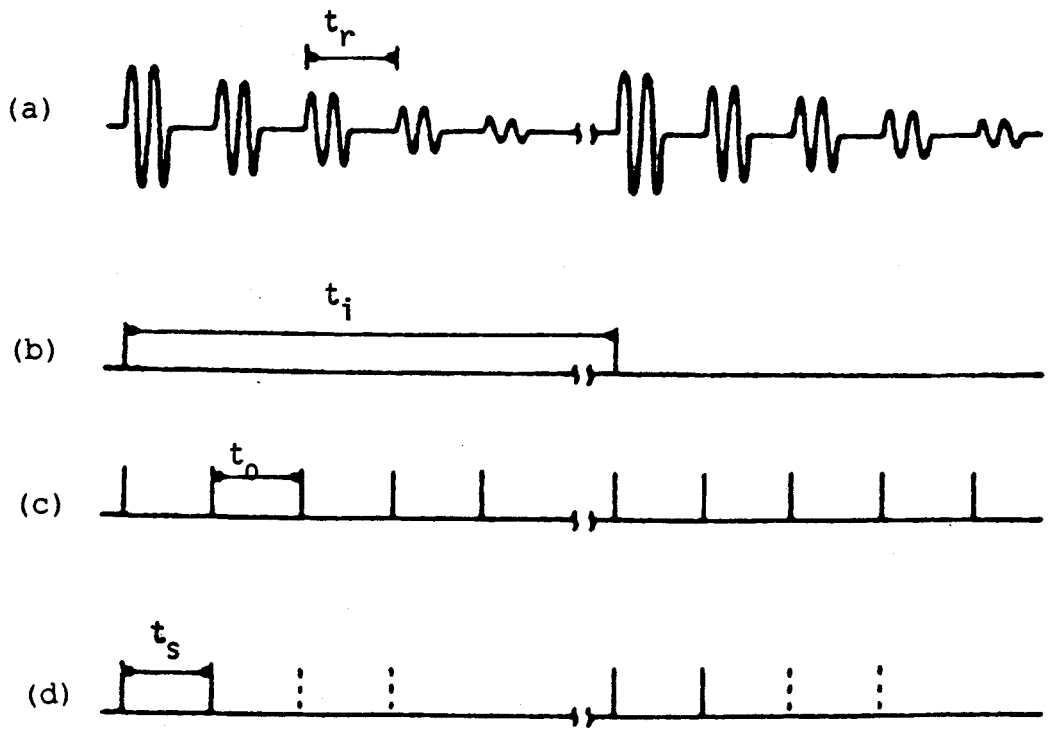

Fig. 2.11 (a) Pulse echoes. (b&c) Trigger pulses for PEO method. (c&d) for the SPEO method. (c) is for the X axis sweep of the oscilloscope[16].

the round-trip time t_r through the specimen is determined and hence the velocity. The in-phase condition of the echoes is determined when the amplitude of the superposed echoes becomes a maximum with respective superposed echoes having the same phase with each other. This can be seen on the oscilloscope.

3. THERMAL ANALYSIS TECHNIQUES

3.1 INTRODUCTION

In thermal analysis techniques, physical properties of a material are measured as a function of temperature, when the material is subjected to a controlled temperature-time program. Some of the physical parameters which can be measured by thermal analysis instruments are temperature and energy of a phase transition, dimensional changes, and viscoelastic properties. Other applications of thermal analysis include product reliability, compositional analysis, and chemical reactions[3]. The most extensively used group of techniques, which perform thermal analysis of materials, are Differential Scanning Calorimetry (DSC) and Thermo-Mechanical analysis (TMA). Recently Thermo-Microhardness analysis (TμHA) has also been introduced as a further technique. These techniques are described in this Chapter to lay down the principles of techniques used for thermal analysis. A preview with some applications of the Thermoacoustic analysis (TAA) technique from the present literature has also been included to elucidate its usefulness.

3.2 DIFFERENTIAL SCANNING CALORIMETRY (DSC)

This thermal analysis technique is principally based upon the detection of changes in heat content (enthalpy) or the specific heat of the sample. The specific heat of the material varies slowly with temperature when the material is in a

particular state. However, it varies discontinuously when there is a change of state taking place. Some of the processes which are accompanied by changes in enthalpy are melting, decomposition, and heat of reaction of a material. Enthalpy changes related to these processes can be detected by DSC[3].

In DSC, a sample to be analyzed and a thermally inert reference material are both placed in identical environments. This environment is constituted of metal cans on individual bases each having a platinum resistance thermometer and a heater as shown in Fig. 3.1(a). Thermal mass of the holders is minimised so as to increase the response of the thermometers. The heater power is adjusted such that any temperature difference between the sample and reference is nulled. Thus the temperatures of both the reference and the sample are the same as the programmed temperature. This null temperature difference is maintained even in case of a thermal event taking place in the sample[3]. The amount of energy which is either supplied or withdrawn from the sample is measured against the temperature of the sample. A typical DSC curve called a thermogram for a sample is depicted in Fig. 3.1(b). The ordinate is proportional to the specific heat of the sample since it corresponds to the rate of heat input into the sample. Exothermic and endothermic enthalpy changes give rise to peaks as shown in the thermogram in Fig. 3.1(b).

A number of DSC instruments are commercially available, but all require to be calibrated accurately prior to use. Some

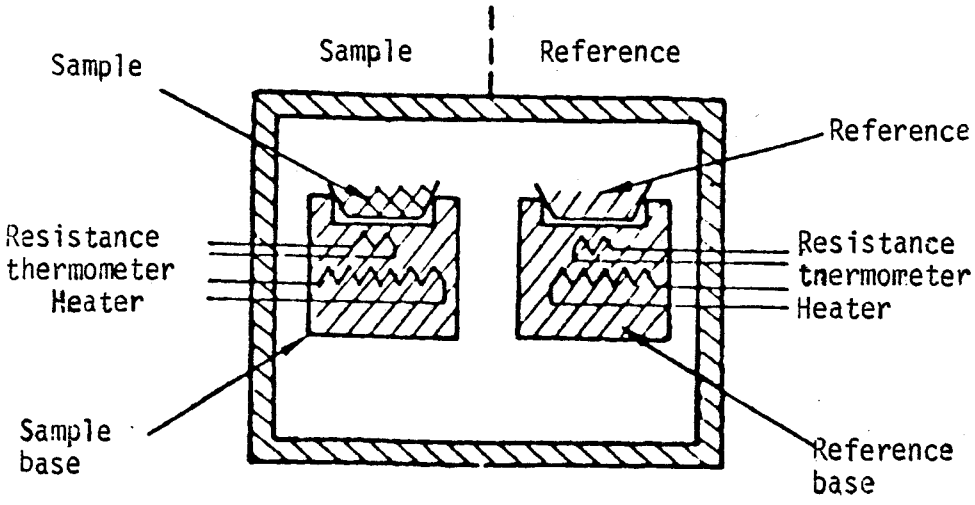

(a)

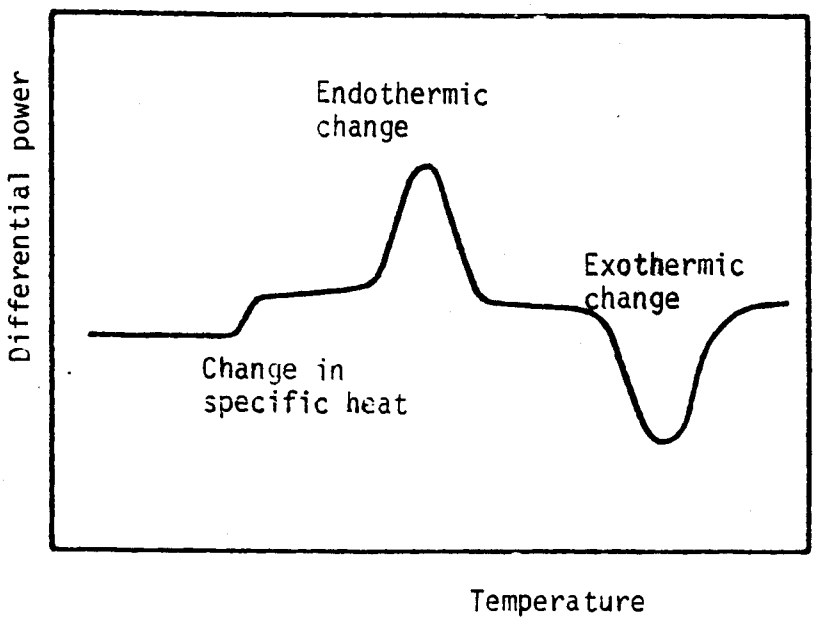

(b)

Fig. 3.1 (a) DSC Experimental arrangement[17]. (b) Typical curve[17].

of the factors which can affect DSC measurements are given below[3]:

(a) Furnace atmosphere
(b) Speed and response of recording instrument.
(c) Particle size.
(d) Packing density.
(e) Amount of sample.
(f) Degree of crystallinity.

3.3 THERMOMECHANICAL ANALYSIS (TMA)

Using this thermomechanical analysis[17](TMA) technique mechanical deformations of the material, e.g. expansion or contraction of material, as a function of programmed temperature can be determined. The amount of deformation is usually monitored when stress, which is normally non-oscillatory, is applied to the sample, so that deformation under a permanent load is measured. As in the case of DSC, TMA instruments are also commercially available. The principles behind these measurements are the same in all the commercial instruments. Fig. 3.2 illustrates a typical TMA apparatus. A probe is connected to the core of Linear Variable Differential Transformer (LVDT). The core is in turn coupled to the sample by a quartz tube containing a thermocouple for measuring the sample temperature. The movement of the sample is transformed into an electrical signal, by the LVDT, which is directly proportional to the displacement of the probe, and hence to the deformation of the sample. Expansion or contraction of the sample is indicated by the sign of the transformed electrical signal. The apparatus shown in Fig. 3.2 can operate from liquid nitrogen temperature to 850°C[17]. A weight tray which is

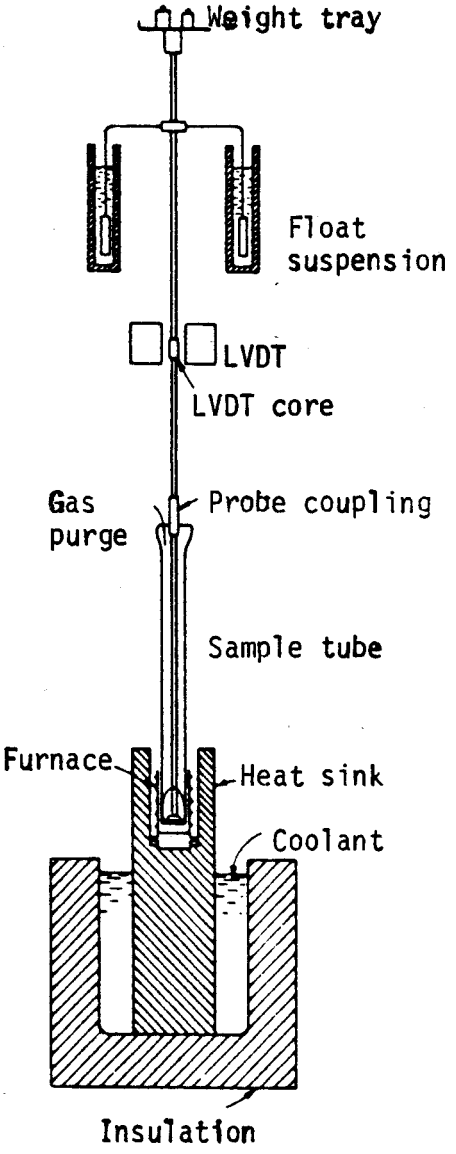

Fig. 3.2 TMA experimental arrangement[17].

attached to the upper end of the probe allows predetermined force to be applied. A small tip diameter probe[17] and loaded weight tray are used when sensitive detection of the softening temperature (e.g. glass transition temperature, T_g) of the material is required. For determining the coefficients of expansion larger tip diameters and zero loading are used. Samples as thick as 1-1.5[17]cm can be analyzed by TMA.

3.4 THERMOMICROHARDNESS (TμH)

Hardness as defined by the American Society of Metals "is the measure of the resistance of a material to indentation by an indenter of fixed geometry, under a static load." There are various schools of thought regarding the definition of the term *microhardness*. For example Buckle's[18] definition of *microhardness* is "Indentations with lowest possible loads upto a maximum of 200 gm". In contrast Lysaght's[18] definition for the same term is "Tests performed with loads of under 1000 grams". Thus the term "microhardness testing" is generally accepted as implying the measurement of hardness at low loads, but the precise range of loading considered varies with different workers.

The most commonly used indenter for microhardness testing is the Vickers 136° diamond pyramid. Other indenters, e.g. steel balls, are also used, particulary in the U.S.A. Hardness numbers are used to express hardness, measured by different techniques, for example Vickers hardness number (VHN), Knoop hardness number (KHN). Vickers hardness test involves using a

diamond indenter to press against the material at a constant load of F kgf. This diamond indenter has the shape of a square pyramid with an apex angle of 136° as shown in Fig 3.3(a). After a fixed loading the pyramidal indenter is removed and the diagonals d_1 and d_2 of the indentation are measured. VHN is load per unit surface area of impression. VHN (kg/mm^2), is given by[19]

$$VHN = 1.854 \frac{F}{d_{av}^2} \qquad (3.1),$$

where

d_{av} = Average diagonal in mm,

F = Constant load.

In thermo-microhardness measurements, the hardness number (or its log) is plotted against temperature, in order to determine the various structural transformations in the material under test.

Fig. 3.3(b) illustrates a TμHA instrument designed by Kasap and Yannacopoulos[19]for TμH analysis. Buehler micromet II microhardness tester operates a diamond indenter for Vickers indentations on the test sample under the selected load for a selected duration. The sample is mounted on to an aluminum plate by means of thermal high conductivity paste. The heater in the aluminum plate is connected to an autotransformer, which as seen is controlled by a Labmate data acquisition system and a computer, through a relay. The temperature of the sample is sensed by attaching a thermocouple to its surface

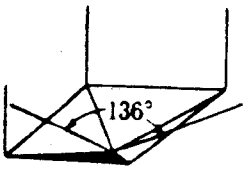

(a)

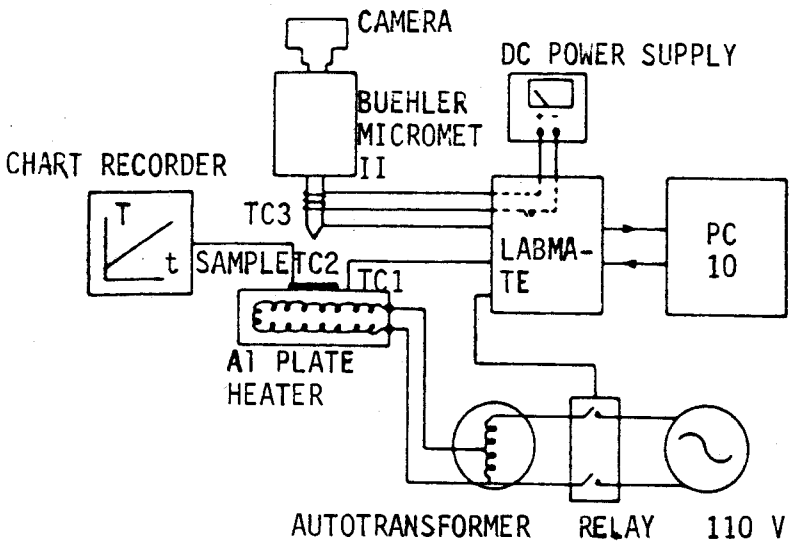

(b)

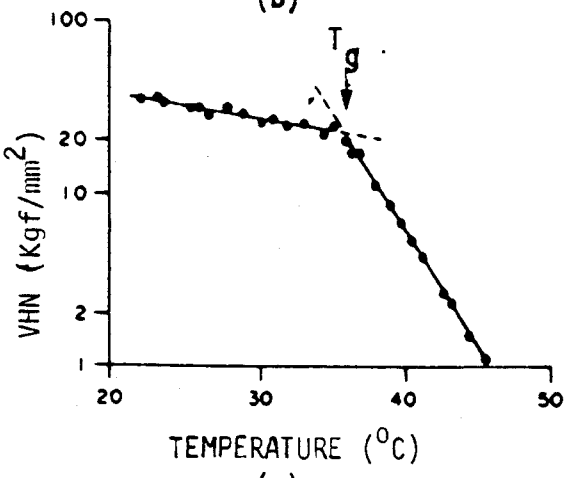

(c)

Fig. 3.3 (a) The Vickers pyramidal indenter. (b) Schematic diagram of the TμHA system. (c) Log VHN vs. temperature plot for amorphous $Se_{.997}As_{.003}$, for a heating rate of 0.05°C/min[19].

and this temperature appears on the chart recorder. Each VHN measurement is marked on the chart corresponding to the temperature.

In order to avoid the cooling effect of the indenter tip, its temperature is maintained close to that of the sample by the data acquisition system in conjunction with the relay and power supply. The hardness measurements on this instrument can be carried out for heating rates from .02°C/min to a maximum of 3°C/min. However, the heating rate is maintained constant over a VHN versus temperature measurement. A typical plot of VHN versus temperature is depicted in Fig. 3.3(c). From the graph it can be seen that there is a point of inflection at temperature T_g which corresponds to the phase transformation called *the glass transition temperature.* In general, for microhardness the Ito-Shishokin[20] relation given below is applicable

$$H = A\, e^{-BT} \qquad (3.2),$$

where

A = Intrinsic hardness constant,

B = coefficient of thermal softening[19].

Some of the sources of errors which can affect TμH measurements are listed below[20]:

(a) Rate of application of the load.
(b) *Chisel tip* of the indenter which is inherent in the design of both Vickers as well as Knoop indenters.
(c) Resolution of the microscope.
(d) Contrast at the edge of impression.

It must be emphasised that the tensile strength of many materials is related to hardness of the material. Thus, TμHA, effectively monitors the changes in the tensile strength as the material is heated.

3.5 THERMOACOUSTIC ANALYSIS (TAA)

This is a relatively new technique of thermal analysis compared to those described above. Two parameters may be measured as a function of temperature. a) Relative changes in ultrasonic wave velocity or absolute velocity changes, in the sample under analysis. b) Attenuation of the ultrasonic waves within the sample. From the measurement of both or either of these two parameters, different physical properties of the sample can be studied. These include phase transformations, the strength of material, rate of relaxation, types and concentration of defects, behaviour of a bond between two materials, welds, and changes in the concentration of constituents in the alloy. An important inherent advantage of this technique is that the physical properties of the sample can be measured by non-destructive means.

TAA technique can also be used isothermally. Kittinger[21] used this technique at room temperature to determine the rate of relaxation in vitreous selenium at different storage temperatures (T_g value of vitreous selenium is 30°C). He subjected samples of amorphous selenium prepared from a given batch to different storage temperatures. The results obtained by Kittinger shows changes in sound velocity at different

storage temperatures as illustrated in Fig. 3.4. The changes in the sound velocity are due to the process of structural relaxation which is highly temperature dependent.

Lakshmikumar et al.[22] used the TAA technique to determine precisely the longitudinal and shear velocities near the glass transition temperature in amorphous $Se_{80}Te_{20}$ and $Se_{90}Te_{10}$ (T_g ~60°C). They prepared cylindrical samples of diameter 6-8 mm and of thickness 10-15 mm, and analysed the samples by using McSkimins[14] pulse superposition technique. They employed ultrasonic waves at 10 MHz with the sample subjected to an average heating rate of 5 to 6 K/hr. The TAA cell used by them, and the variation of longitudinal and shear velocity in these alloys with temperature are shown in Fig. 3.5 and Fig. 3.6 respectively. It is observed that both the velocities decrease abruptly around 333 K (60°C) where there is a glass transformation in the material.

Kartha et al.[23] measured the variation of sound velocity in $Se_{90}Ge_{10}$ (T_g ~87°C) and $Se_{85}Ge_{15}$ (T_g ~102°C) with temperature also by employing Mcskimins[14] pulse superposition technique. A graph of longitudinal and shear velocities versus temperature in both the samples is shown in Fig. 3.7 where it can be seen that there is an abrupt change in velocity around the glass transition temperatures of the two samples.

Similar measurements were also carried out by Kostial et al.[24] on amorphous Se-Te alloys, who found the glass transition temperature of the alloy to depend on the Te concentration.

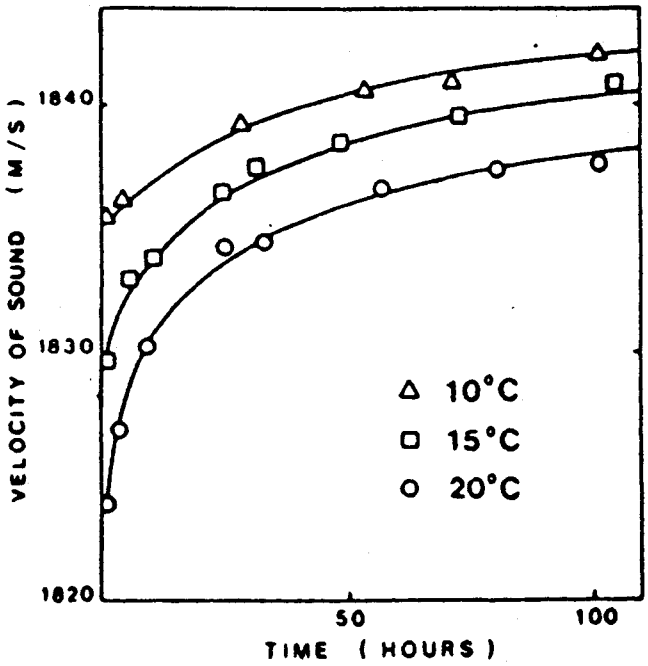

Fig. 3.4 Time dependence of ultrasonic wave velocity in vitreous Se during storage at different temperatures[21].

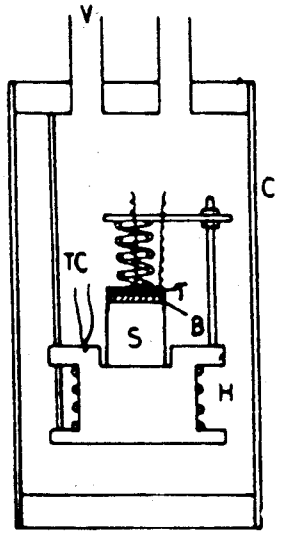

Fig. 3.5 TAA cell. T: transducer; S: sample; H: heater, B: bond; TC: thermocouple; C: calorimeter; V: vacuum connection[22].

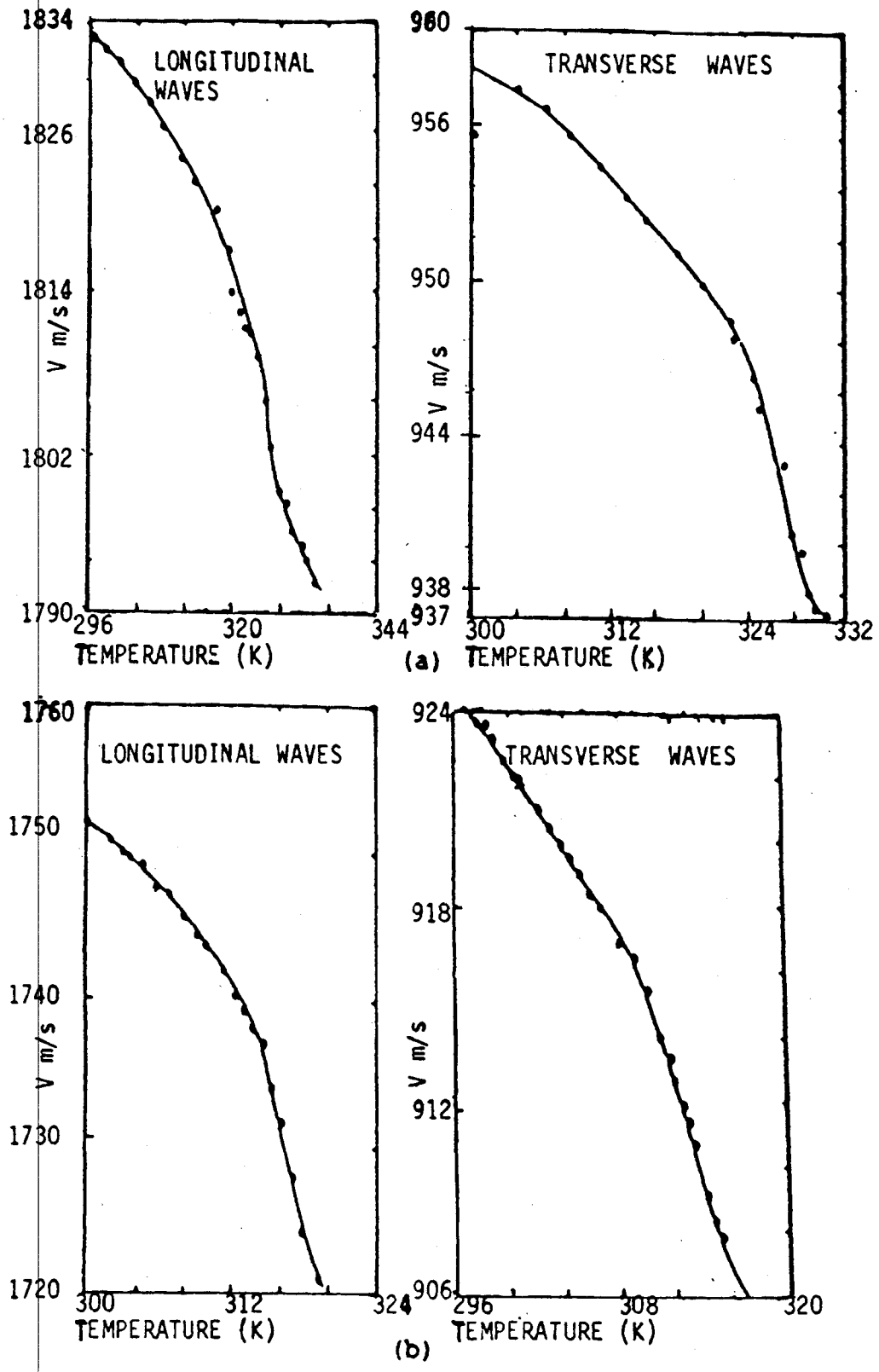

Fig. 3.6 (a) Longitudinal and transverse wave velocities in $Se_{80}Te_{20}$ near the glass transition. (b) Longitudinal and transverse wave velocities in $Se_{90}Te_{10}$ near the glass transition temperature[22].

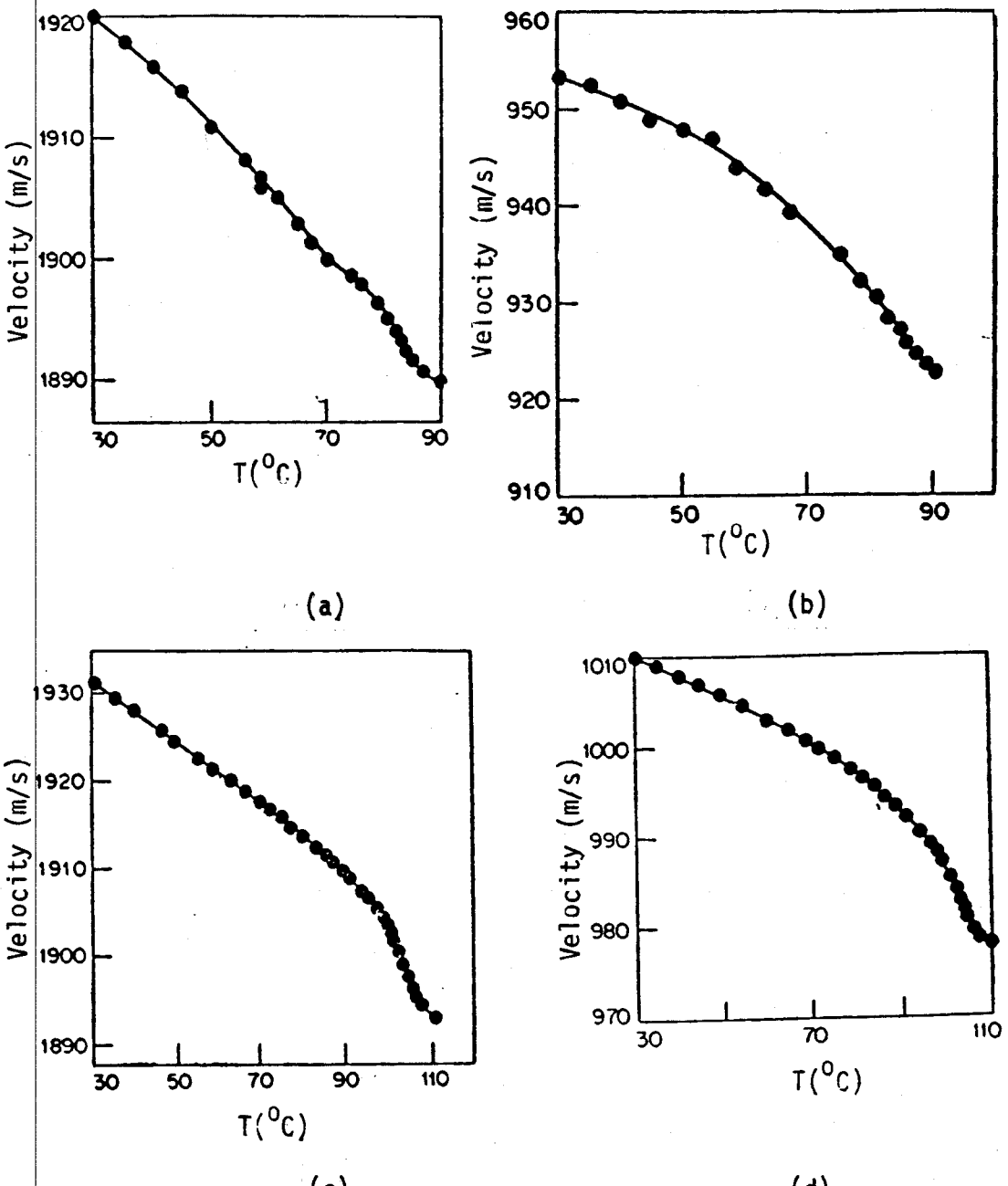

Fig. 3.7 (a) & (b) Longitudinal and transverse wave velocities in $Ge_{10}Se_{90}$ respectively near glass transition temperature. (c) & (d) Longitudinal and transverse wave velocities in $Ge_{85}Se_{15}$ respectively, near glass transition temperature[23].

They subjected the cylindrical samples to a 1 K/min temperature ramping rate. The fundamental frequency of the Lithium Niobate transducer which they used was 3.5 MHz. The results obtained by Kostial et al. are in agreement with Kasap's[25]DSC experiments. There are two transitions obtained one is independent of Te (tellurium) concentration and the other increases with an increase in Te concentration. The second transition is the glass transition temperature T_g of the alloy[24]. Similar experiments by Carini et al.[26] on Se-Te alloys show a disagreement in that Tg is observed to decrease with an increase in Te concentration. It would be interesting to carry out further studies on the amorphous $Se_{1-x}Te_x$ system to clarify the experimental disagreement.

Robinette[27]has investigated the influence of thermal treatment on amorphous As_2Se_3 (36.4 atomic % As) alloy. He subjected the samples from the same batch to different cooling rates immediately after their preparation. Some were allowed to cool rapidly by air convection and others were allowed to equilibrate at 160°C in an oil bath for several hours. The samples in oil bath were then cooled at different rates i.e. 10, 30, 50, 100 hrs. to room temperature. The velocities were measured by the pulse echo overlap technique[15]on 1 cm thick samples. Robinette found that there was a significant increase in sound velocity in samples with slower cooling due to bulk densification. For the fastest cooled sample (~ 1 hour) bulk densification continued at room temperature for several

months. Another aspect of his investigation was the thermal cycling effect. He found that rapidly cooled samples completely relax with subsequent slow cooling. Whereas, slow cooled samples when subjected to subsequent rapid cooling have some influence of their previously more relaxed state. Thus the time-temperature history, specifically cooling from T_g to room temperature, can have an effect on the physical properties of amorphous glasses such as As_2Se_3.

Changes in the ultrasonic velocity and absorption with stress have already been studied by a number of researchers. For example, using their self designed instrument, Ordu et al.[28] measured relative changes in the ultrasonic velocity and attenuation in 99.999% pure aluminum subjected to cyclic stress. The stress cycles are numbered from 1-10 in Fig. 3.8. They observed an increase in attenuation $\Delta\alpha$ and a decrease in the normalised sound velocity $\Delta V/V$ at low stresses, which is shown in Fig. 3.8. However, at higher stresses a second range of variation takes place due to the onset of plastic strain. Similarly Nagata et al.[29]have used acoustic measurements to study the high pressure phase in polyethylene.

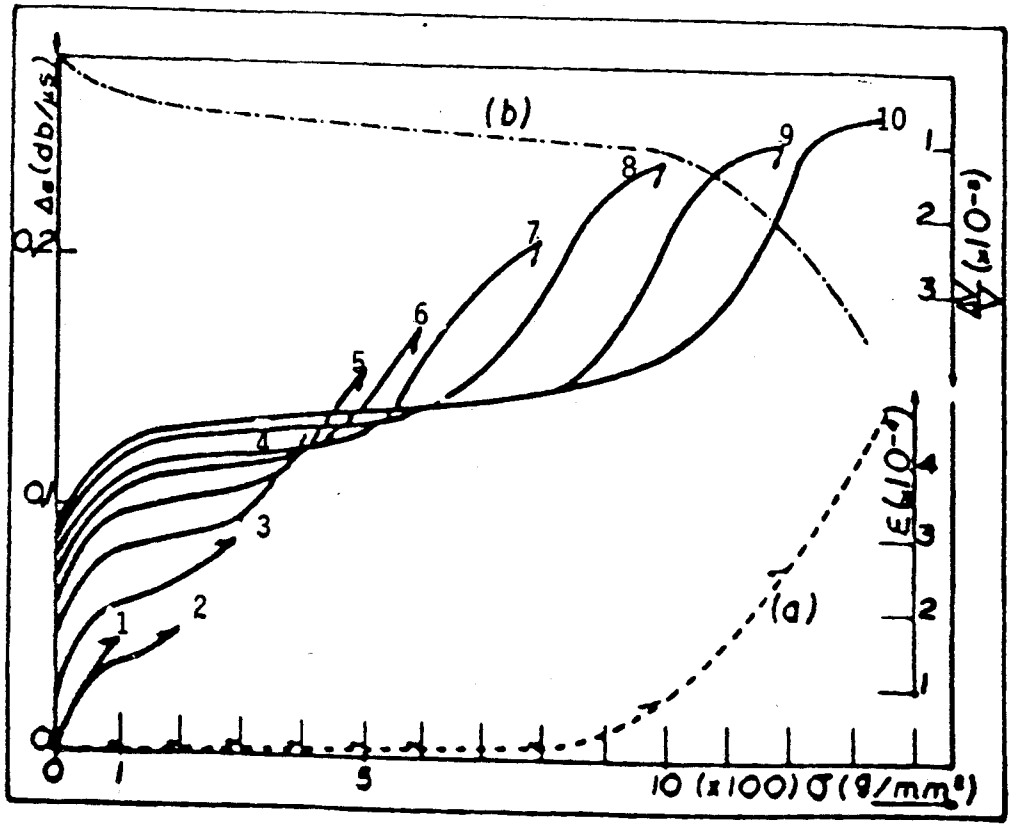

Fig. 3.8 Curves 1-10 show the variation of attenuation versus the applied cyclic stress. Variation of velocity is represented only in case of cycle 10^{28}.

3.6 CONCLUSION

Although Differential Scanning Calorimetry (DSC) and Thermomechanical analysis are well established thermal analysis techniques with a number of commercial instruments available to carry out the experiments, there is nonetheless a need to explore the use of ultrasonic techniques for thermal analysis. Only a few authors[21-24,26,27] have recently attempted to use ultrasonic measurements in thermal analysis of materials. For example, using TAA, the glass transformation phenomenon has been studied in a-$Se_{1-x}Te_x$ alloys. In all cases[21-24,26-34] the TAA instrument was designed adhoc and quite often without a well defined temperature-time profile. Furthermore, the transducers were bonded directly to the sample and the instrument could not accept a variety of specimens which can be readily changed. It is clear that there is therefore a need to develop a convenient TAA apparatus.

4. EXPERIMENTAL PROCEDURE

4.1 INTRODUCTION

The purpose of the TAA apparatus designed and implemented in this thesis is to measure relative velocity changes of longitudinal ultrasonic waves, ΔV, and relative attenuation $\Delta\alpha$ as a function of temperature in a wide variety of engineering materials. The details of the design and construction of the TAA apparatus and the experimental procedure used for carrying out the acoustic experiments are described in this Chapter. Many workers[21-24,26-28,30-33] have coupled the acoustic transducer directly to the sample and the sample has often been heated along an undefined temperature-time profile[22-24,26]. One of the most important requirements for TAA is a well defined heating rate so that the ultrasonic data obtained from the experiments can be sensibly analysed by the current thermo-analytical methods.

The TAA apparatus in the present work was implemented from commercially available components and with some workshop machining. The loading of the sample for the ultrasonic measurements was kept as convenient as possible to allow a variety of samples to be readily studied.

4.2 GENERAL SYSTEM DESCRIPTION & METHOD

A block diagram of the complete TAA system and a photograph of the experimental set-up are shown in Figs. 4.1 and 4.2 respectively. Two X-cut quartz transducers for

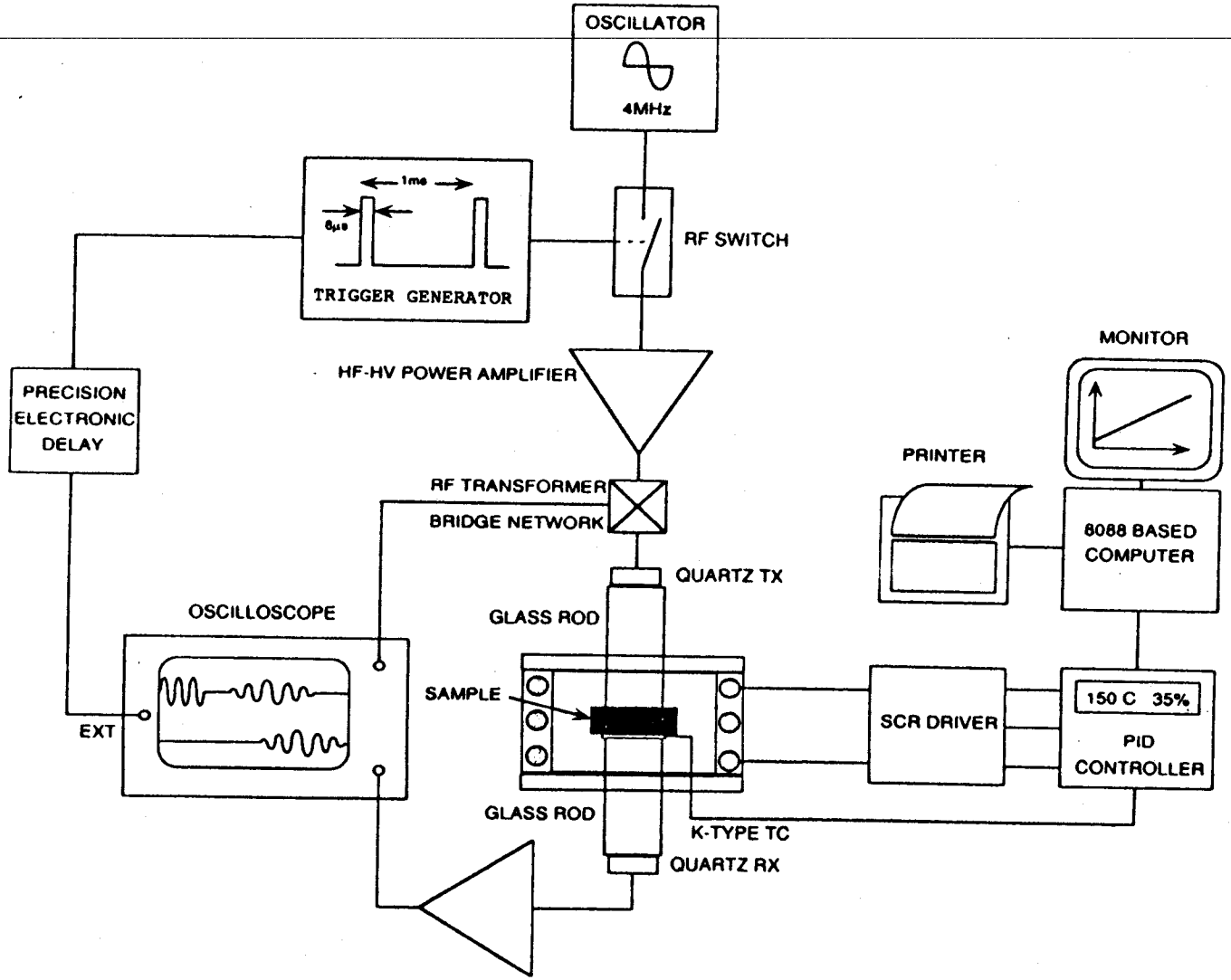

Fig. 4.1 Block diagram of TAA apparatus.

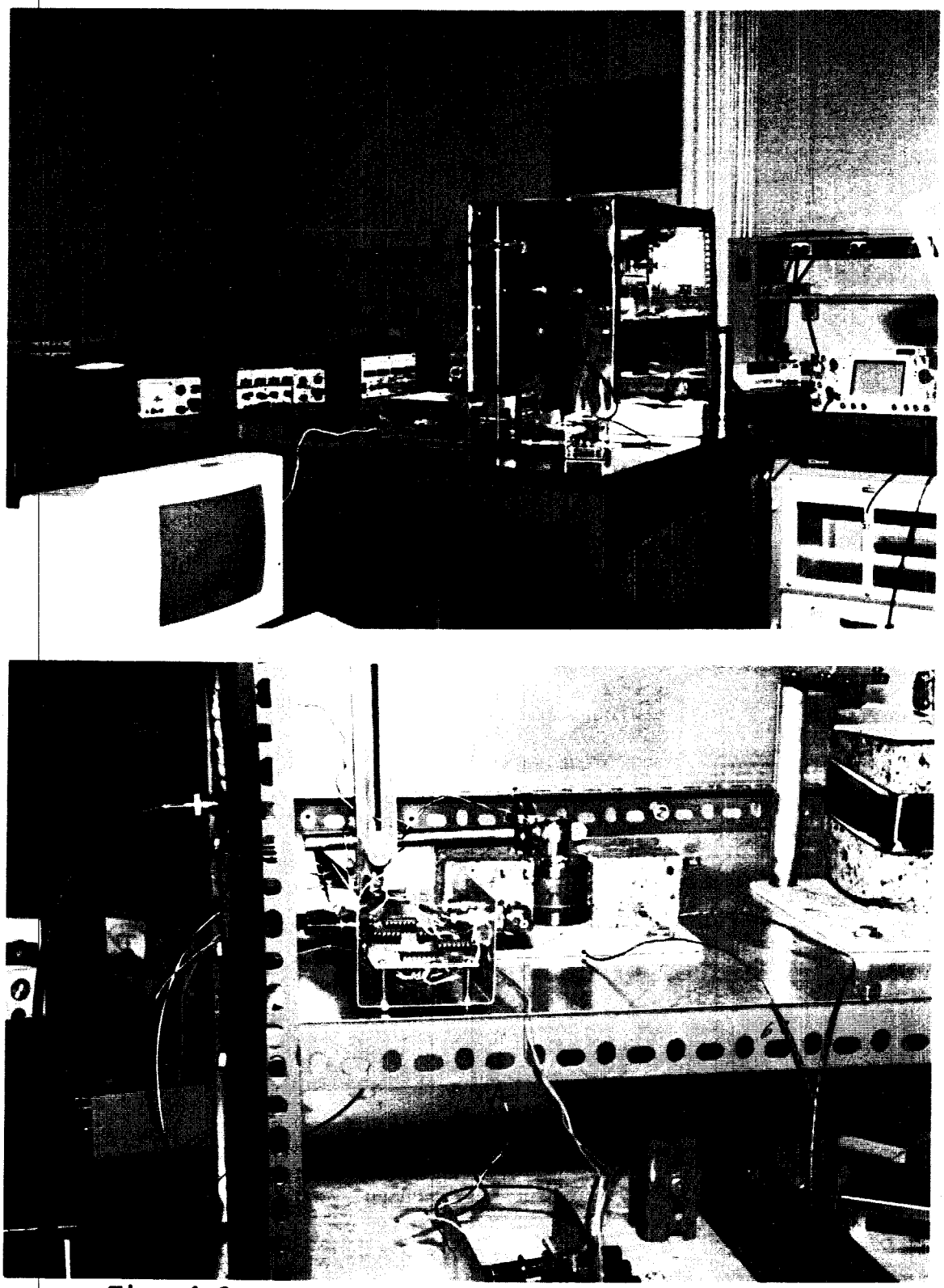

Fig. 4.2 Photograph of Experimental setup.

producing and detecting longitudinal ultrasonic waves were attached onto two pyrex glass buffer rods using a thin layer of adhesive. Both the pulse echo and the sing-around techniques (Section 2.6.1 & 2.6.2) were employed in order to increase accuracy and reliability of the measurements. The pulse echo technique was implemented by an RF bridge circuit which keeps the transmitting and the receiving channels isolated. Accordingly, one of the transducers works as a transmitter (generator) as well as a receiver of ultrasonic waves, whereas the other transducer functions only as the receiver of ultrasonic waves.

It can be seen in Fig. 4.1 that the sample under study is sandwiched between the two glass buffer rods in the TAA cell. Fig. 4.3 gives a schematic sketch of the TAA cell which is placed on a 1/4" thick asbestos sheet of dimensions 6" X 6". Two buffer rods made of pyrex glass and of dimensions 1.90 cm in diameter and 4.00 cm in length were used to sandwich the sample and to pass the waves through the sample. The upper rod was used to couple the waves into the sample and the lower rod was used to couple the waves from the sample to the receiving transducer. The upper buffer rod could be moved vertically upwards or downwards by a mechanical clamp-sliding arrangement whereas the lower buffer rod was fixed. An aluminum ring with a small notch and a miniature tightening screw was attached around the lower buffer rod at the sample end. A K-type thermocouple junction head was firmly fixed inside the notch

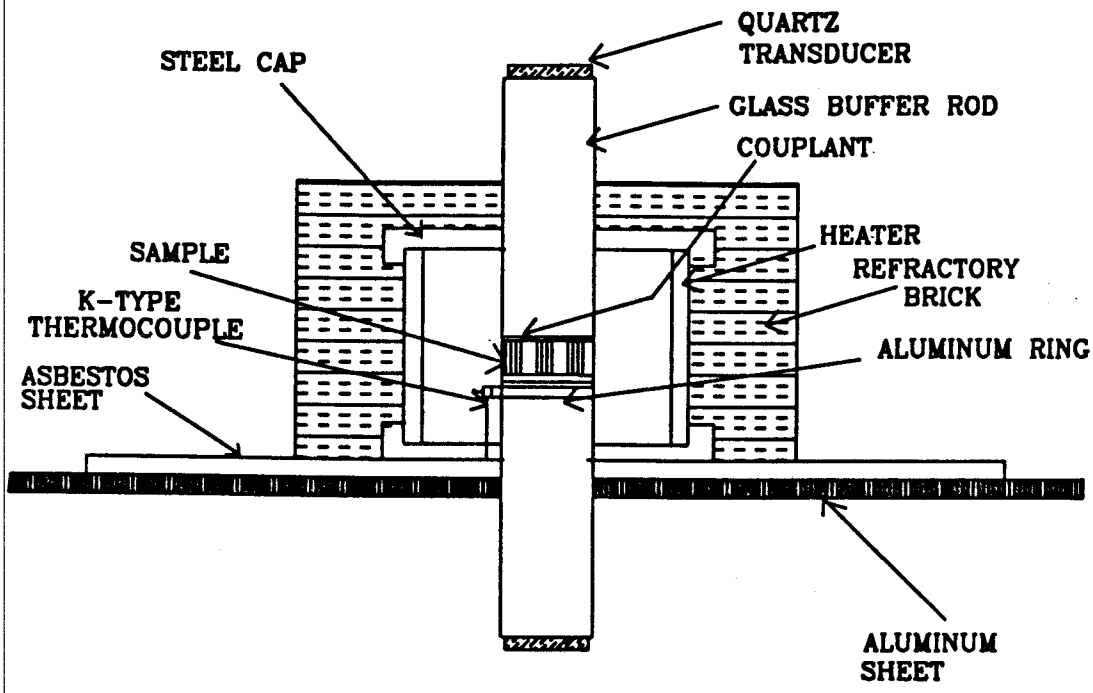

Fig 4.3 TAA cell

by means of a miniature screw. Two thin aluminum foils circular in shape and having the same diameter as the buffer rods were placed at the sample ends of the buffer rods by a special high temperature grease.

The sample to be studied is required to have parallel surfaces and be preferably cylindrical in shape with a thickness in the range of 1.5 mm to 8 mm. Thickness of the samples was measured by a thickness measurement system manufactured by Sylvac Measuring systems, Switzerland. The thickness was measured at 6-7 different points on the sample and the average value of the thickness was obtained. Maximum accuracy of the thickness measuring system as given by the manufacturer is around 0.1 μm.

The sample, after being smeared with a thin layer of grease (Slick 50), was placed onto the aluminum foil attached to the lower buffer rod. The purpose of the aluminum foil is to establish a reasonably uniform temperature across the contact surfaces of the sample and the glass buffer. A number of control runs with thermocouples attached to the sample and ring on various samples like aluminum, polymers, glassy alloy showed that the thermocouple attached to the aluminum ring sensed the sample temperature to within 1°C. The sample temperature in the TAA apparatus was read by a PID temperature controller by means of the K-type thermocouple fixed in the aluminum ring around the lower buffer rod. The sample placed on the lower buffer rod was then surrounded by an electrical

heater. The latter was cylindrical in shape and had the dimensions of 1.25" in diameter and 1.25" in height. This heater basically forms the TAA cell, which is shown in Fig. 4.3. The upper buffer rod was then lowered and placed on the sample. The sample was thus sandwiched between the upper and lower buffer rods with the heater surrounding the sample and part of the buffer rods. The heater was covered at its ends by machined aluminum plates to allow only buffer rods to pass through into the TAA cell. The entire TAA cell was then surrounded by appropriately shaped refractory bricks for thermal insulation and adiabatic heating of the sample. The TAA cell could be operated at a maximum heating rate of 10°C/min. The TAA cell and parts of the electronic circuitry were housed in a grounded aluminum box which was divided into two sections so as to separate the transmitting and the receiving transducers as shown in Fig. 4.2. This also prevented to a large extent the RF pick-up and interference in the detector section.

The PID temperature controller allowed accurate temperature ramping and soaking options. It was necessary to carry out a careful tuning of the PID controller to the TAA cell heater by carrying out several runs on dummy samples. The heater was powered by the temperature controller through a Triac interface unit. This temperature controller was interfaced to an IBM computer by an RS 232 interface. The desired heating rate could be entered through the computer and

the temperature profile of the sample could be monitored in real time along with the desired temperature profile. After the heating process was over, a hard copy could thus be obtained.

The electronic circuitry for the acoustic velocity and attenuation measurements basically generated and detected the ultrasonic waves. The transmitter part of the electronic circuitry produced RF pulses of 165 Vp-p amplitude, 4 MHz frequency, 6 μs pulse width, at a pulse repetition rate of 1 kHz. These high voltage RF pulses excited the transmitting X-cut quartz transducer to generate longitudinal ultrasonic waves. The generated ultrasonic waves then traversed through the buffer rods with the sample sandwiched between them and were finally detected by a receiving transducer to produce RF voltage signals which were amplified and displayed on a Cathode Ray Oscilloscope (CRO).

During the transit of the ultrasonic wave, a part of it gets reflected at the interface between the sample and the upper buffer rod (due to mismatch in acoustic impedance) and is received by the transmitting transducer. The echo signal is obtained after a time corresponding to the transit through twice the upper buffer rod length. This signal was then fed directly to the CRO. On the other hand, the signal received by the receiving transducer corresponds to the transit time of the ultrasonic waves through the upper and lower buffer rods and the sample. Thus by observing both the signals on the CRO,

the time difference between the two signals could be determined. This time difference corresponds to the transit time of the ultrasonic waves through the sample alone provided that the buffer rods are of equal length. By knowing the thickness of the sample, the absolute velocity through the sample could be readily determined.

The relative changes of the ultrasonic transit time with temperature of the sample were determined by taking as a time reference the zero crossing of the beginning of a cycle of the echo signal at the transmitting end. The time changes (δt) of the zero crossing of the beginning of a cycle of the received signal at the receiving transducer with respect to the above reference gives the change in acoustic transit time. Thus by measuring this time δt on the CRO at different temperatures with the sample heated at a controlled rate, the relative changes of ultrasonic transit time through the sample could be readily obtained. This data was then used to obtain normalised velocity; normalised with respect to the velocity through the sample at room temperature. The attenuation of the ultrasonic waves through the sample with temperature at a particular heating rate was obtained by measuring the received amplitude (Vp-p) of the RF voltage signal on CRO in the storage mode. The reference Vp-p was taken at room temperature. The resolution of the apparatus for measuring relative changes in transit time was improved by using a delayed triggering technique to trigger the CRO externally. The delayed trigger

was produced by using the trigger generator (Fig. 4.1) or RF pulse to trigger a precision electronic delay comprised of Pulse Generator PG 58 (Advance Instruments) in the external trigger mode. The delay of the pulse produced by the pulse generator was set so as to get resolution of 10 ns in measuring changes of transit time. The resolution for measuring the signal amplitude was about 1 mV.

The working of the apparatus at room temperature was verified by measuring the velocity of longitudinal ultrasonic waves through the two pyrex glass buffer rods coupled to each other by a thin layer of Slick 50 grease. The measured transit time of the ultrasonic waves through the coupled pyrex buffer rods was 14.64 μs. With the length of the combined buffer rods being 8.00 cm, the velocity of longitudinal ultrasonic waves obtained was 5.46×10^3 m/sec. The value of longitudinal ultrasonic waves in pyrex glass obtained from the literature[13] is 5.57×10^3 m/sec, the discrepancy is thus around 2 %.

The whole experimental system shown in Figs. 4.1 and 4.2 can be considered as an integration of three major subsystems.

1) Electronic instrumentation subsystem.
2) Thermal subsystem.
3) Mechanical subsystem.

4.3 ELECTRONIC SUBSYSTEM

The main purpose of the electronic subsystem is the generation and detection of ultrasonic waves which requires the use of acoustic transducers as discussed in Section 2.4.

Transducer design and techniques for coupling of the transducer to the sample under study are important parts of the electronic subsystem. Another important constituent of the electronic subsystem is the design and implementation of the circuits for excitation of the transducer to generate longitudinal ultrasonic waves and to detect these waves after transit through the sample.

4.3.1 TRANSDUCER DESIGN

Transducer design involves determining the type of transducer, transducer material, and the various parameters associated with the transducer; viz. diameter, resonant frequency (f_r), type of crystal cut, geometry and material of electrodes, and material for contact leads.

As TAA had to be performed on small samples of diameter around 2 cm, it was necessary to use high frequency excitations and small diameter transducers. Thus electromagnetic, electrostatic, magnetostrictive, thermal and mechanical type transducers described in Appendix A were not feasible and only piezoelectric and ferroelectric type of transducers could be used.

Since the sample undergoing TAA was to be subjected to temperatures as high as 250-275°C, the use of a transducer which could withstand high temperatures was essential. Though ferroelectric transducers; viz. Barium titanate have a high efficiency of 20 % to 50 % (Table 2.1) most of them lose their piezoelectric properties around 70°C[1]. In contrast, quartz can

withstand temperature as high as 573°C[1] without losing its piezoelectric properties, but has a lower efficiency of about 11 % (Table 2.1). As quartz satisfied most of the present requirements, X-cut quartz crystal was selected as a transducer to generate and detect the longitudinal ultrasonic waves.

A circular crystal geometry was used because, circular crystals are less vulnerable to breakage due to absence of sharp corners and also they radiate more strongly than do square crystals[4].

The choice of resonant frequency (f_r) of the transducer was based on the diverse nature of the materials which would have to undergo TAA. At high frequencies, the wavelength of the ultrasonic wave becomes comparable to the microscopic defects in the material hence more attenuation of the ultrasonic wave will take place. Other practical disadvantage is that quartz crystals having high resonant frequency are very thin and hence vulnerable to damage. The thickness of crystal is given by $2t=\lambda$, where t is the thickness and λ the wavelength of longitudinal ultrasonic wave generated[4]. Too low a frequency would result in a large diameter transducer, hence large samples. The increased size of the samples would result in a non uniform heating of the sample at a high heating rate. Thus 4 MHz was chosen as a compromise value for the frequency of the X-cut quartz crystal.

The diameter of crystal was based on the average diameter of the sample for TAA that would be available and also on the diameter of X-cut quartz crystals of resonant frequency 4 Mhz made available by the manufacturer (VALPEY-FISHER, MA. U.S.A.). Thus transducers of diameter 0.5 inch were chosen.

X-cut quartz crystals having coaxial type of electrodes made of vacuum deposited gold, and copper wires as leads for contacts, were found to be suitable as transducers. In the coaxial type of electrode configuration, electrical accessibility is provided to both the surfaces through leads on one side of crystal only; both the leads emerge from one surface of the transducer. The leads are soldered to the gold plated electrodes. Fig 4.4 illustrates a quartz crystal with coaxial type of electrodes.

The X-cut quartz crystals obtained from the manufacturer with the above mentioned specifications were flat to within .00002", parallel to within .00005" and the diameter tolerance was +/- .001".

4.3.2 BUFFER ROD TECHNIQUE

The simplest technique used to transmit longitudinal ultrasonic waves through a material, is to bond the transducers directly on to the material by means of bonding agents such as transformer oil, grease, epoxy resin, cements, and organic compounds such as glycerin, glycerol[2,4] etc.

However, in the case of TAA, the material under test may be subjected to temperatures as high as 250-275°C. As the

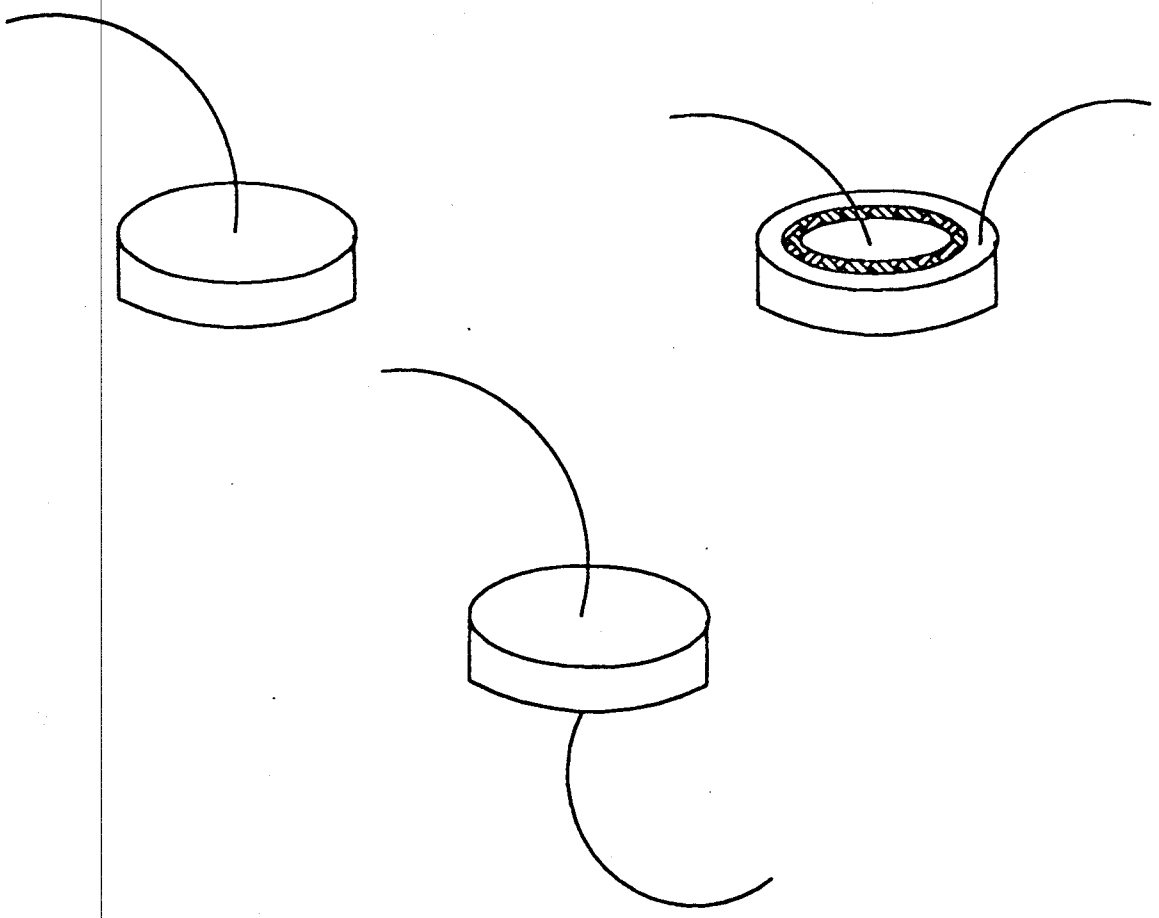

Fig. 4.4 Conventional patterns of quartz transducer (left to right): Solid electrode with centered lead, Solid electrode with one lead on each side, Co-axial electrode.

leads of the transducer were soldered, such high temperature could melt the solder contact. Furthermore, as the TAA apparatus was to be used time and again on a variety of samples, which could be easily mounted, it became apparent that the buffer rod technique was the most convenient method.

Two buffer rods each 4.00 cm in length and 1.90 cm in diameter made of pyrex glass were used to sandwich the sample. The transmitting and the receiving transducers were each bonded by an adhesive to one end of the buffer rods. The sample undergoing TAA is sandwiched between the two buffer rods. Pyrex glass buffer rods have been used because:

(a) pyrex can readily withstand temperatures as high as 500°C.
(b) it has very low attenuation to the longitudinal ultrasonic waves
(c) it is a good thermal insulator, hence the transducers are subjected to much lower temperature than the sample.

The dimensions of the buffer rods were chosen approximately as close as possible to satisfy the acoustic dispersion relation for a frequency of 4 MHz (Equation 2.3).

4.3.3 COUPLING AGENTS

Coupling of longitudinal ultrasonic waves between different media is important from the point of view of attenuation due to change in acoustic impedance. The coupling may be looked upon as a transformer which matches the acoustic impedances of the crystal (transducer) to that of the work. An ideal coupling agent should satisfy the following relationship[2]

$$Z_C = \sqrt{Z_{m1}\, Z_{m2}} \qquad (4.1),$$

where

Z_C = the acoustic impedance of the couplant,

Z_{m1}, Z_{m2} = the acoustic impedances of the two media in contact with the couplant viz. transducer and the other transmission medium.

Two of the experimental parameters which affect the nature of a bond are frequency and temperature[36]. High frequency waves require thin bonds, and the stresses caused by thermal expansion should be minimal.

Experiments were performed with the sample sandwiched between the buffer rods and subjected to the maximum heater temperature of 400°C. The temperature at the places on the two buffer rods where the transducers were to be adhered was then monitored. Maximum temperature at these places was found to be around 80°C. This required the adhesive to be stable at 80°C. Extensive experiments were performed on a number of adhesives such as Superbonder 430 applied with Speedbonder Quickset 404, Cermabond 503, and Speedbonder 312 applied with Primer NF for quicksetting. Finally, Speedbonder 312 adhesive applied with Primer NF was found to be the most stable and efficient couplant amongst the adhesives studied.

Similarly a coupling agent was required to couple the sample to the buffer rods in order to provide low acoustic impedance to the longitudinal ultrasonic waves. After

extensive market search, a high temperature coupling agent Slick 50 grease was found. It could be used to temperatures as high as 250°C.

4.4 ELECTRONICS DESIGN SPECIFICATIONS

As mentioned earlier the basic aim of the electronics design was to generate and, after transit through the sample under study, detect the longitudinal ultrasonic waves. This required the excitation of the transducer by means of high voltage RF pulses. Thus the important specifications relevant in the design of the electronics were related to the following parameters:

(a) RF pulse Voltage amplitude.
(b) RF frequency.
(c) RF pulse width.
(d) RF pulse repetition.

The RF pulse amplitude determines the extent of amplitude of vibration of the X-cut quartz transducer at its resonant frequency. The higher the pulse amplitude, Vp-p, greater is the vibration of transducer. This in turn determines the extent to which the longitudinal ultrasonic waves can transit through highly attenuating samples, greater path lengths, and still be detected.

From the available literature[35], it was apparent that RF pulse amplitude in the range 150-200 V needed to be used to obtain a detected signal which could be displayed on the oscilloscope.

The RF frequency required for excitation of the X-cut quartz crystal for generating longitudinal ultrasonic waves

must be equal to the resonant frequency of the crystal viz. 4 MHz. This would result in producing maximum amplitude of vibration of the quartz crystal at the exciting RF pulse voltage amplitude.

The specification pertaining to the pulse width was important in two ways. Too high a RF pulse width would affect the resolution in the determination of the transit time of the waves through the sample. The RF pulse width specification depends on the transit time of the longitudinal ultrasonic waves through the buffer rods and the sample. Too low RF pulse width results in less power available for excitation of the transducer thus resulting in less intensity of generated ultrasonic wave, which makes the detection by the receiving transducer difficult. To get an approximate estimate regarding the pulse width, the available data[13]on the longitudinal sound velocity in pyrex glass was taken into consideration. The transit time of ultrasonic waves thus obtained through the buffers was 14.36 μs. Thus a value of 6 μs was found to be a reasonable specification for the RF pulse width.

The specification regarding the pulse repetition rate was chosen after taking into consideration the ringing effect due to high Q of the quartz transducer which occurs when the crystal is set into vibration[13]. Too high a repetition rate would result in the superposition of received signals and hence would affect resolution of the acoustic transit time, whereas too low a repetition rate would result in an unstable

view of the received signal on the CRO. Thus after preliminary experimentation 1 ms was taken as a reasonable specification for the RF pulse repetition rate.

4.5 ELECTRONICS DESIGN & IMPLEMENTATION

The electronic instrumentation which was designed and implemented in order to meet the above mentioned specifications consisted of different modules. The modular design approach was followed because of the ease in the implementation and troubleshooting of the different circuits.

All the designed modules were implemented on single sided printed circuit boards (PCB's). The copper plane on these PCB's were used as a ground plane thus resulting in low capacitances and inductances. The leads of all the components used were kept as short as practically possible and bypass capacitors of 0.1 μF and 10 μF were used at the supply pins. All the discrete components used were kept as close as possible to the pins of the Integrated circuits used to minimize interference.

The different modules which have been designed and implemented are described below.

4.5.1 RF OSCILLATOR

The RF oscillator produced the RF sinusoidal waves to excite the transducer. Keeping in view that the oscillator would be required in future to excite the transducer at different harmonic frequencies or different crystals with different resonant frequencies, prompted the use of variable

frequency type oscillator. The circuit diagram and schematic are depicted in Fig. 4.5. The integrated circuit MC 1648P was chosen, as it is the only one of its kind which can generate a wide range of frequency oscillations upto a maximum of 225 MHz. In contrast, other VCO (Voltage controlled oscillator) chips such as LM556, XR2207 have a maximum frequency range of 1 MHz. Another major advantage of MC 1648P is the small variation in output frequency because of internal noise (20 Hz at 4 MHz). The MC1468P is basically a VCO which requires an external tank circuit consisting of an inductor and a capacitor. It also requires a + 5 V/-5 V d.c. power supply. The voltage swing of the tank circuit provides drive for the output buffer and the AGC (Automatic Gain Control) potential directly affects the output waveform. The manufacturer suggests inductor value in the range of μH in the tank circuit for a frequency of few MHz. Thus an external inductor of 15 μH and a variable capacitor (Trimmer) of ~ 10 - 150 pF were used in the external tank circuit. Using this combination, a frequency variation from ~ 1 MHz to 12 MHz could be readily obtained. The output waveform from the oscillator circuit at a frequency of 4 MHz is shown in Fig. 4.5(c). Adjustments to the output level of the oscillator signal could be made by an external 10 KΩ potentiometer connected between pin 5 of the IC and the ground.

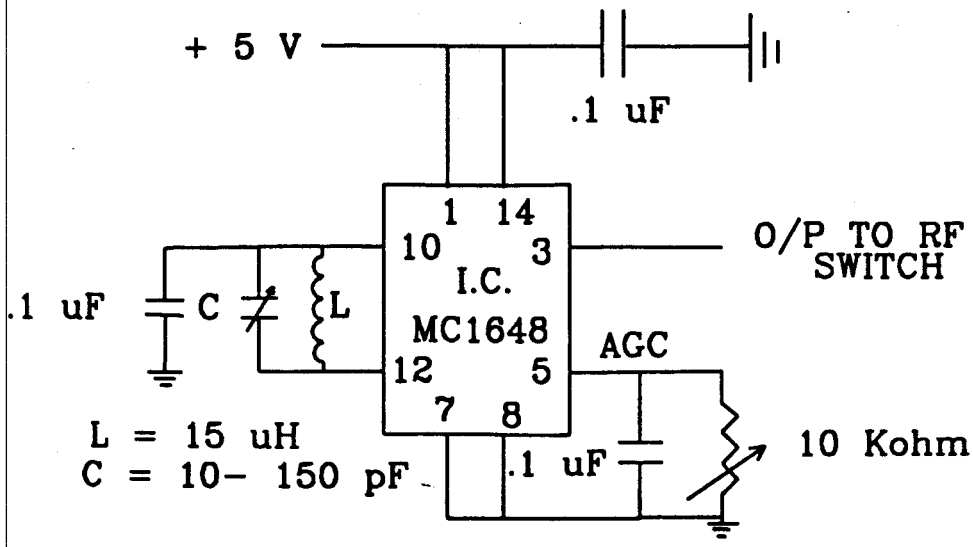

(a)

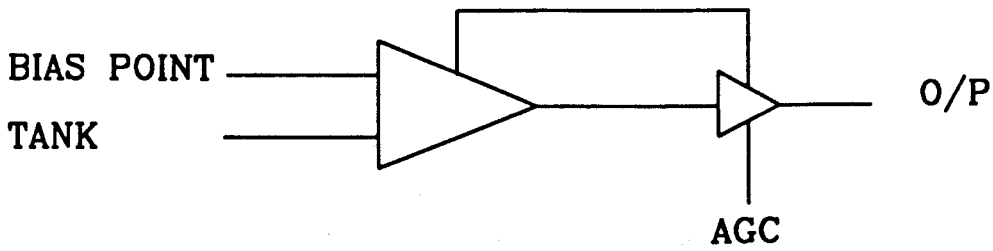

(b)

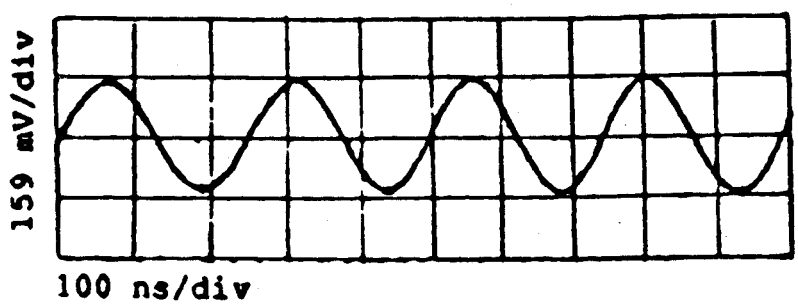

(c)

Fig. 4.5 (a) RF oscillator circuit schematic. (b) RF oscillator functional diagram. (c) Display of o/p waveform of RF oscillator.

4.5.2 RF /VIDEO SWITCH

The main purpose of the RF/Video switch IC IH5341 was to chop the continuous RF wave produced by the oscillator IC MC1648P, to produce RF pulses. Thus the output of the oscillator was fed to this switch. Some of the salient features of this switch are:

(a) On resistance < 75 Ω from dc to 100 MHz.
(b) Off isolation > 60 dB @ 10 MHz.
(c) Directly compatible with CMOS/TTL
(d) Wide operating power supply range.
(e) Break before make switching
(f) Fast switching (80 ns/150 ns typ.)

The circuit diagram of this module and the functional diagram of the switch are shown in Fig. 4.6. IH 5341 uses a series/shunt (T switch) configuration to obtain high OFF isolation while maintaining good frequency response in the ON position.

The switch is turned ON by applying TTL high pulse to the control pin. The ON and OFF time of the switch is governed by the duration of the high and low logic levels in a rectangular wave. The duration of the ON time basically decides the RF pulse width which, as described earlier, was required to be around 6 μs. The period of the rectangular wave determines the repetition period of the RF pulses.

In order to turn the switch ON and OFF, and vary the duration of the ON time, an IC MC1455 timer in the astable mode of operation was used. External resistors and capacitors were chosen so as to produce a rectangular wave of 1 ms period. In order to decrease the duty cycle of the rectangular

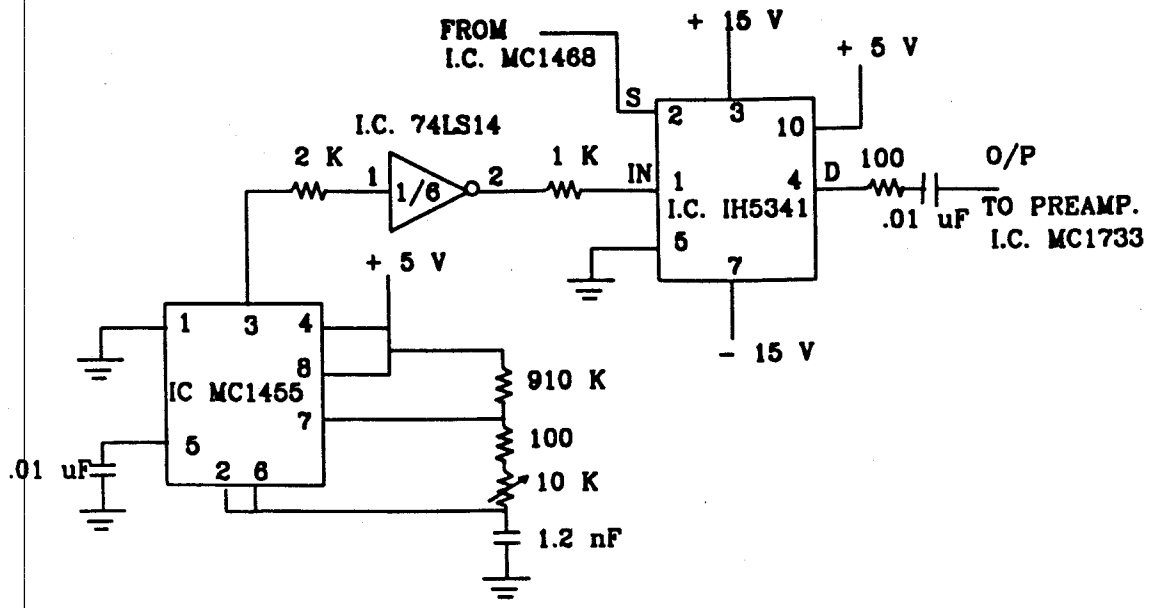

(a)

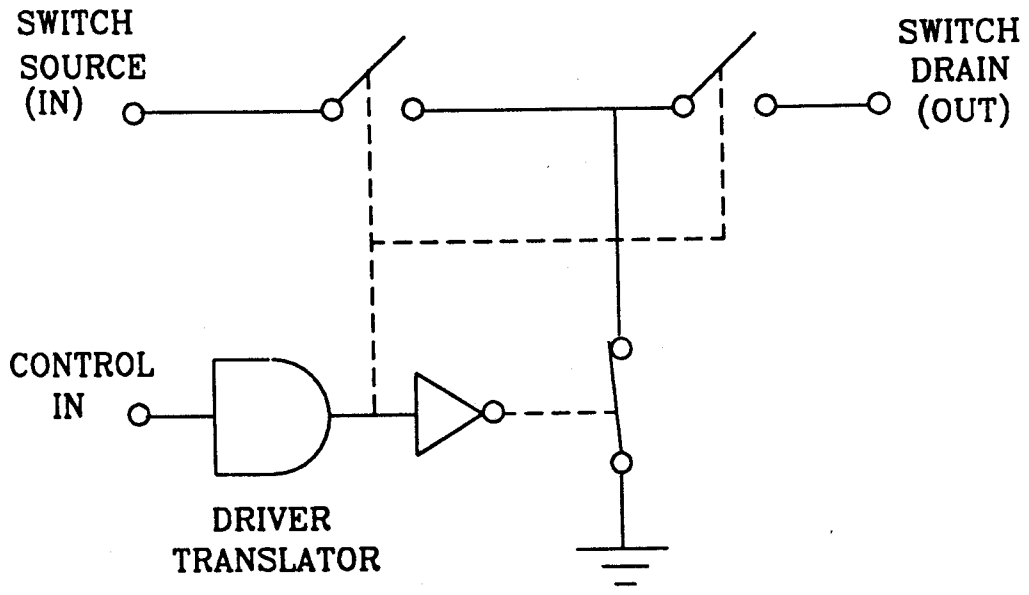

(b)

Fig. 4.6 (a) Circuit schematic of RF switching. (b) RF video switch functional diagram.

wave, the output of IC MC1455 was inverted by a Schmitt trigger hex inverter IC 74LS14. This produced an output TTL high comparable to 6 μs which could be adjusted by the 10 KΩ potentiometer. The two components, IC MC1455 and IC 74LS14, thus form a trigger generator to switch ON and OFF the RF switch at desired times.

4.5.3 RF PREAMPLIFIER

The output of the RF Switch had an amplitude of around 0.3 Vp-p which is about a factor of 500 smaller than a typical voltage required to drive the transducer. A preamplifier IC MC1733 Fig. 4.7(a) was used to amplify the RF oscillations to a level suitable for driving a power amplifier. MC 1733 is a wideband differential amplifier IC having a bandwidth of 120 MHz at a gain of 10. Another major advantage of MC 1733 was that the gain could be fixed at 10, 100, 400 or made user adjustable. This preamplifier was used in the variable gain setting to obtain the desired output voltage to drive the power amplifier.

4.5.4 RF BUFFER

The data sheets of the MC1733 Differential video amplifier indicate that it can supply a maximum current of 4 mA at the operating supply voltage of +/- 6.5 V. This current could not drive an RF amplifier with a low input impedance of around 50 Ω. Therefore, an RF buffer LH 0033 was used as the next modular stage after the Preamplifier. Fig. 4.7(b) shows the circuit diagram of the buffer.

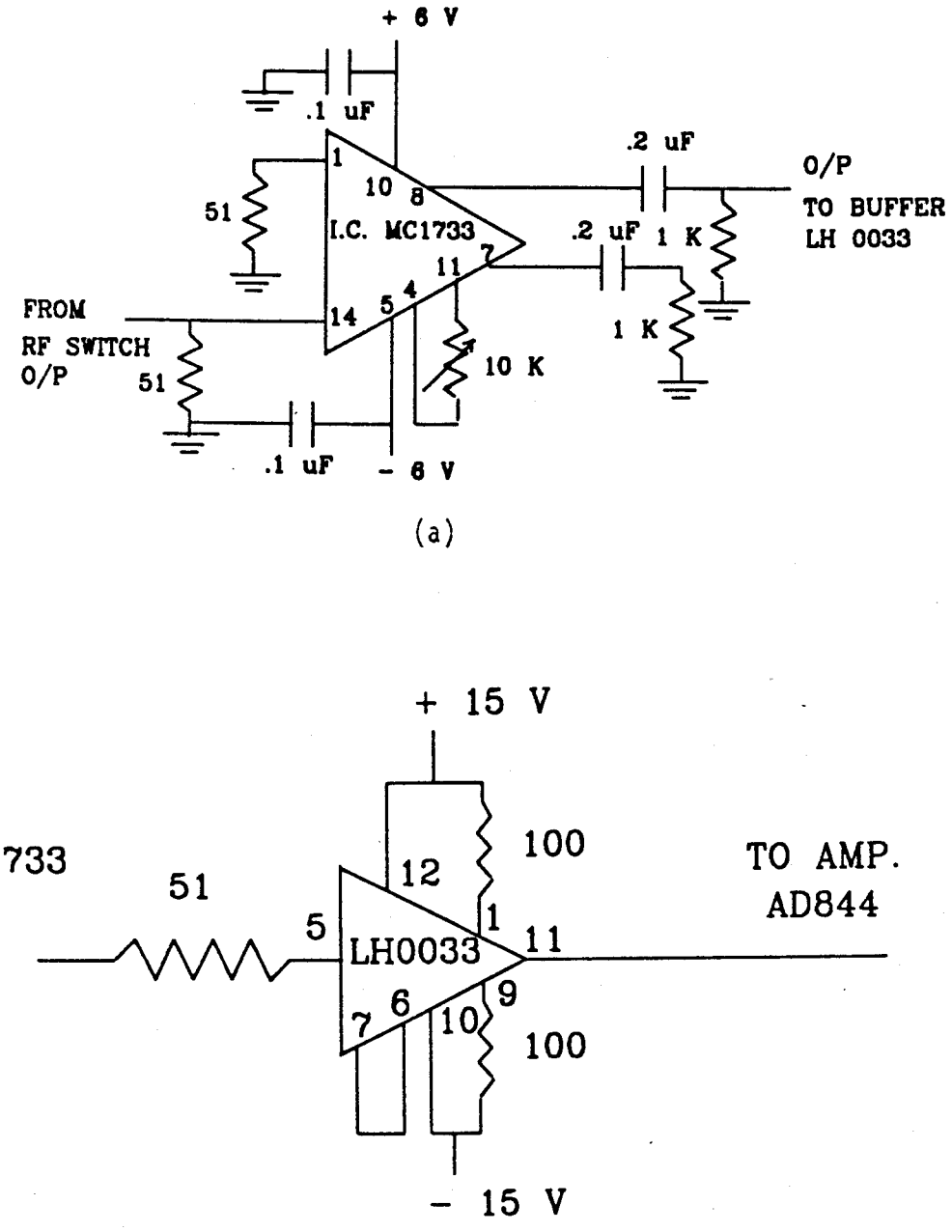

Fig. 4.7 (a) Preamplifier module circuit schematic. (b) Buffer module circuit schematic.

The LH 0033 Buffer is a high speed FET input buffer designed to provide high current drive at frequencies from dc to over 100 MHz. LH 0033 can source or sink a current of 100 mA peak with a 1 KΩ load at a slew rate of 1500 V/μs. Some other salient features of this buffer are:

(a) Wide range single or dual supply operation.
(b) Low phase non linearities.
(c) Fast rise time 2 ns.
(d) High input impedance $10^{12}\Omega$.

4.5.5 RF AMPLIFIER AD 844

The purpose of this amplifier was to amplify the RF pulses received from the buffer LH 0033. The salient features of this Integrated circuit (IC) are:

(a) Wide 60 Mhz Bandwidth at a gain of -1 and 33 Mhz. at a gain of -10
(b) Very high output slew rate; 2000 V/μs.
(c) High output drive +/- 50 mA into 50 ohms.
(d) Low distortion, low noise, and low drift.

Amplifier AD 844 has a current feedback architecture. It is optimised for use in current to voltage conversion applications and as an inverting amplifier. In the present case, as shown in Fig. 4.8, AD 844 was used in the inverting mode and was designed for a gain of 10. The values of R_1, R_2 were chosen after referring to the table for optimisation of the band width given by the manufacturer. RF pulses from the output of the LH033 buffer (Section 4.5.4) could be amplified to a maximum of 20 Vp-p amplitude at a frequency of 4 MHz.

4.5.6 RF POWER AMPLIFIER TP 1465

In order to further amplify the RF pulses an additional RF amplifier was necessary. Thus a special Teledyne-Philbrick

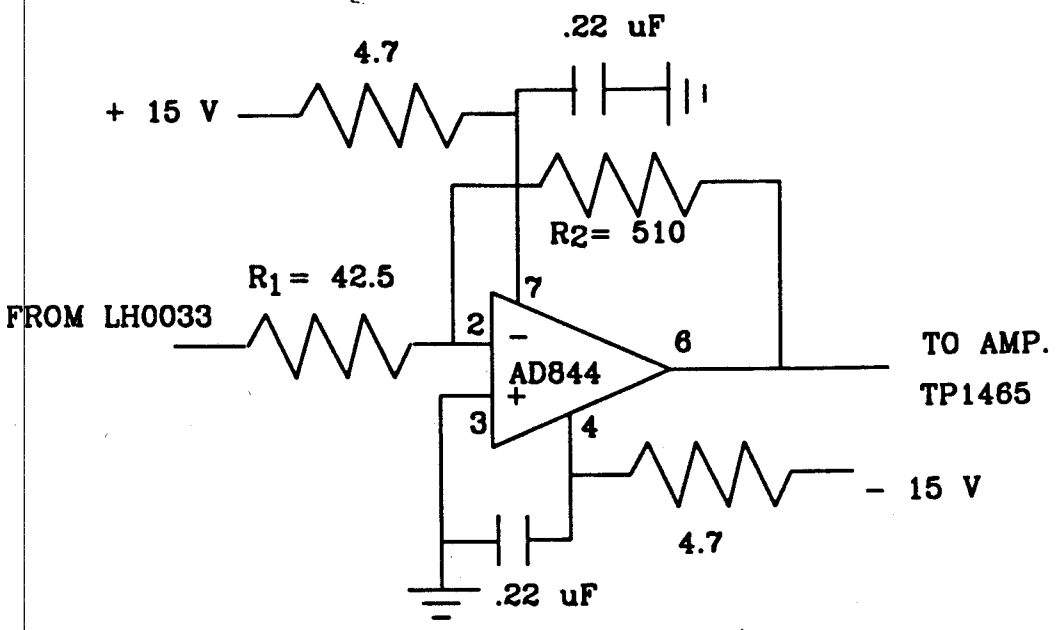

Fig. 4.8 Amplifier AD 844 module circuit schematic.

(TP 1465) wide bandwidth IC was used to obtain 50-60 Vp-p RF output. TP 1465 received RF pulses directly from the AD 844 amplifier described above. Fig. 4.9 shows the TP 1465 amplifier circuit. TP 1465 IC is an extremely fast, FET input, VMOS output power operational amplifier which can be operated from dual dc voltages ranging from +/- 15 V to +/- 40 V. It can provide output voltages and currents upto +/- 34 V, +/- 750 mA respectively. Furthermore, it has a Gain-Bandwidth product of 2.5 GHz and a slew rate of 1000 V/μs. It also has a thermal shutdown feature for protection against any destructive over heating.

The circuit was designed to provide a gain of 10 in the inverting mode by choosing R_1= 220 Ω and R_2= 2.2 KΩ. The output of the TP1465 amplifier was fed through 75 Ω resistor to a BNC connector. A shielded cable of 50 Ω characteristic impedance carried the RF pulses to the RF transformer placed inside the shielded aluminum cage of the TAA apparatus. The 75 Ω resistor protected the output of amplifer in case of shorting to ground. The amplifier amplified the RF pulses of 6-7 Vp-p fed from the amplifier AD844 to a maximum of 50-58 Vp-p. Input and output signals of IC TP1465 are shown in Fig. 4.9(b). The pulsed nature of signals is due to switching by RF switch IC IH5341.

4.5.7 RF TRANSFORMER

In order to deliver very high voltage for excitation of the quartz transducer, further boosting of voltage was

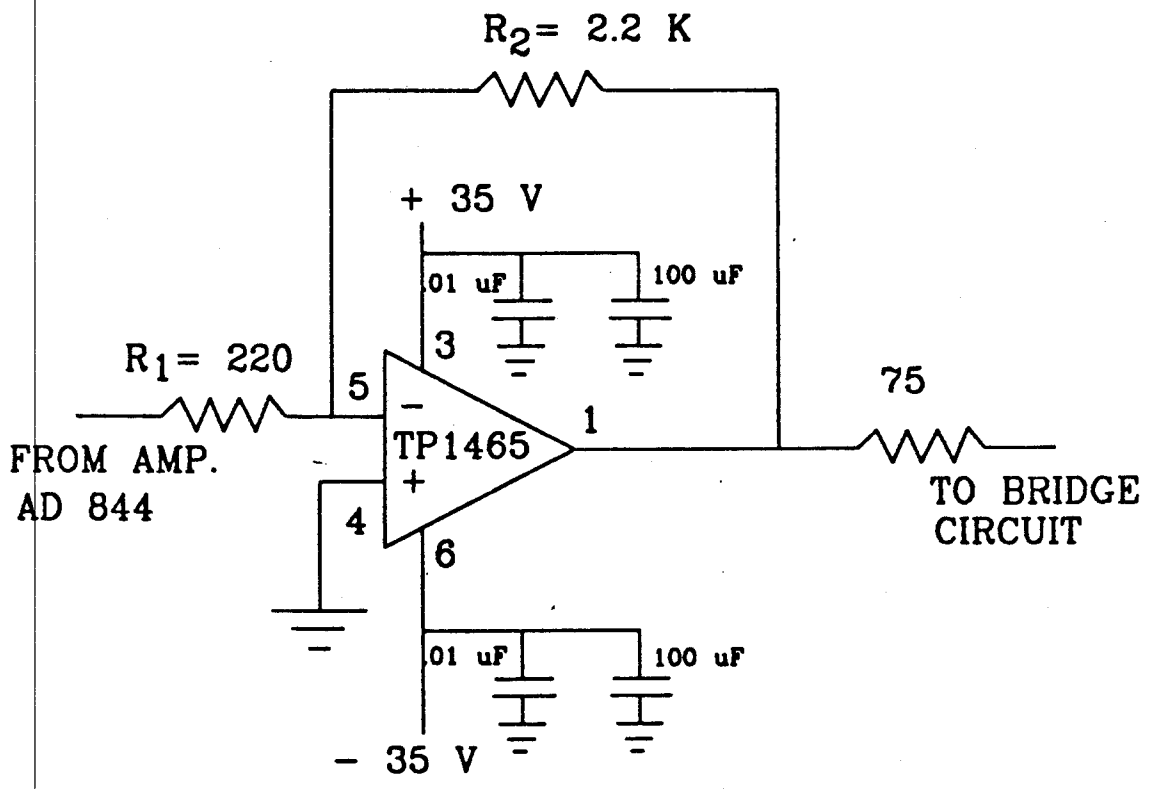

(a)

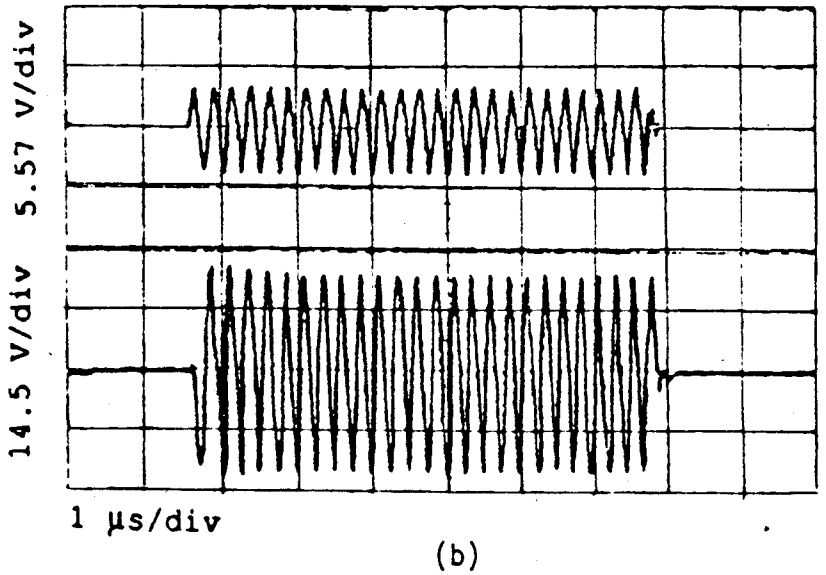

(b)

Fig. 4.9 (a) Amplifier TP1465 module circuit schematic.
(b) Input and output waveforms of TP1465.

necessary. Thus, boosting of TP 1465 power amplifier output voltage was carried out by a RF transformer having the necessary turns ratio.

The secondary turns winding acts as an inductor to "tune" out the inherent capacitance between the transducer electrodes as discussed in the equivalent circuit of the transducer (Section 2.5). Only part of the current supplied to a crystal transducer is used to maintain the vibrations, the remainder is short circuited through the capacitance C_o[1]. This is prevented by connecting a coil of inductance L_o across the crystal to tune out C_o. The value of L_o is chosen to satisfy equation given below

$$f_r = \frac{1}{2\pi\sqrt{L_o C_o}} \qquad (4.2),$$

where

f_r = the resonant frequency[4].

The RF transformer used was model No. TT25-1 (Mini circuits supplier). It has an impedance transformation ratio of 25:1, a continuous maximum power rating of 250 mW and could be used in the frequency range 20 KHz to 30 MHz. In contrast to RF transformers, the ordinary transformers have limited frequency response due to significant leakage inductance and stray capacitance of the windings.

4.5.8 TRANSDUCER BRIDGE CIRCUIT.

A bridge circuit depicted in Fig. 4.10 was designed primarily to use the same transducer as the transmitter of

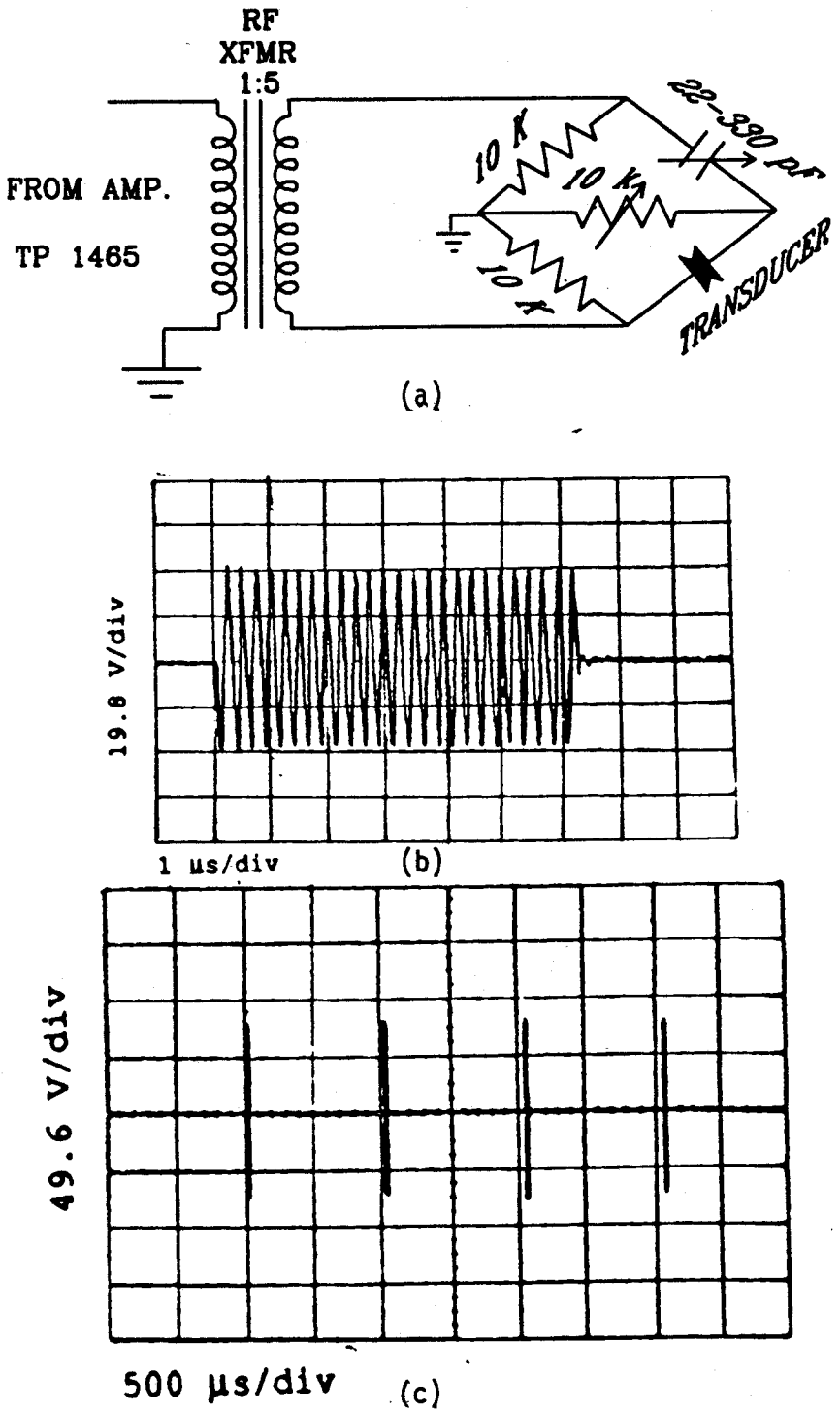

Fig. 4.10 (a) Bridge circuit module schematic. (b) Transducer excitation voltage. (c) Output (secondary) of RF transformer after being cascaded to the bridge circuit.

longitudinal ultrasonic waves as well as the receiver of the ultrasonic waves reflected at the interface of the buffer rod and the sample as discussed in Section 4.2. Thus the bridge circuit provided isolation between the transmitting and the receiving channels.

The bridge circuit received the RF pulses from the RF transformer with an X-cut quartz crystal transducer forming one arm of the bridge. Two arms of the bridge each have resistors of 10 KΩ which prevent loading of secondary output by the bridge. A variable capacitor 22-335 pF forms one arm of the bridge to balance out the crystal capacitance. A variable resistor 10 KΩ across the diagonal acts as a load for the received echo RF signal.

The bridge was carefully balanced by a variable capacitor until the received signal, as seen on the CRO, contained minimum voltage amplitude of the exciting RF pulse. This minimum was about 2 Vp-p. After balancing the bridge, an RF pulse voltage of 85-90 Vp-p amplitude excited the transducer. Fig. 4.10(b) illustrates this excitation voltage for the transducer. Fig. 4.10(c) illustrates the secondary output of the RF transformer after being cascaded with the bridge circuit. RF pulses of 6 μs duration, 165 Vp-p amplitude and a pulse repetition period of 1 ms can be seen in Fig. 4.10(c).

4.5.9 RF RECEIVER AMPLIFIER

The ultrasonic waves after their transit through the buffer rods and the sample were received by the receiving

transducer which was adhered on to the lower buffer rod. The RF signal thus generated by the receiving transducer was amplified so that it could be observed on the CRO for samples with different attenuation properties at different temperatures. The differential video amplifier IC MC 1733 was used as the RF receiver amplifier.

4.5.10 SYSTEM MONITOR

The signals received by both the transducers were monitored on a Digital Storage Oscilloscope Model No. 468 (Tektronix) in order to make transit time and attenuation measurements. Fig 4.11(a) illustrates the reflected RF signal obtained by the bridge circuit. Similarly, Fig. 4.11(b) depicts the transmitted RF signal. A very small RF pickup is seen at the beginning of both the signals. Time difference between the beginning of reflected and transmitted signal envelopes, is the actual transit time through the sample. The RF envelopes observed after the first echoes are due to the ultrasonic waves reflected to and fro in the buffer rods. The CRO was triggered externally to improve the resolution by a pulse generator PG 58 (Advance Instruments) in the external trigger mode. This pulse generator was in turn triggered by a trigger generator formed by RF/video switch module (4.5.2) or by RF pulse. The measurements were made as described earlier in Section 4.2.

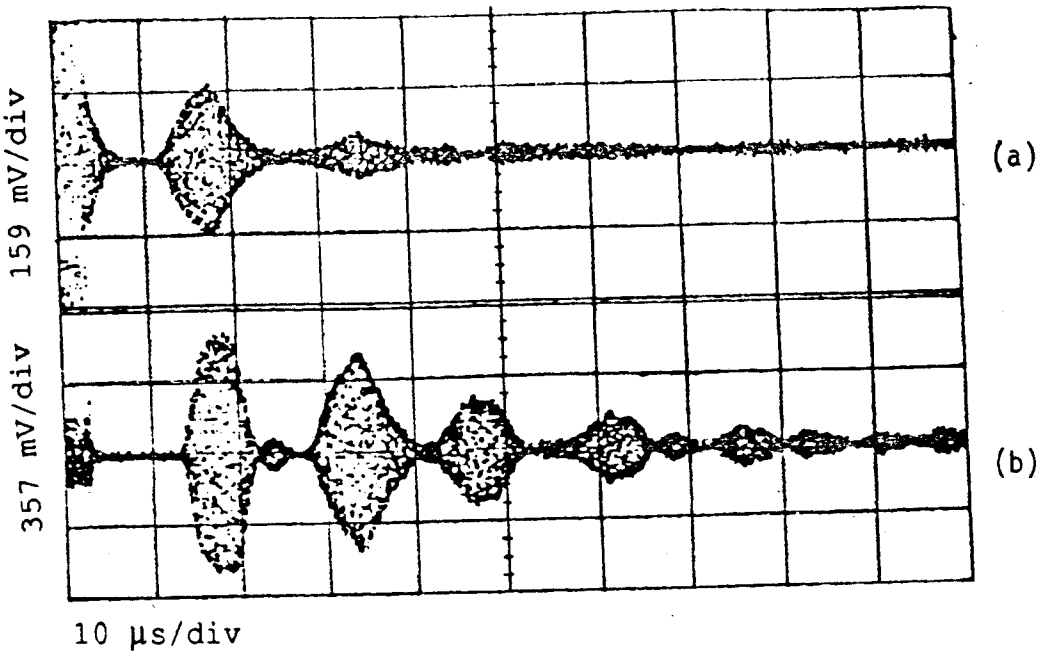

Fig. 4.11 (a) RF echo signal, received due to reflection at the sample-buffer interface. (b) RF transmitted signal, received after transit through the sample and the buffer rods.

4.6 THERMAL SUBSYSTEM

The prime purpose of this subsystem is to control the temperature of the sample accurately as determined by a user desired heating rate. This subsystem consists of a PID temperature controller, triac interface unit, and a TAA cell

A) PID TEMPERATURE CONTROLLER

The OMEGA CN-2010 Series Programmable Controller is a microprocessor based temperature controller. Input to this controller is a K-type Thermocouple, whereas the output is a controlled current through an external heater.

CN-2010 features ramp and soak functions. Upto eight temperature-time intervals can be programmed into the controller to hold the temperature constant or at a constant rate of change. Each of the temperature intervals can have a time duration of upto 100 hrs and upto 254 repeat cycles. It also has a digital communications option available to interface CN-2010 to a computer through an RS 232 interface. In the present apparatus the PID temperature controller was interfaced to an IBM computer through which the heating rate could be entered. Temperature profile of the sample in real time could be obtained and compared with the desired profile.

The following procedure, which is recommended by the manufacturer, was followed to tune the controller. As per the procedure, various parameters which control the tuning of the controller are first determined by making use of the heater without the controller. K-type thermocouples were attached to

the heater and the aluminum ring. The TAA cell, surrounded by refractory bricks, was powered directly from the ac (alternating current) mains through a variac. Ring temperature was noted from an Omega model 871A Digital thermometer every minute until the heater temperature reached 400°C. From the graph of ring temperature versus time for the above process, the time (T_d) it took for the temperature to reach a maximum slope and the maximum slope itself were found. This time T_d corresponds to the lumped system delay. From these two parameters the PID parameters were obtained.

The PID parameters thus obtained were then entered into the Controller. A number of dummy runs at a high heating rate of 10 °C/min were performed with the heater surrounded by insulation, and powered by the controller through a Triac interface unit. This was done to examine whether the temperature profile of the dummy material exhibited any temperature overshoot or oscillations. Fine tuning was done by changing the PID parameters one at a time and then observing the process response. Fine tuning and adjustment of PID parameters were carried out several times until the desired temperature profile and the obtained temperature profile were almost identical as shown in Fig. 4.12.

B) TRIAC POWER SWITCH INTERFACE UNIT

CN-2010 controller has a solid state relay as an output which can supply a maximum current of 1 Ampere, whereas it was observed that heater when powered from 120 V ac mains voltage

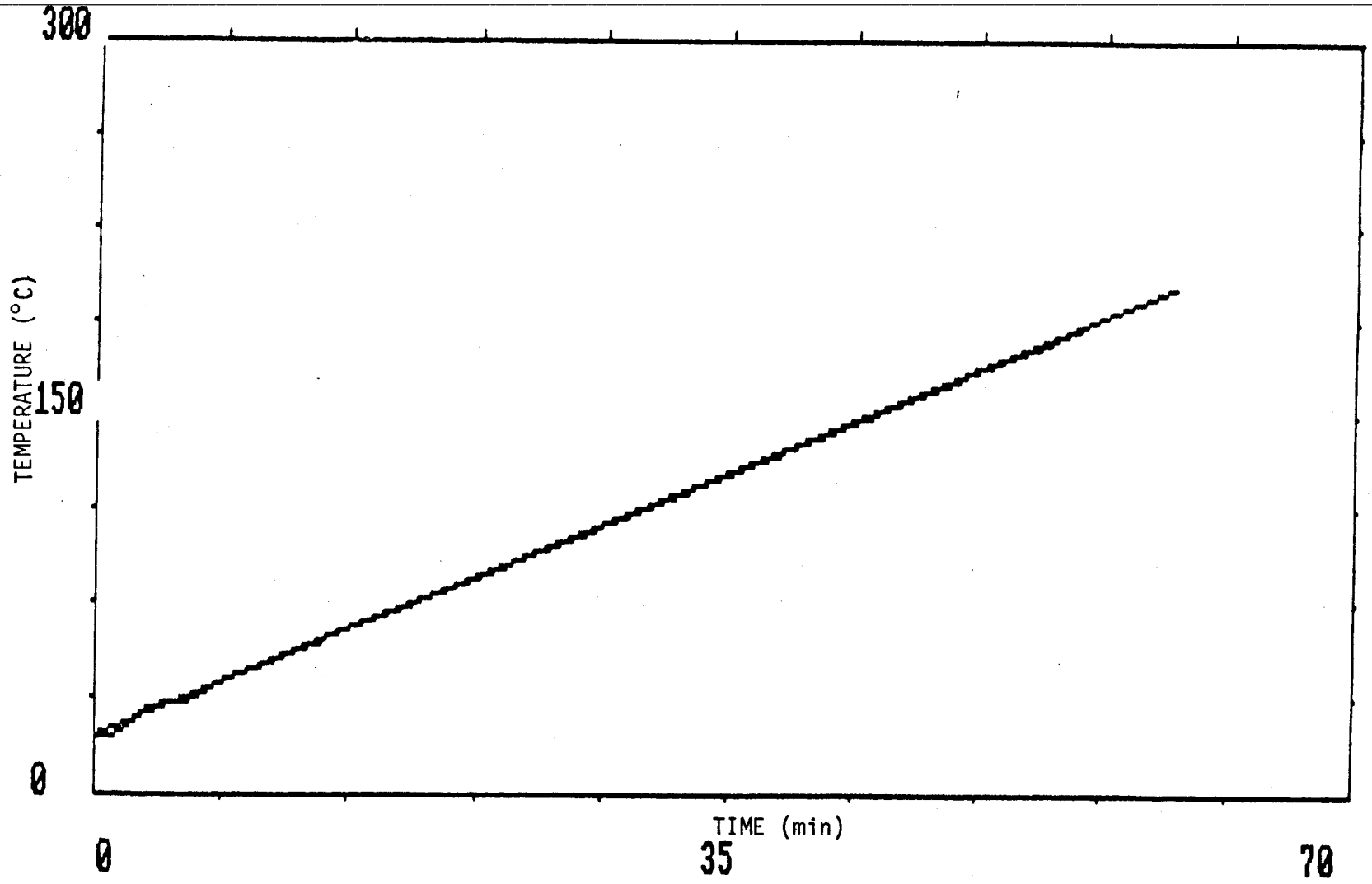

Fig. 4.12 Temperature profile at 3 °C/min after tunning.

drew a current of 1.3 A. The heater was thus powered by a triac switch. A 400 V, 6 A Triac (9C89) was used to power the heater. As shown in Fig. 4.13 gate potential is fixed by a potential divider circuit which is powered by the output of the controller. The AC HI terminal of CN-2010 was shorted to one of the current carrying triac terminal i.e. MT1. The other terminal of triac i.e. MT2 was shorted to AC LO of the controller. Care was taken in the design to check that the triac neither continues to be in the ON state, due to the internal triac leakage current, nor does it continue to be in the OFF state.

(C) HEATER & INSULATION

The heater of the TAA cell was a *quick* responding mica insulated one piece band heater (Omega Engineering Model No.MB1E1E1A1). It is cylindrical in shape and the dimensions of the heater are 1.25" internal diameter and 1.25" in height. To avoid hot spots on the heater and to provide a uniform heating it was tightly clamped on to a cylindrical piece of stainless steel cylinder of dimensions 2 mm thickness and 2.75 cm in internal diameter. To complete the TAA cell, stainless steel lids had to be machined to close the heater assembly and to allow the glass buffer rods to pass through them. To provide insulation for the TAA cell, two refractory bricks had to be chiseled so as to enclose the heater and the assembly. As described earlier the heater assembly and refractory bricks were placed on an asbestos sheet of dimension 6" x 6" and

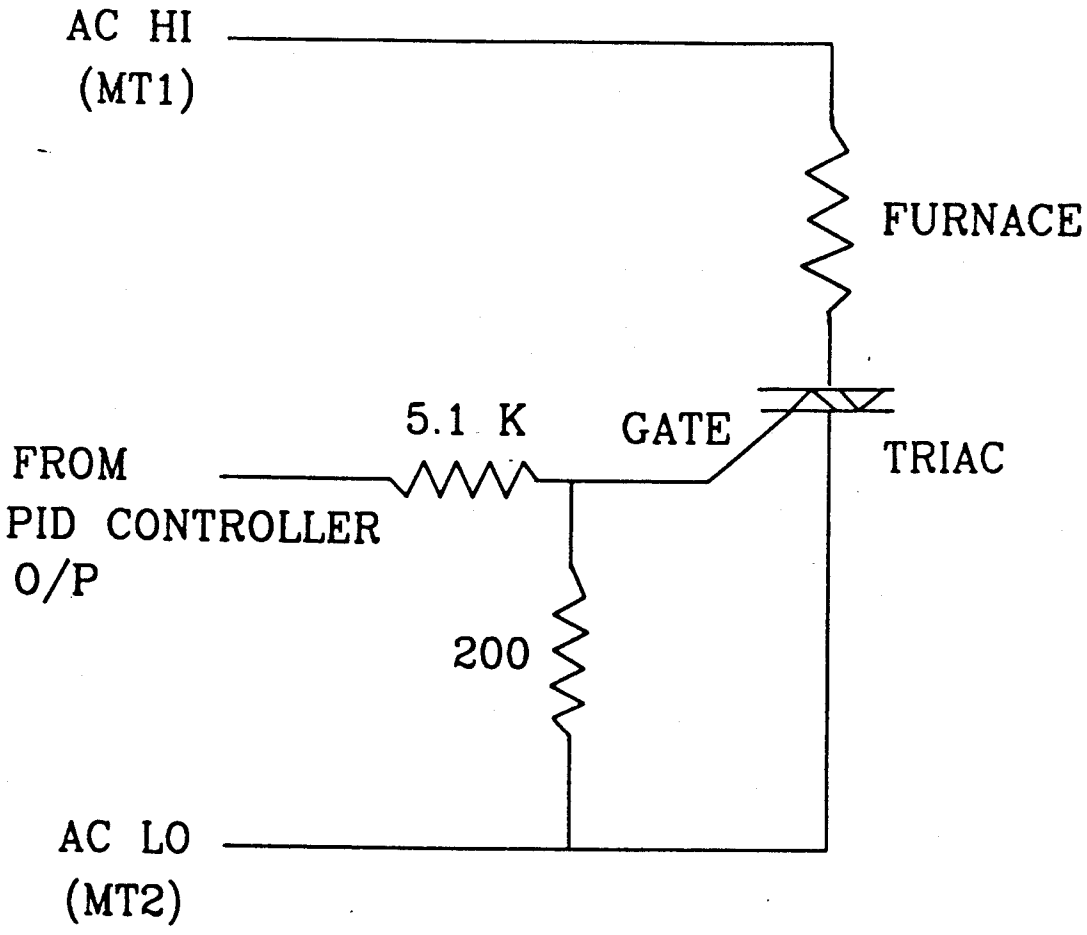

Fig. 4.13 Triac interface box circuitry.

1/4" thick, fixed to the aluminum partition dividing the transmitter and the receiver section.

4.7 MECHANICAL SUBSYSTEM

The TAA cell, buffer rods, RF bridge, RF receiving amplifier were housed in a shielded box made of dexions and covered with aluminum sheets. The entire box was grounded to provide shielding against capacitive interference. This box was partitioned into two sections to separate the transmitter and the receiver operations as can be seen from the photograph in Fig. 4.2. Only a hole of 21 mm dimension was drilled in the aluminum partition to allow the lower buffer rod to pass through.

The mechanical clamp holding the upper buffer rod could be moved vertically along a groove in the stand fixed to the aluminum partition. The entire mechanical assembly for holding the upper buffer rod was machined out of brass and stainless steel. The TAA cell assembly was placed on an asbestos sheet attached to the aluminum partition.

Twisted pair cables ran from the contact points for the leads of transmitting and receiving transducers, to the bridge circuit and receiving amplifier respectively. In order to provide shielding, all electronic modules were housed in grounded aluminum boxes.

5. RESULTS AND DISCUSSION

5.1 INTRODUCTION

The contents of this Chapter provide the results of the experiments carried out on important engineering materials using the TAA apparatus developed in this work. Furthermore, the experimental data has been analysed in terms of the current theories of ultrasonic wave propagation and phase transformations to obtain:

(a) elastic modulus of various materials.
(b) glass transition temperatures of various materials at different heating rates.
(c) evidence of any secondary transitions in the phase transformation processes.
(d) correlation between the TAA technique with other thermal analysis techniques viz. DSC, TμHA, to verify the TAA technique.
(e) the values of activation energies for the phase transformation processes.

A brief discussion of polymers is given in Appendix B and the interpretation of results for phase transformations in amorphous materials has been given by considering various principles underlying it.

Materials were analysed by the TAA apparatus at room temperature, and also from room temperature to temperatures as high as 250°C, at controlled heating rates. These materials include a wide variety of engineering polymers, composites, and a near stoichiometric amorphous semiconductor alloy of arsenic and selenium used in electrophotography. Thermal analysis techniques based on DSC and TμHA have been correlated

with an extensive TAA analysis carried out for polycarbonate (PC). From the correlation plots, the *activation energy* for the glass transformation of polycarbonate has been determined.

5.2 ACOUSTIC VELOCITY MEASUREMENTS AT ROOM TEMPERATURE

For analysis of materials at room temperature by the TAA apparatus, it was necessary to have samples with parallel surfaces. The average sample thickness was found after determining the thickness of the sample at different places on the surface by the thickness measurement system described in Section 4.2. The sample, was then smeared with a thin layer of coupling agent Slick 50 grease. With the sample placed on the lower buffer rod, the upper buffer rod was then lowered so as to sandwich the sample between the two buffer rods (Fig. 4.1). The transmitting circuitry then excited the X-cut quartz crystal at its 4 MHz resonant frequency, with a RF pulse width of 6 μs. Repetition rate of the RF pulses was 1 ms.

As the two buffer rods were of the same length, the echo signal received at the transmitting transducer corresponds to the transit time of the acoustic waves through the two buffer rods. This received signal was isolated from the transmitting channel by the bridge circuitry (Section 4.5.8) and displayed on the oscilloscope. Whereas, the signal received at the receiving transducer corresponds to the transit time of the ultrasonic waves through the two buffer rods and the sample. This signal was displayed on the second vertical channel of the oscilloscope. The external trigger signal, generated as

described in Section 4.2, was used to trigger the oscilloscope. External triggering increased the resolution of the transit time measurement. Thus, the time difference between the beginning of the two received signals corresponds to the transit time of the ultrasonic waves through the sample alone. An example of this measurement is illustrated in Fig. 5.1 for the case of a polycarbonate sample of thickness 2.00 mm. Fig. 5.1(a) illustrates both the waveforms i.e. the echo and the transmitted waves (A and B) on a larger time base scale of the oscilloscope. RF excitation pulse-pick ups can be seen in the beginning of both the waveforms A and B. A number of echoes can also be seen in both the waveforms which are mainly due to the reflections of the ultrasonic waves from the interfaces between the buffers and the material. In Fig. 5.1(b), waveform A is the signal received at the transmitting transducer, whereas the lower waveform B is the signal received at the receiving transducer. From the transit time measurement and the thickness of the sample determined earlier, absolute velocity of the acoustic waves through the sample could be determined. Similar waveforms have been presented in Fig. 5.2 for measurement of transit time in a near stoichiometric amorphous alloy of arsenic and selenium (a-As_2Se_3). The sample thickness of the alloy was 2.77 mm.

The TAA analysis at room temperature was carried out on amorphous polymers viz. Polycarbonate (abbreviated as PC), Poly (methyl methacrylate) (abbreviated as PMMA),

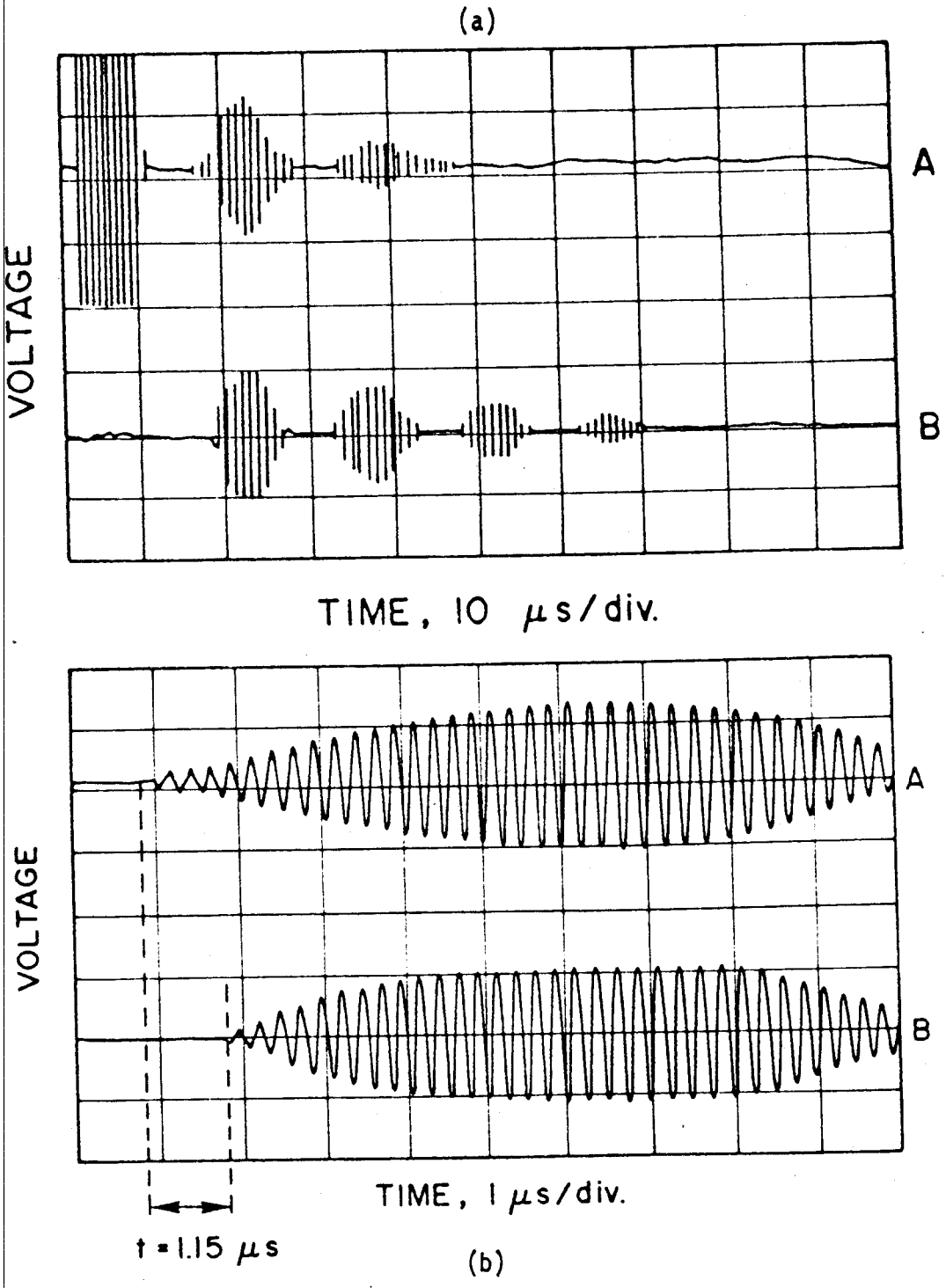

Fig. 5.1 (a) A-Reflected wave, B-Transmitted wave, obtained during TAA of PC at room temperature. (b) Measurement of longitudinal ultrasonic wave transit time through PC.

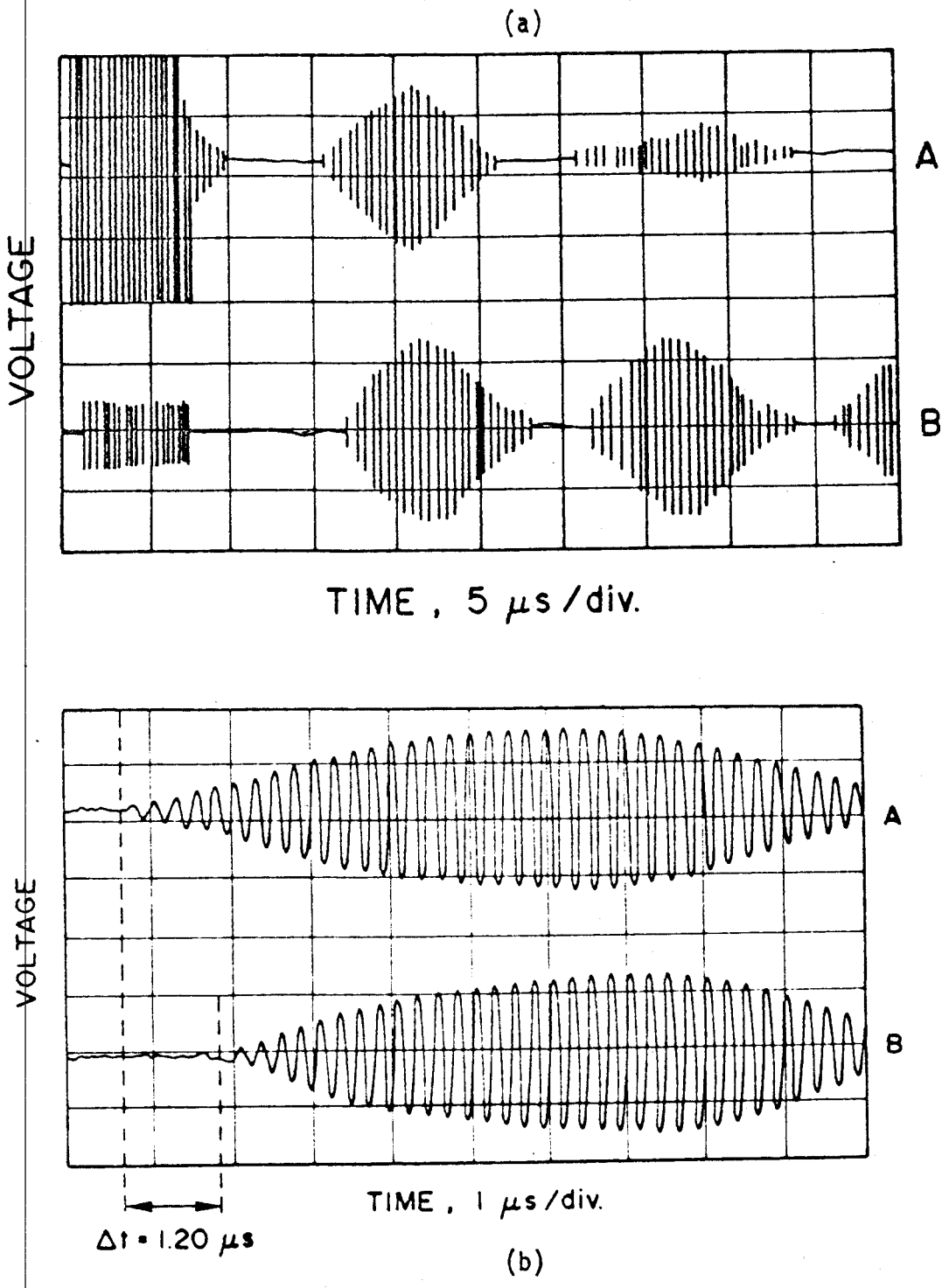

Fig. 5.2 (a) A-Reflected wave, B-Transmitted wave, obtained during TAA of a-As_2Se3 at room temperature. (b) Measurement of acoustic transit time in a-arsenic triselenide.

Polyphenylene sulphide (PPS). TAA was also performed on an near stoichiometric amorphous alloy of arsenic and selenium (a-As_2Se_3), and three types of thermally cycled composite materials comprising of glass fiber reinforced polymers. The structure of polymers are discussed in Appendix B.

Polymers form an important class of engineering materials for numerous reasons viz. low density, resistance to environmental attack, ease of processing into intricate shapes, high electrical resistance (insulation), high strength (for example when the polymer chains are aligned as in Nylon tyre cords) and less cost/weight for equal strength in comparison to metals[37]. Due to their extreme importance as engineering materials, study of polymer properties is generating world wide interest. Thus, the polymers cited above were studied in this research by using TAA first at room temperature and then as a function of temperature. The results of the absolute velocity obtained in these polymers at room temperature have been tabulated in Table 5.1. The acoustic velocity in a polymer is basically dependent on the density of the polymer and the elastic modulus[38]. The calculated elastic modulus from the ultrasonic velocity for some of the polymers is summarized in Table 5.2. Table 5.2 further compares the data of this work with that available in the literature. The relationship between the elastic modulus Y and the longitudinal acoustic velocity c_L is[5]

$$c_L = \sqrt{\frac{Y}{\rho\, f(\nu)}} \qquad (5.1),$$

where

ρ = density of material

$f(\nu)$ = function of the Poisson's ratio given by

$$f(\nu) = \frac{(1-\nu)}{(1+\nu)\ (1-2\nu)} \qquad (5.2),$$

where

ν = Poisson's ratio of the material.

Table 5.1: Absolute acoustic velocity in some materials.

Material	**Absolute velocity (X 10^3) m/s.**
Polycarbonate	1.73
PMMA	2.52
PPS - Matrix	3.08
Composites	
(i) Short fiber random orientation matrix	2.72
(ii) Continuous uniaxial matrix.	3.22
(iii) Continuous bidirectional fibre matrix.	2.69
As_2Se_3	2.30

Table 5.2: Comparison of elastic modulus of some polymers, obtained from TAA results, with the values in the literature.

Material	Y from absolute vel. (GPa)	Y from data sheets (GPa)	Comment
PC	2.26	2.2-2.4 (Goodfellow Metals Ltd., UK)	$\nu = 0.35$ Good agreement
PMMA	3.58	3.78[39]	$\nu = 0.4$ Good agreement

Equation 5.1 assumes that the acoustic wavelength λ is much shorter than the sample thickness L. In calculating Y we had to assume a Poisson's ratio for the polymers. For most plastics the Poisson's ratio is in the range 0.35-0.40[40]. So that typical values of $\nu = 0.35$ and 0.4 were used for polycarbonate and PMMA respectively. Evaluation of Y from c_L is discussed in more detail later in this Chapter.

A similar study has been done on a near stoichiometric amorphous semiconductor alloy of 63 % selenium and 37 % arsenic which is a commercially important alloy known as xerographic arsenic triselenide (As_2Se_3). Square samples of 15 mm X 15 mm and thickness 2.0-3.5 mm, were prepared from vitreous pellets of the alloy obtained from Noranda Technology Centre, Pointe Claire, Quebec. These vitreous pellets were sealed in an evacuated square glass tube of dimensions 18 mm X 18 mm X 150 mm. The resulting vacuum inside was about 10^{-3} torr. It was ensured that the material occupied 1/2-1/3rd

length of the tube. This was necessary to allow space for expansion of the alloy when it was melted. The pellets enclosed in the square glass tube were heated to their melting temperature of 540°C for about 15 minutes. The glass tubes were rotated from time to time during heating in order to ensure homogeneity. When the sample tube was cooled in air the melt formed glass. The material was left for about 15-17 days after quenching in air for the structure of the material to stabilise. Subsequently, the material along with the glass tubing was cut to about 11 samples each of thickness 2-4 mm with the aid of a diamond saw on a Isomet low speed saw (Model No. 11-1180). The samples were then ground and polished on the Struers polishing wheel. The acoustic velocity measured in one of these samples is given in table 5.1. Soga et al.[41] have found velocity of longitudinal acoustic waves in As_2Se_3 to be 2261 m/s. There is a discrepancy of 2 % in the results for the two experiments. The difference is probably due to the fact the As_2Se_3 samples of this work were not stoichiometric (i.e. of composition 40 % As - 60 % Se) but slightly Se rich (37 As - 63 % Se).

Thermally cycled composite materials were analysed by using TAA apparatus at room temperature for the following reasons:

(a) To investigate the variation of absolute acoustic velocity, and hence elastic modulus, through the composites with the number of thermal cycles.
(b) To determine the attenuation of acoustic waves caused by the thermally cycled composite materials relative to uncycled composite of the same type.

Hence normalised attenuation coefficient of the composite was studied.

(c) Finally, to examine if there is a correlation between the acoustic velocity, normalised attenuation, flexural strength with the number of thermal cycles.

The composite materials obtained from Dr. Yannacopoulos consisted of a general purpose polyester resin as the matrix material. E-type glass had been used for the fibres and a silane coupling agent for the fibre-matrix bond reinforcement. The three types of composite materials analysed by TAA were (i) a short fibre random orientation matrix (ii) a continuous uniaxial matrix and (iii) a continuous bidirectional fibre matrix. Before these composites were obtained, they had already been subjected to high or low temperature thermal cycling and some to no thermal cycling. The flexural strength of these composites had been already determined[42], after various thermal/fatigue cycles, by a mechanical method called the three point bend test. The velocity of the acoustic waves through the three composite materials before thermal cycling is given in Table 5.1. Table 5.3 gives the Young's modulus (Y) of the three uncycled composite materials obtained from the corresponding velocity data. These values of the Young's modulus are compared with the theoretically expected result for the Young's modulus of the composites by two Mixture Rules, given by Equations 5.3 and 5.4[43].

$$Y_{11} = X_g Y_g + X_p Y_p \qquad (5.3),$$

$$Y_{22}^{-1} = X_g Y_G^{-1} + X_p Y_p^{-1} \qquad (5.4),$$

where

Y_{11} and Y_{22} = Young's moduli of the mixture for the isostrain case and isostress case respectively,

Y_p and Y_g = Young's modulus of the polyester and glass respectively,

X_g and X_p = the molar concentrations of the glass and polyester respectively.

Similarly the Poisson's ratio ν of the mixture is given by

$$\nu = \nu_g X_g + \nu_p X_p \qquad (5.5),$$

where

ν_g and ν_p = the Poisson's ratio for the glass and polyester respectively.

As seen from Table 5.3 mixture rule 1 is more applicable to the composites than mixture rule 2. The density of composite samples (belonging to any of the three types) was determined at room temperature by the Archimedes method with a sensitive Mettler microbalance TG30 and ethanol as the buoyant medium. Furthermore, the value of the function $f(\nu)$, which is given by

$$f(\nu) = \frac{(1-\nu)}{(1-2\nu)\ (1+\nu)} \qquad (5.6),$$

Table 5.3: Comparison of Young's modulus obtained for composites by TAA with the values from the mixture rule.

Material	Y from TAA. GPa.	Y from mixture rule 1 GPa.	Y from mixture rule 2 GPa.	Comments (Compared with mixture rule 1)
Composite type 1	5.78	5.69	2.51	1.76 % error. Good agreement
Composite type 2	7.5	7.3	2.6	2.74 % error. Good agreement.
Composite type 3	5.73	6.27	2.54	8.61 % error. Satisfactory agreement.

was calculated based on a Poisson's ratio of the composites obtained by using Equation 5.5 for all the composites. Value of $f(\nu)$ was assumed to be relatively constant when compared with changes in the elastic modulus in the thermally cycled composites. This assumption is justified by a plot of $f(\nu)$ against ν as illustrated in Fig. 5.3. Wide class of materials ranging from polymers to metals have Poisson's ratio in the range of 0.3-0.4. As can be seen from the plot in Fig. 5.3 the value of $f(\nu)$ changes by a maximum of 10-15 % for a practical variation of ν by 10 % within a given class of materials. Based on this assumption the variation of elastic modulus against flexural strength is shown for composite materials of type 1 in Fig. 5.4(a). The density of all the composite

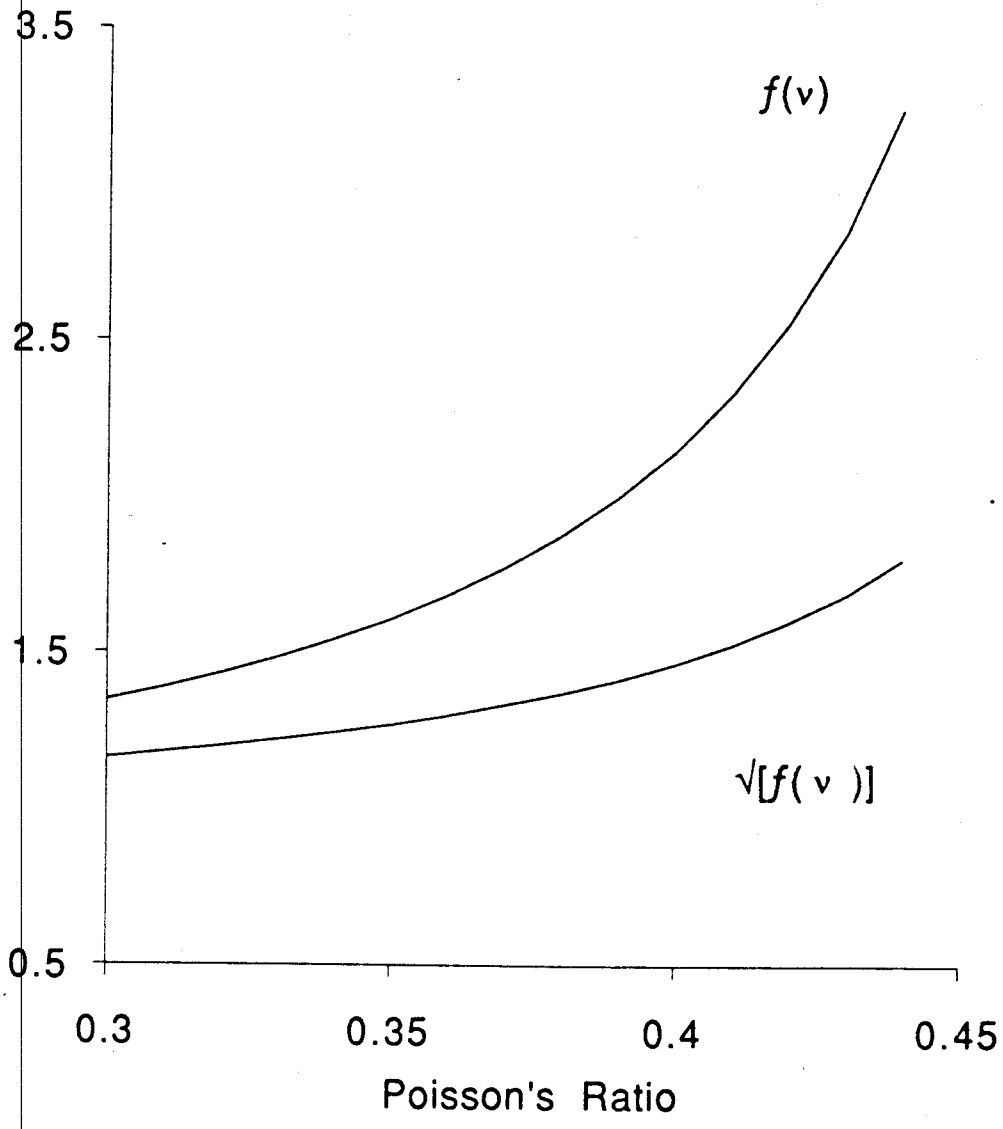

Fig. 5.3 Graph showing variation in f(ν) for the typical range of Poisson's ratio ν.

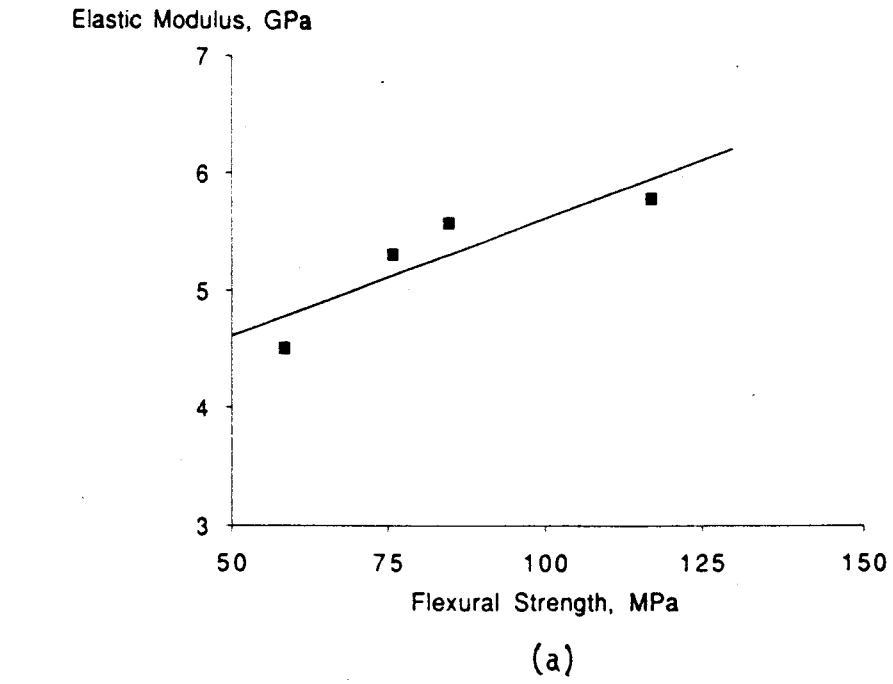

(a)

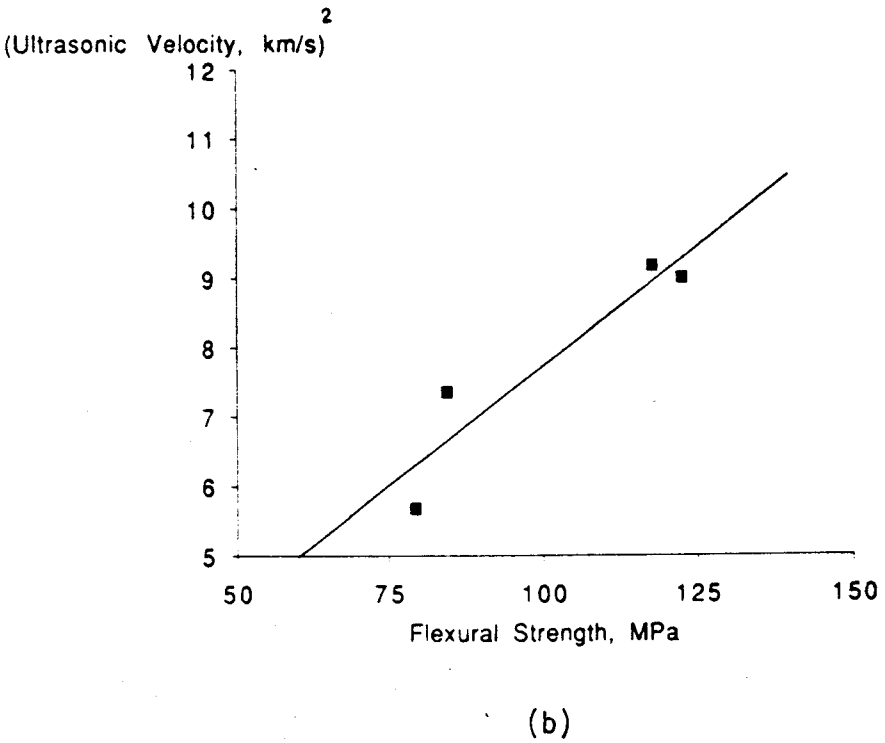

(b)

Fig. 5.4 Variation of elastic modulus with flexural strength in (a) Composite material of type 1 (b) Composite material of type 2.

samples were determined to be almost constant. As f(V) was also assumed relatively constant, square of velocity is proportional to the elastic modulus. For samples of type 2 and 3 square of velocity has been plotted against flexural strength in Fig 5.4(b) and 5.5 respectively. From Fig. 5.4 and Fig. 5.5 it can be seen that the elastic modulus for all the three types of composites increases with the increase in flexural strength. Both the elastic modulus and the flexural strength depend on the fiber-matrix bond. Before the thermal cycling the fiber-matrix bond is strong, whereas, during thermal cycling debonding occurs. With less surface area of bonding between the fibers and the matrix, both the elastic modulus and the strength decrease. Although the two quantities are not directly related they are nonetheless both dependent on the fiber matrix bond.

The correlation of velocity, flexural strength[42], normalised attenuation with the number of high and low thermal cycles is shown in Fig. 5.6, by plotting these parameters against the number of thermal cycles. This is done for samples of the composite material type 1. From Fig. 5.6 it is clear that the ultrasonic velocity decreases with the decrease in flexural strength. This is to be expected, since the ultrasonic wave propagation as discussed above is dependent on the fiber-matrix bond. The normalised attenuation, as seen in Fig. 5.6 increases, with the number of thermal cycles. Thermal cycling tends to develop microscopic cracks/defects due to

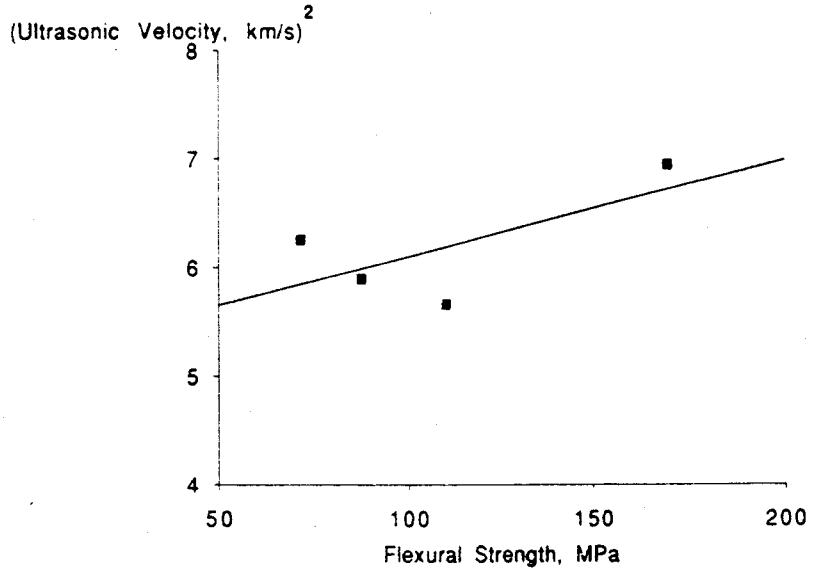

Fig. 5.5 Variation of elastic modulus with flexural strength in composite of type 3.

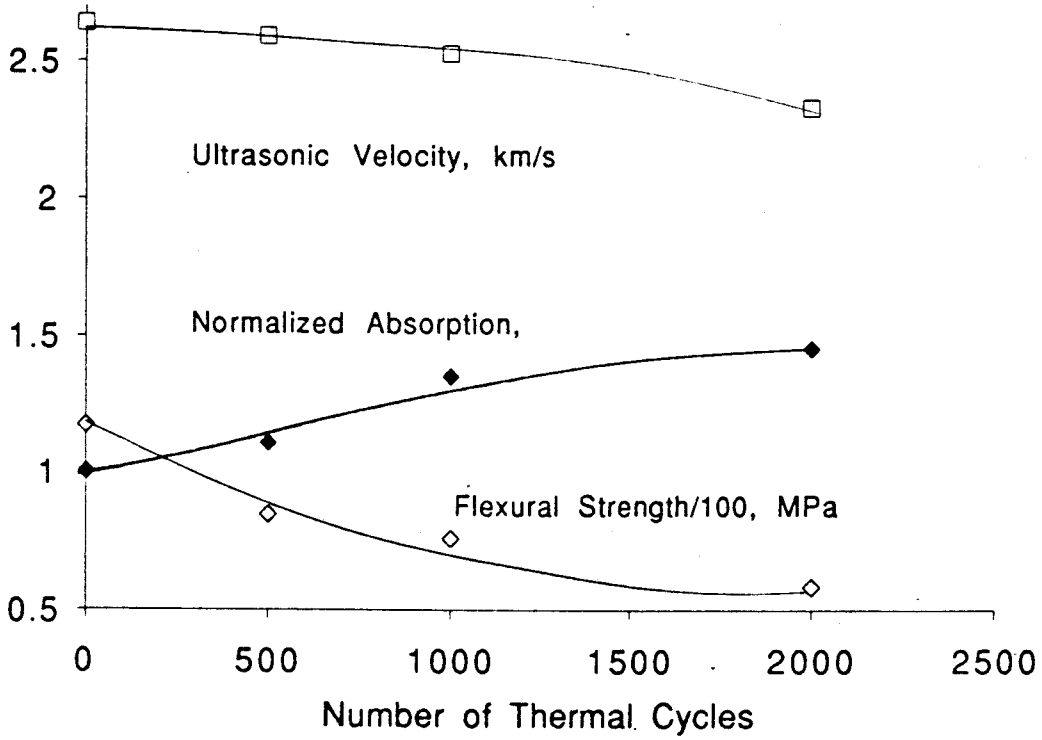

Fig. 5.6 Correlation of velocity, normalised attenuation and flexural strength[42] with number of thermal cycles in composite material of type 1.

debonding between the fiber and the matrix, which in turn causes discontinuities in the propagation medium. The microcracks generally develop because of the inevitable mismatch in the thermal expansion coefficient of the materials constituting the composite[44]. Due to these discontinuities in the medium there is scattering of the ultrasonic waves, and hence divergence of ultrasonic energy from the main beam resulting in an increased attenuation with an increase in thermal cycles. Similar reasoning can be applied to explain Fig. 5.7 for samples of composite material of type 2 and 3.

The above sets of experiments using the TAA apparatus illustrate the usefulness of TAA apparatus even at room temperature.

5.3 THERMOACOUSTIC ANALYSIS OF POLYCARBONATE

Polycarbonate is an important engineering polymer belonging to the thermoplastic group of plastics i.e. it can be moulded and remoulded by heating into different shapes. The first polycarbonate was synthesised around 1902[45]. Since then much work has been done in synthesising new varieties of linear polycarbonates by Eastman Kodak and General Electric company. The polymer is based on the readily available monomer, bisphenol-A. It has an all-around balance of properties in particular impact strength. A limitation of polycarbonates is the tendency to crack or craze under tensile stress. Polycarbonate can be obtained in various forms viz. sheets, films, rods and as a polycarbonate resin. However,

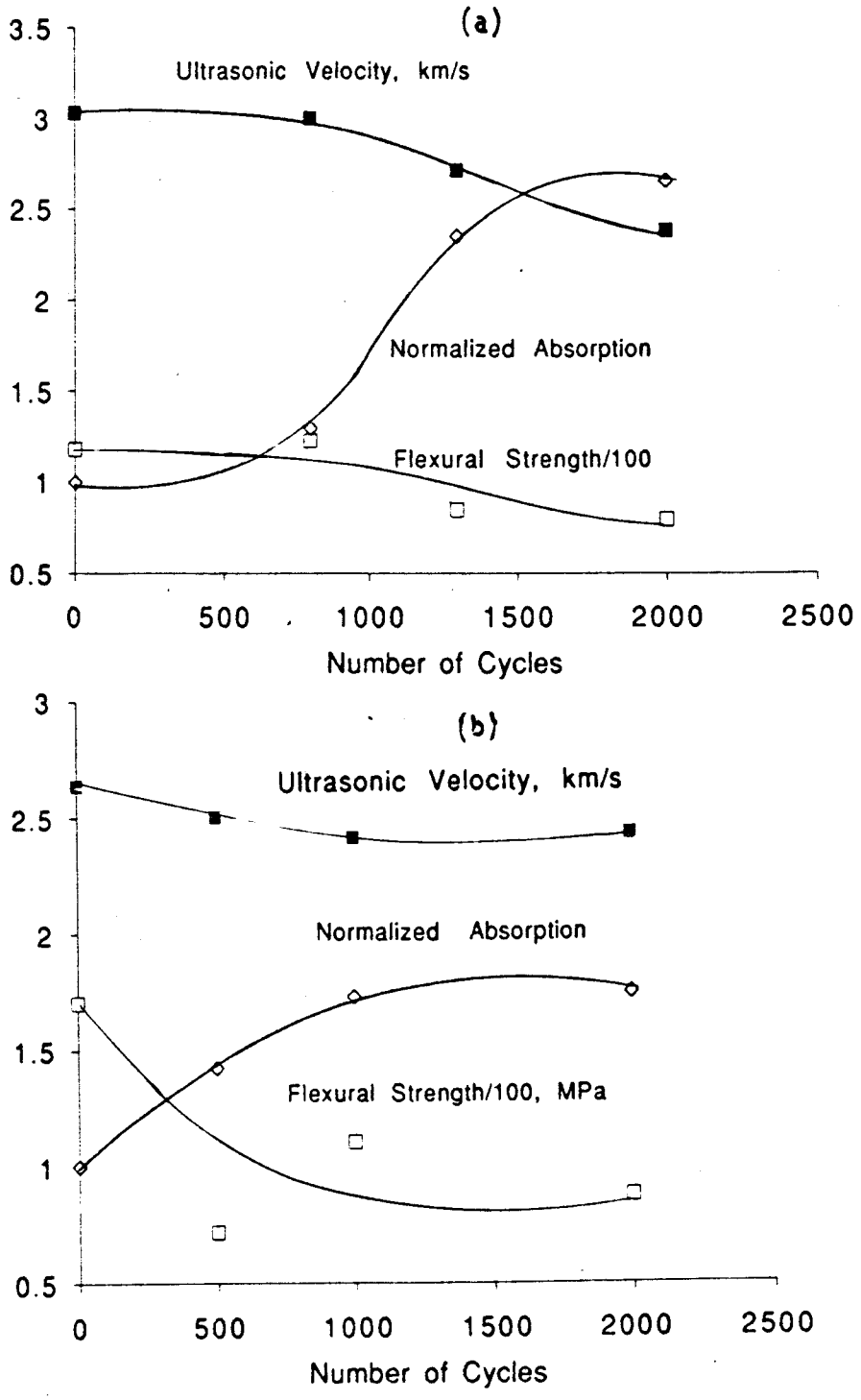

Fig. 5.7 Correlation of ultrasonic velocity, normalised attenuation and flexural strength[42] with the number of thermal cycles in (a) Composite of type 2 (b) Composite of type 3.

polycarbonate resin is a thermosetting plastic i.e. it cannot be remoulded, but has superior abrasion and dimensional stability characteristics.

5.3.1 EXPERIMENTAL RESULTS - PC

Amorphous polycarbonate sheet of dimensions 150 x 150 mm and of thickness 2 mm (obtained from Goodfellow Metals Ltd., Cambridge, U.K.) was cut into cylindrical samples of diameter 19 mm. TAA was performed on polycarbonate samples at different heating rates viz. 0.2, 0.5, 1, 3, 5 and 10°C/min, from room temperature (23°C) to a maximum of 200°C. Relative changes in transit time of the longitudinal ultrasonic waves through the sample were measured as a function of sample temperature, as described in Section 4.2. Similarly, the voltage amplitude (peak- to-peak) of the received signal was measured as a function of temperature to obtain the relative attenuation of the ultrasonic waves in the sample. The temperature of the sample was noted from the PID controller while making these measurements. The velocity of the waves through the sample at any temperature T, was normalised with respect to the velocity at room temperature. The equation used for calculating this normalised velocity is

$$V_n(T) = \frac{V(T)}{V(T_o)} = \frac{tr_o}{tr_o + (\delta tr_t - \delta tr_o)} \qquad (5.7),$$

where

$V(T)$ and $V(T_o)$ = the velocities of the ultrasonic waves through the polycarbonate sample at any temperature T and at room temperature respectively,

t_{ro} = the transit time of the waves through the sample at room temperature,

δt_{ro} and δt_{rt} = the time difference between the beginning of a cycle of the received signal nearest to the reference at room temperature and at any other temperature respectively. The reference was taken as the beginning of a cycle of the echo signal received at the transmitting transducer, as described earlier in Section 4.2. A factor to be considered here is the deformation of the viscoelastic material under the pressure exerted by the buffer rods and its own weight. This would introduce a contraction in the sample after the transition. Since in the derivation of Equation 5.7 only the room temperature length of the sample has been considered (in the absence of thermal expansion data) the actual calculations of normalised velocities at different sample temperatures are therefore slightly obscured by changes in length of the sample due to the sample contraction. However, in the determination of T_g it is the indicative nature of the graph of V_n vs T (of the type in Fig. B.2 shown in Appendix B) and not the actual magnitude of the change in the physical property measured (specific volume in the case of Fig. B.2 shown in Appendix B) which is important. For example, Kartha et al.[23] have reported

measurements of ultrasonic velocities in $Se_{90}Ge_{10}$ and $Se_{85}Ge_{15}$, by taking room temperature length of samples for calculating changes in the acoustic velocity. Their measurements also do not take into account the contraction of the sample. The glass transition temperature for any heating rate can be found from the graph of the normalised velocity against sample temperature since at T_g there is a sudden change in the acoustic velocity as illustrated in Fig. 5.8 for PC samples heated at different heating rates. Fig. 5.8 also displays the glass transition temperature for each V_n vs T thermogram at the heating rate shown. The glass transition temperature can be seen to increase with the increase in heating rate. It can also be seen from Fig. 5.8 that there is a significant decrease in the normalised velocity in the glass transition region. This can be attributed to the transition of the amorphous material to a liquid-like state in the glass transition region. The relative attenuation of the waves, by the sample at different temperatures was obtained by the expression

$$\Delta\alpha = -\frac{1}{L}\mathrm{Ln}\left(\frac{V_t}{V_o}\right) \qquad (5.8),$$

where

L = the thickness of the sample in meters,

V_t and V_o = the amplitude (peak-to-peak) of the received signal at any temperature T and at room temperature respectively.

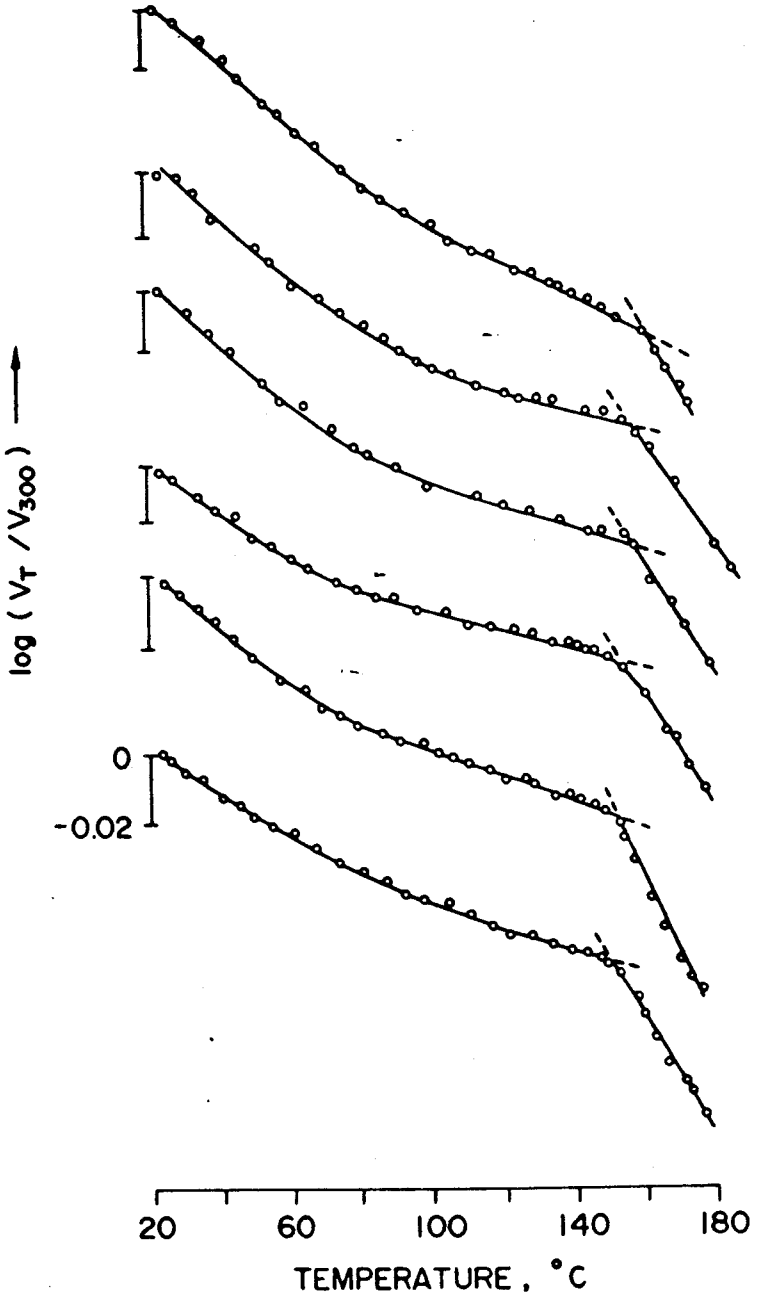

Fig. 5.8 Normalised acoustic velocity vs temperature at different heating rates for PC: (a) at r = 0.2°C/min, T_g = 147.8°C. (b) at r = 0.5°C/min, T_g = 150.5°C. (c) at r = 1°C/min, T_g = 151°C. (d) at r = 3°C/min, T_g = 154°C. (e) at r = 5°C/min, T_g = 155°C. (f) at r = 10°C/min, T_g = 157°C.

In Equation 5.8, the room temperature length of the sample has been also used as in Equation 5.7. Fig. 5.9 shows a plot of relative attenuation $\Delta\alpha$ against the sample temperature for PC heated at a rate of 1°C/min. There is a peak observed at a temperature of 150.5°C which is the glass transition temperature as determined by the thermoacoustic attenuation method. The peaking occurs due to the transit of the polymer from glassy state to a rubbery state. In the glass transition region the elastic modulus decreases sharply which rapidly increases the attenuation. Elastic modulus in the rubbery state remains more or less constant[46]. Also just in the rubbery state following the T_g transformation the polymer chains can move in the direction of the applied stress and return to their original state[46], which causes slightly less attenuation compared to that in the glass transition region. This can be seen in Fig. 5.9. As the temperature is further increased, the state of the material tends to be more and more viscous, due to which the attenuation of the ultrasonic waves again starts increasing.

The changes in transit time with respect to the reference, and the peak-to-peak voltage of the received signal were measured at the same sample temperature only for slower heating rates of 3°C/min and below. For heating rates greater than 3°C/min only one of the parameters i.e. changes in transit time or peak to peak voltage was measured as a function of temperature to obtain a sufficient number of

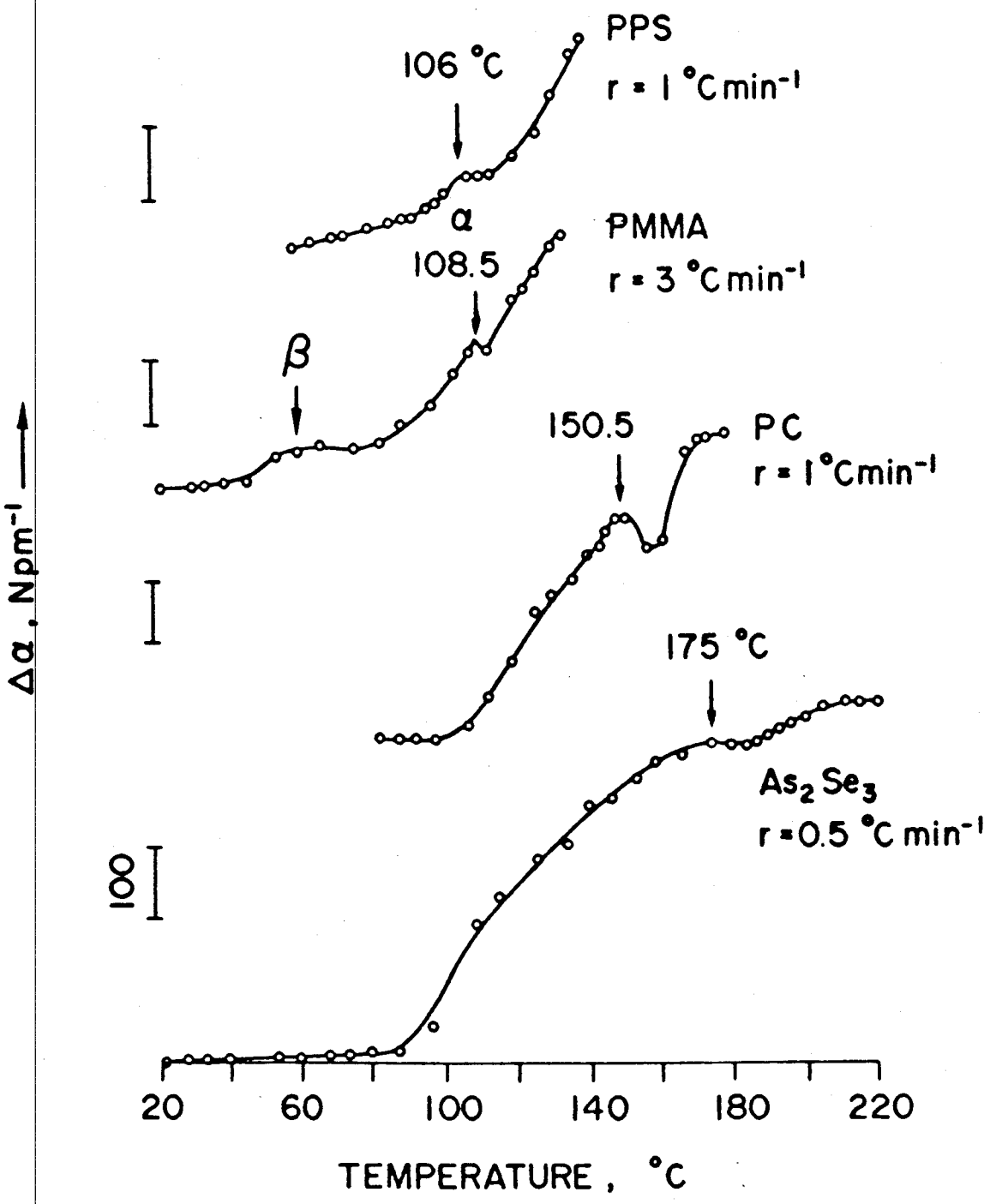

Fig. 5.9 Relative attenuation of longitudinal ultrasonic waves vs temperature in different materials obtained by TAA.

experimental data points to observe the T_g transformation. Each experiment was performed on a different polycarbonate sample so as to ensure that the acoustic measurements were on samples with identical thermal history. It is well known that T_g transformation depends on the thermal history. Thermal analysis of Polycarbonate material was also carried out by DSC and TμHA[47]. This was done to verify the measurements obtained by TAA and also to obtain a correlation between the three thermal techniques.

DSC experiments were carried out using a Mettler Instruments TA3000 Thermal Analyzer system which consisted of a model TC10 Thermal Analyzer and a model DSC30 Differential Scanning Calorimeter. TμHA experiments were carried on the apparatus described in Section 3.4. Fig. 5.10 depicts the thermograms for the three thermal analysis techniques, namely TAA (both normalised velocity and relative attenuation), DSC and TμHA carried out on polycarbonate samples at a heating rate of 1°C/min. The T_g values obtained from all these three thermal analysis techniques differ by a maximum of only 1°C, when DSC T_{gm} is taken into consideration rather than the onset temperature T_g. Some differences in the T_g values can be expected because of the inherent errors which can occur during thermal analysis techniques as discussed in Sections 3.2 and 3.4. Furthermore, K-type thermocouples unless specially calibrated generally have a resolution of ~1°C.

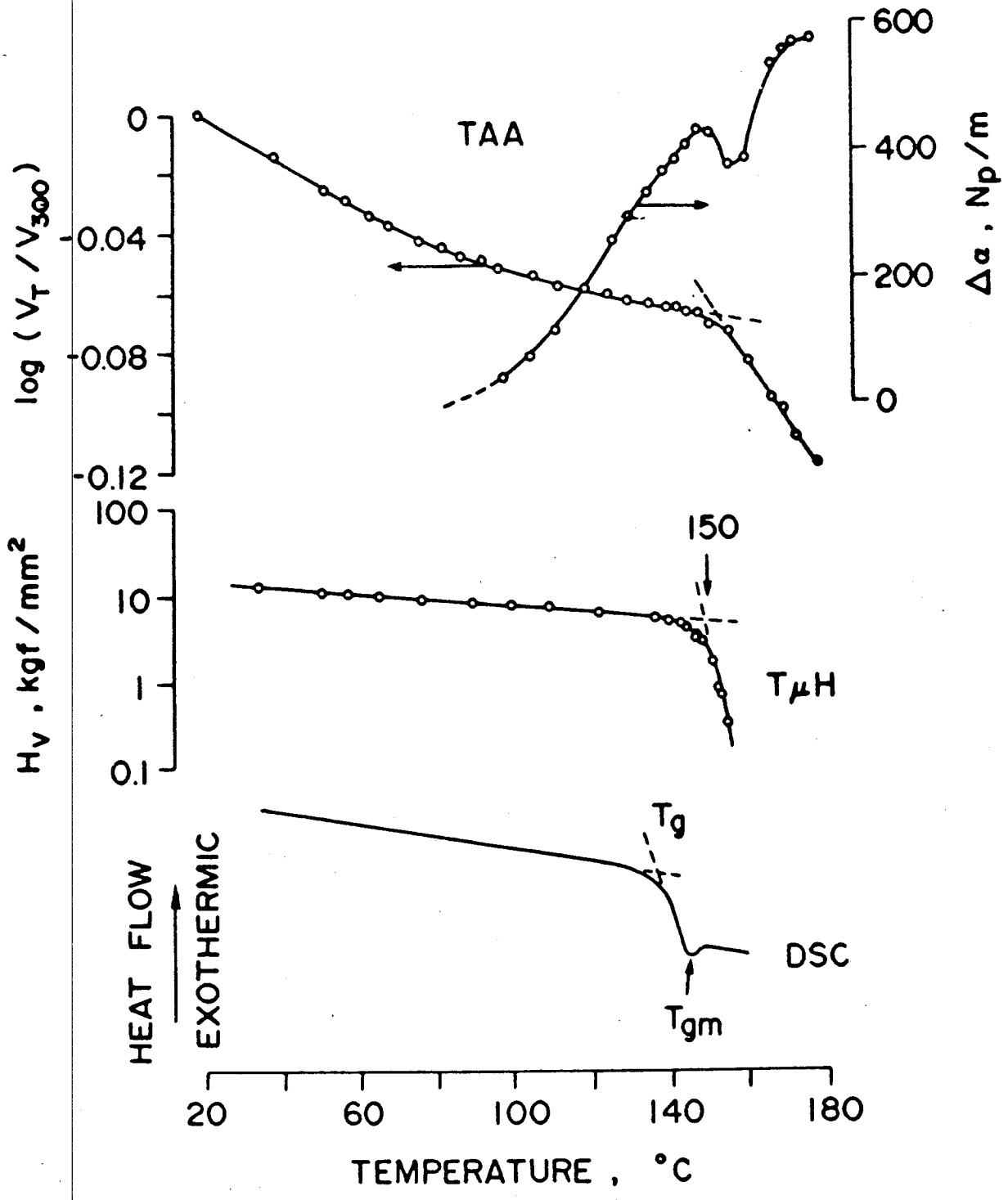

Fig. 5.10 Correlation of TAA with different conventional thermal analysis techniques viz. DSC, TμHA[47] for polycarbonate.

Another major aim of the analysis was to obtain the value of activation energy for the phase transformation of polycarbonate and to correlate these to the viscosity. The activation energy is the height of the energy barrier to a reaction which must be surmounted by thermal excitation.

There are various glass transformation theories presently in use. The most widely used interpretation is that which describes the glass transformation process by a kinetic structural relaxation process[48]. This interpretation is widely used as it is able to predict readily the cooling and heating rate dependence of the observed glass transition behaviour[48]. In its simplest form of interpretation, the temperature range of interest, T_2-T_1, may be divided into N isothermal events each lasting a time $\Delta t = (T_2-T_1)/rN$, where r is the heating rate, as shown in Fig. 5.11(a). Fig. 5.11(b) shows the enthalpy vs temperature behaviour of a typical glass-forming material. It can be seen in Fig. 5.11(b), that on cooling of the melt, the enthalpy of the melt deviates from the equilibrium value of enthalpy $H_E(T)$, as the structure does not relax fast enough i.e. $\tau >> \Delta t$ (τ is the relaxation time). Once the glassy state has been reached the glass is at a temperature T_A, then by means of structural relaxation the enthalpy will relax towards the enthalpy of the metastable equilibrium state, $H_E(T_A)$. When the glassy material is heated from the state $H_E(T_A)$ relaxation process is slow, which results in deviation of enthalpy of glass from the equilibrium

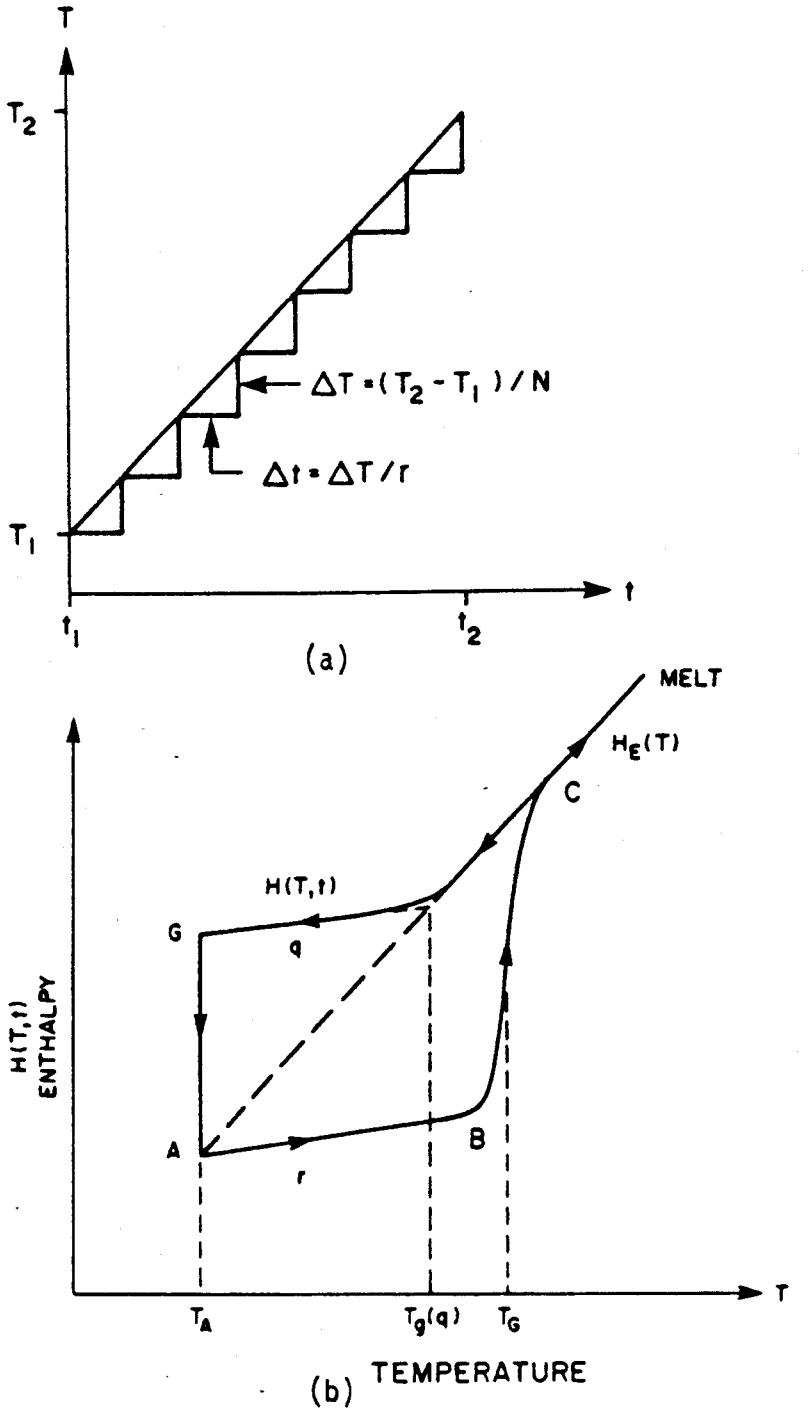

Fig. 5.11 (a) Temperature-time profile can be considered to be N isothermal events each lasting for a period Δt (b) Enthalpy vs T behaviour of a typical glass -forming liquid[48].

value of enthalpy $H_E(T)$. However, with further heating the relaxation process becomes rapid and when $\tau << \Delta t$ the structure becomes liquid like. At $\Delta t = \tau$ the system recovers towards $H_E(T)$ and the temperature at which this occurs is defined as the *glass transition temperature*. Assuming a first order relaxation process with some characteristic relaxation time τ, then the relaxation rate of the enthalpy $H(T,t)$ at a constant temperature can be written as[48]

$$\left[\frac{\partial H(T,t)}{\partial t}\right]_T = -\frac{[H(T,t) - H_E(T)]}{\tau} \qquad (5.9),$$

The thermally activated structural relaxation process can be written as[48]

$$\tau = \tau_o \exp\left(\frac{E_g}{kT}\right) \qquad (5.10),$$

where

τ_o = is a structure dependent factor.

k = Boltzmann constant.

The structural relaxation rate can also be described reasonably well by a Vogel expression of the form[48].

$$\tau(T) = \tau_o \exp\left[\frac{A}{T-T_o}\right] \qquad (5.11),$$

where

A = constant,

T_o = the characteristic temperature.

As at T_g by definition $\Delta t = \tau$ we have from Equation 5.10

$$\tau_o \exp\left(\frac{E_g}{kT_g}\right) = \frac{(T_2 - T_1)}{Nr} \qquad (5.12),$$

Rearranging Equation 5.12 we get

$$\ln r = \frac{-E_g}{kT_g} + \text{constant} \qquad (5.13),$$

Equation 5.13 is the equation of a straight line with a slope $(-E_g/k)$. Thus, from the plot of log r vs $1/T_g$, the activation energy E_g for the phase transformation process can be determined. However, if Equation 5.11 is used then the resulting plot of log r vs $1/T_g$ will be a curve. In this case the slope of the tangent to this curve gives the value of activation energy at that temperature.

The T_g values obtained for all the heating rates by different thermal techniques, in the case of PC, were used to obtain the graph depicted in Fig 5.12. Another important parameter plotted is the reciprocal of the coefficient of viscosity. This has been measured for PC by Macho et al.[49] As all the plots for the different techniques i.e. DSC (T_{gon})[47], DSC ($T_g$min)[47], reciprocal of viscosity[49], TμHA[47], TAA-normalised velocity, TAA-relative attenuation are parallel, the activation energy obtained from all techniques is thus approximately the same. The activation energy calculated from the slope of tangent to curve is ~530 kJ/mole at the temperature of ~149°C while that obtained by Macho et al. is ~526 kJ/mole. The identical values for activation energies

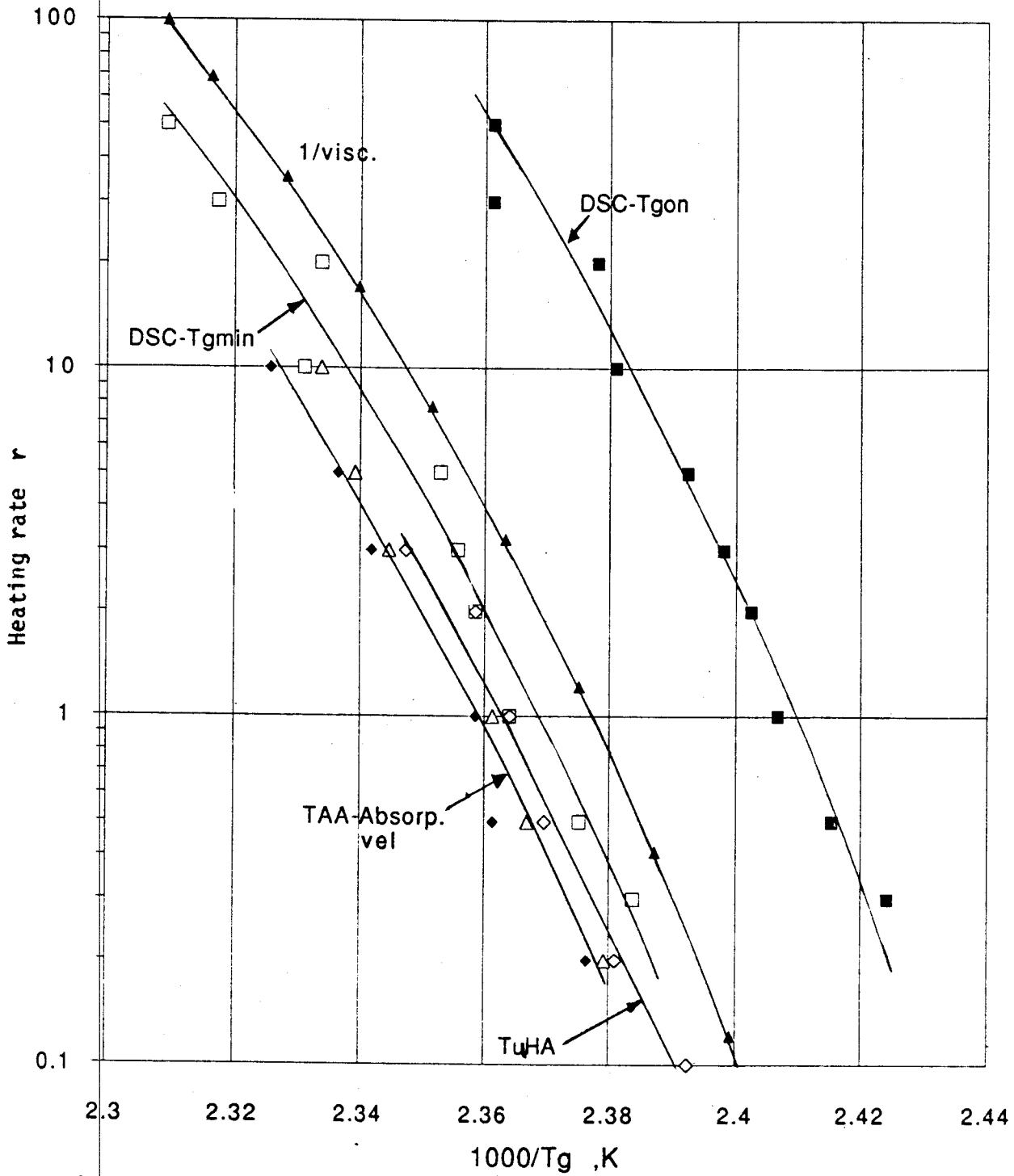

Fig. 5.12 Correlation of different thermal analysis techniques[47] and $1/\eta$[49] with TAA for PC, showing that almost identical values of activation energy are obtained in all the cases.

obtained by different techniques suggests that the same concept of relaxation kinetics is applicable in all these techniques. Thus, in the case of TAA analysis the relaxation kinetics is also applicable to the elastic modulus of the medium of propagation.

5.4 TAA APPLICATIONS TO DIFFERENT MATERIALS

Phase transformations were also investigated in other polymers such as Poly (methyl methacrylate), PPS composite and in near stoichiometric alloy of amorphous arsenic-selenium a-As_2Se_3. In the past studies of these polymers have been conducted by using static and dynamic mechanical methods mostly[50]. There have been very few measurements of ultrasonic velocities near the glass transition temperature. Etienne et al.[51] have reported measurement of ultrasonic velocities in amorphous Selenium near T_g. Padaki et al.[52] have reported measurement of ultrasonic velocities near T_g in amorphous Se-P. Acoustic studies have been carried out in alloys of Selenium viz. $Se_{1-x}Te_x$ by Kostial et al.[24] and Carini et al.[26]However, for non-stoichiometric As_2Se_3 (with As 37 %) Robinette[27]has studied the acoustic properties of the alloy at room temperature only. There is no published information about the investigation of this alloy by acoustic means at high temperatures.

PMMA was developed in the late 1930s by Hill and Crawford of ICI[46], and is also referred commonly by the name perspex when it is rolled into sheets. PMMA falls in the family of

thermoplastics. As mentioned in Appendix B a polymer is made up of repeat structures called monomers, which in the case of PMMA is illustrated in Fig. 5.13. PMMA is commonly used in bathroom fixtures, knobs, combs, illuminated signs. The optical property of PMMA is used in applications where transparency is at a premium.

An amorphous PMMA sheet of thickness 5.0 mm (obtained from Goodfellow, Cambridge, U.K.) was cut into cylindrical samples of diameter 19 mm for acoustic measurements. TAA was carried out on PMMA, by measuring the normalised ultrasonic velocity and relative attenuation, as per the procedure described in 4.2 and 5.3. PMMA samples were analysed at different heating rates viz. 0.5, 1, 3 and 5°C/min. Fig 5.14 illustrates typical results, at a heating rate of 1°C/min, by plotting normalised velocity against temperature for PMMA, as well as for the other materials. From Fig. 5.14 it can be observed that the glass transition temperature of PMMA is 114°C. Similarly, a plot of the relative attenuation vs temperature for PMMA is illustrated in Fig. 5.9. The value of the glass transition temperature obtained from Fig 5.9 for PMMA, when it was heated at 3°C/min, is 108.5°C. The values of glass transition temperature obtained by other methods are 105°C[37, 46] 107°C[53], 117°C[54], 111°C[55] at 10 C/min and 115°C, 119°C by Kawagoe et al.[56] and Cheng et al.[39] respectively. The apparent variation in the measured values of Tg for PMMA, is mainly due to differences in the rates of heating used by the workers as

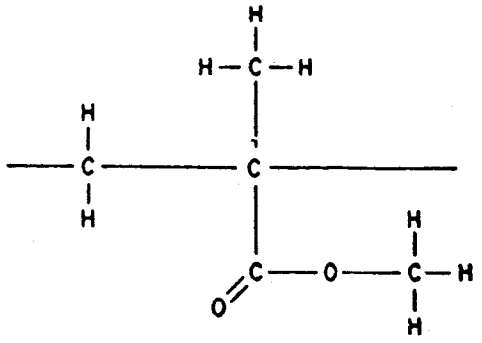

Fig. 5.13 Monomer structure of PMMA[57].

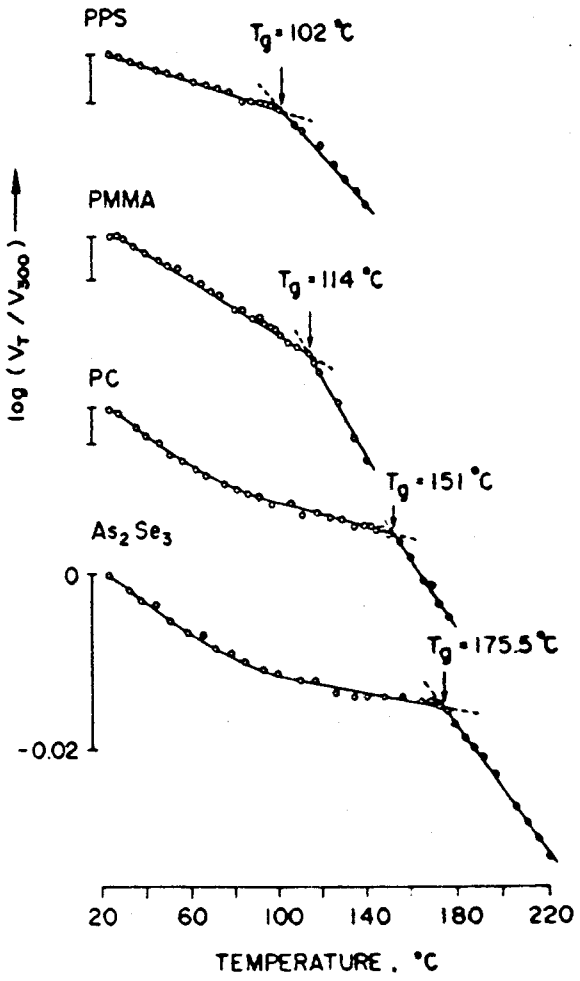

Fig. 5.14 Normalised velocity vs temperature for different materials, showing the T_g values obtained therefrom.

well as the thermal history of the samples. It could also be due to the configurational effects in the polymer. From Fig. 5.9 it can seen that the relative attenuation for PMMA shows two peaks. The peak at higher temperatures is due to the glass transition and is termed the α-peak. The other peak observed at lower temperature is due to a secondary transition and is termed the β-peak.

The α-peak temperature corresponds to T_g, because it represents the maximum amount of chain flexibility (short of solution) that a polymer network can possess. Essentially, the sample becomes liquid like after a short rubber-like state, thus a significant increase in attenuation is to be expected above Tg. When this flexibility is frozen at the glass transition temperature there may remain some limited freedom either of short segments or of side groups, which cause multiple transitions[37]. The β-transition peak occurs at 60°C while that obtained by other methods is 55°C[54] and around 40°C[57]. The secondary transition is attributed to the motion of the $-COCH_3$ group[57].

PPS is another important polymer which is used in the electrical industry as an insulator at high temperatures[58]. Electrical resistivity of PPS film at room temperature is about 10^{18} Ω-cm[58]. Temperature dependence of the conductivity changes abruptly around the glass transition temperature. Fig. 5.15 shows the molecular structure of PPS and table 5.1 shows the acoustic velocity in PPS. Amorphous PPS composite of

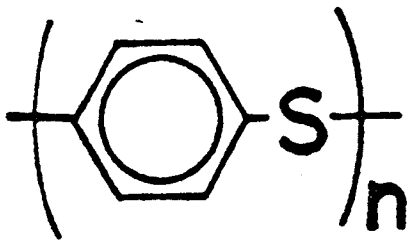

Fig. 5.15 Molecular structure of PPS[58].

Aramid fibre matrix, in the shape of a rod of diameter 6.35 mm (obtained from Goodfellow, Cambridge, U.K.) was cut into cylinders of thickness 6 mm. The sample was heated at a uniform heating rate of 1°C/min from room temperature to 140°C, for TAA to be performed. Fig. 5.14 depicts that the glass transition temperature of PPS occurs at 102°C. The value of T_g for a PPS film is around 90°C[58]. The T_g value of PPS composite should be higher because of less flexibility for the molecular rearrangement to take place in a composite, as compared to pure PPS. From Fig 5.9 the T_g value obtained from the relative attenuation data is 106°C.

The amorphous As_2Se_3 samples were prepared by the method described earlier in Section 5.2. Amorphous As_2Se_3 is used commonly as a photoresistive element in photocopier machines. TAA was performed on a square As_2Se_3 samples at different heating rates viz. 0.5, 1, 3, 5 and 7°C/min. Typical results of the analysis have been presented in Fig. 5.14 for a heating rate of 1°C/min. The value of T_g obtained for a heating rate of 1°C /min is 175.5°C which agrees with the T_{gmin} value of 177.5°C obtained from DSC experiments performed at the same heating rate, on the same batch of samples. The value of T_g obtained from relative attenuation at 0.5°C in Fig. 5.9 is 175°C.

The glass transition temperatures obtained for different materials, by different techniques at a heating rate of 1°C/min is summarised in Table 5.4.

Table 5.4: Comparison of T_g values obtained by different techniques for materials at r=1°C/min.

Material	T_g-TAA Norm. vel. °C	T_{gmin}-DSC °C[48].	T_g-TμHA °C[48]	T_g-Literature	Comments
PC	151	148	150	152 (Min)	Excellent agreement
PMMA	114	115.5	111	105, 107, 111, 115	Good agreement
PPS-Matrix	102	Not detected	~97	90 for PPS film	Good agreement
As_2Se_3	175.5	177.5	Not done	165-170	Large difference probably due to thermal history.

5.5 CONCLUSIONS

The TAA technique was used to determine some mechanical and thermal properties, of important engineering materials viz. polymers, composite materials, and an amorphous semiconductor. This was done at room temperature, and also from room temperature to temperatures as high as 250°C at different controlled heating rates. It was shown that the elastic modulus and absolute velocity obtained by the TAA technique for different materials at room temperature, agreed well with that available in the literature. Agreement was also shown in case of the elastic modulus of composites obtained by TAA and that obtained through the mixture rules.

The results obtained by TAA technique correlated well with those obtained by other thermal analysis techniques viz. DSC and TμHA, as shown in the particular case of polycarbonate. It also correlated with the reciprocal of the coefficient of viscosity data obtained by Macho et al.[49] This verifies TAA technique and the apparatus as a useful thermal analysis tool. The TAA technique not only showed primary transitions but also the secondary transitions. By using a higher frequency of longitudinal waves such transitions would appear much more prominent. The use of the TAA technique gives an insight to the understanding of material properties over a wide temperature range. Increasing this temperature range would be very effective in investigating the thermal properties of many other materials such as metallic alloys.

This is the first time a complete thermoacoustic analysis has been carried out on an amorphous solid and results critically compared with the conventional methods of DSC and TμHA. The work herein has shown that the TAA technique is sufficiently sensitive to obtain the phase transformation temperature over a range of heating rates from 0.2 to 10°C/min and from room temperature to 250°C.

6. CONCLUSIONS AND SUGGESTIONS FOR FUTURE WORK

6.1 CONCLUSIONS

The present research has resulted in the investigation of some of the important mechanical and thermal properties of engineering materials by a non-destructive thermal analysis technique using ultrasonics. A method and an apparatus were developed to carry out a thermoacoustic analysis (TAA) of materials. The principle of the TAA technique is based on generating and transmitting an ultrasonic wave through a material and monitoring the changes in the acoustic velocity and attenuation as a function of sample temperature, as the sample temperature is ramped. The TAA technique is also applicable for making measurements at room temperature or isothermally at any other temperature.

As shown in this thesis a convenient TAA apparatus can be built by using an RF oscillator, RF switch, RF buffers, amplifiers and a transformer to excite an X-cut quartz transducer at its resonant frequency. The excitation of the transducer results in the generation of longitudinal ultrasonic waves. These waves can be coupled to the sample by a pyrex glass buffer rod. Another pyrex buffer rod of identical dimensions as the first one can couple the waves transmitted through the sample to a receiving quartz transducer. Thus, in effect the sample is sandwiched between the two buffer rods. Furthermore, a TAA cell comprising mainly

of a heater controlled by a PID temperature controller can be used to control and ramp the sample temperature accurately.

Both the sing-around and pulse echo techniques can be incorporated with the aid of a bridge circuit to increase the accuracy of the transit time measurements through the sample. Thus, the transit time of the acoustic waves through the sample is in effect the time difference between the echo received at the transmitting transducer and the transmitted wave received by the receiving transducer. These signals were monitored on a Cathode Ray Oscilloscope.

The principal sources of error in the measurement of the transit time and attenuation in the present apparatus were due to CRO, dependence on acuity of observation. Accuracy of sample temperature was limited due to temperature gradient between the surface and the bulk of the material. Resolution obtained in transit time measurement was around 10 ns and for the measurement of peak to peak voltage of the acoustic echo was about 1 mV. Resolution of sample temperature was limited to about 1°C due to the use of K-type thermocouples.

The resourcefulness of the TAA technique was established by measuring the elastic modulus of different single phase materials and also of composites, and identifying phase transformations in important engineering materials viz. polymers and an amorphous semiconductor alloy of As-Se.

The technique was first tested at room temperature by measurements on thermally cycled composites. By using the TAA,

acoustical parameters viz. absolute velocity and normalised attenuation in the composites, were correlated with the number of thermal cycles in the same fashion as the flexural strength measured by a mechanical method i.e. three point bending test. Further, the elastic modulus computed from the acoustic velocity measurement with the present TAA showed good agreement with the values found in the literature. The correlation studies and velocity measurements done at room temperature demonstrate the significance and potential of the TAA as a non-destructive technique.

The technique was also applied to study the phase transformations in a number of amorphous materials under controlled heating rates. The measurements done by this technique at controlled heating rates, were used to determine the glass transition temperature. The TAA experiments were performed from room temperature to temperatures as high as 250°C. The normalised velocity in the materials as well as the relative attenuation of the acoustic waves obtained from the TAA data were shown to be effective in determining the glass transition temperature. The results obtained were validated by correlating this technique with other conventional thermal analysis techniques viz. DSC, TμHA as well as with reciprocal of viscosity. A complete correlation was shown to exist in the case of polycarbonate. The activation energy of the phase transformation in polycarbonate obtained by TAA agreed well with that obtained by other analysis techniques and moreover

the relaxation times were found to be proportional to the viscosity. The normalised velocity decreased sharply in the glass transition region, whereas the attenuation exhibited a peak.

Application of the TAA has shown that a secondary transition exists in the case of PMMA polymer in agreement with the literature. It is expected that such transitions would be much more prominent if higher ultrasonic frequencies are used. Similarly, it was found that higher temperatures (500~900°C) and higher frequencies would be required to study transformations in metallic alloys.

The resolution of the apparatus in the measurement of changes in transit time of acoustic waves through the materials was sufficient to determine the T_g to within ~1°C over a wide range of heating rates. This resolution however may not be adequate for detecting small changes in material properties. For example, in Nylon 6,6 the degree of mobility of atoms is very limited due to large molecules in the glass transition region. This tends to produce very small changes in the transit time. Thus, an increased resolution in the measurement of transit time changes would make it possible to study materials with extremely restricted mobility in the glass transition region.

6.2 SUGGESTIONS FOR FUTURE WORK

The TAA technique used in this research was useful in determining some of the properties of amorphous materials by

non-destructive means. The prototype of the TAA apparatus which was designed and implemented for the purpose of this research, could be further improved and made more versatile by the following suggestions.

TAA of most of the metallic alloys requires analysis upto temperatures as high as 500~900°C. For such high temperatures to be generated in the thermal subsystem of the apparatus would require the use of a high temperature furnace, preferably fabricated from stainless steel. In addition, the pyrex glass buffer rods used in the present system would have to be replaced by buffer rods made of materials like Vycor or Quartz. A renewed market search for high temperature couplants would also be a requisite. In order to prevent oxidation of the materials at high temperatures the TAA cell should be designed with an inlet for Nitrogen gas.

Dispersive materials can be studied by TAA if acoustic wave propagation takes place in the material at different frequencies. This would require the usage of a transducer polished for harmonic generation, which could thus be excited at its different harmonic frequencies. The harmonic frequencies that can be generated by piezoelectric materials will only correspond to the odd integral multiples of the fundamental resonant frequency of the transducer. Study of the material over a wide range of frequencies would provide information regarding its relaxation frequency. Also the study of metallic materials at high frequency will yield information

regarding grain boundary movement, and, in the case of polymers, indicate prominent secondary transitions.

Apart from determining the longitudinal wave velocity in materials, it would also be useful to determine the acoustic velocity in materials by using transverse waves. This would enable computation of the Debye's temperature for materials and the shear modulus of materials. Glass transition temperature of amorphous materials, can also be studied in more details by shear waves.

A low Q transducer, viz. Lead Zirconate Titanate (PZT), would be very effective in investigating material properties by the pulse echo technique as well as by the technique presently implemented. This would be mainly due to the enhancement of resolution of the apparatus, when PZT transducers are used. In order to accommodate the PZT transducer in the present system, the electronic amplifier i.e. TP 1465 would have to be replaced with a high power amplifier. Also the RF transformer would have to be removed.

For the study of porous materials, it is strongly recommended either to use low resonant frequency quartz transducers, or to increase the RF voltage amplitude for excitation of the quartz transducer. This would overcome the strong attenuation to the ultrasonic waves within porous materials. Also in order to enhance the analysis of different types of materials at higher temperatures, increased voltage amplitude of the excitation signal would be useful.

An increase in the accuracy of the temperature measurement would be important in determining the glass transition temperature. T-type thermocouples have higher resolution (<0.1°C) and could be incorporated into the subsystem.

System automation would effectively increase the number of materials to be analysed. The system should be automated such that the transit time measurement of the ultrasonic waves through the sample at different temperatures could be monitored by an interfaced computer. Some work was done in this direction during the present research by using Schmitt trigger circuits for producing the triggering waveform from the signal received at the transmitting transducer and the signal received at the receiving transducer. The time between the trigger signals was measured by a HP Universal Counter Model 5315A. However, due to the decrease in peak to peak voltage of the received signal at the receiving transducer with increase in sample temperature, the threshold triggering point for the Schmitt trigger varies. This resulted in producing jittery pulse edges, due to which time measurement between trigger pulses could not be accomplished accurately. However, it is strongly felt that this could be achieved by using an Automatic Gain Control (AGC) circuitry to keep the voltage amplitude of the received signal constant.

Furthermore, a peak detector or an envelope detector should be implemented to obtain the peak to peak voltage of

the received signal. This peak to peak voltage could then be converted by an Analog to Digital converter and monitored by a microcomputer.

By modifying the TAA cell, material properties could be studied at very low temperatures and at high pressures.

It can be seen that the prototype TAA apparatus developed in this work can be further improved and made more versatile to bring the apparatus almost to a level of commercial utilization.

7. REFERENCES

1. Blitz J., Fundamentals of Ultrasonics, 1967, Butterworth and Company Limited, London.

2. Cracknell A.P., Ultrasonics, 1980, Wykeham Publications Limited, London.

3. Wendlandt W.M., Thermal Analysis, 1986, John Wiley and Sons, Inc., New York.

4. Carlin B., Ultrasonics, 1960, Mcgraw-Hill Book Company, Inc., New York.

5. McGonnagle W.J., Nondestructive Testing, 1961, Gordon and Breach Science Publishers, New York.

6. General Dynamics Corporation, Nondestructive Testing, ultrasonic testing, 1967, Convair Division, San Diego, California.

7. Filipczynski L., Ultrasonic Methods of Testing Materials, 1966, Butterworth and Company Limited, London.

8. Crawford A.E., Ultrasonic Engineering, 1955, Butterworths Scientific Publications, London.

9. Halmshaw R., Non-destructive Testing, 1987, Edward Arnold (Publishers) Limited, London.

10. Omar M.A., Elementary Solid State Physics, 1975, Addison-Wesley Publishing Company, Menlo Park.

11. Krautkramer J. and Krautkramer H., Ultrasonic Testing of Materials, 1969, Springer-Verlag Inc., New York.

12. Berlincourt D.A., Curran D.R. and Jaffe H., Physical Acoustics, 1964, Edited by W.P. Mason, Academic Press, New York.

13. Ensminger D., Ultrasonics, 1973, Marcel Dekker Inc., New York.

14. McSkimin H.J., "Pulse superposition method for measuring ultrasonic wave velocities in solids", 1961, J. Acoust. Soc. Am., **33**, 12-16.

15. Papadakis E.P., "Ultrasonic phase velocity by the pulse-echo-overlap method incorporating diffraction phase corrections", 1967, J. Acoust. Soc. Am., **42**, 1045-1051.

16. Negita K. and Takao H., "Superposed pulse echo overlap method for ultrasonic sound velocity measurement", 1989, Rev. Sci. Instrum., **60**, 3519-3521.

17. Willard H.H., Merritt Jr. L.L., Dean J.A. and Settle Jr. F.A., Instrumental Methods of Analysis, 1981, Wadsworth Publishing Company, Belmont.

18. Small L., Hardness-Theory and Practice, 1960, Cushing-Malloy, Inc., Michigan.

19. Kasap S.O., Yannacopoulos S., "Mechanical and thermal properties of the glassy chlorinated $Se_{0.997}As_{.003}$ used as an X-ray imaging material", 1989, Can. J. Phys., **67**, 686-693.

20. Armstrong P.E., Denton A.A., Dunegan H.L., Krafft J.M., Petty E.R., Post D., Tatro C.A., Tetelman A.A. and Wilshaw R.R., Measurements of Mechanical Properties, Edited by Bunshah R.F., 1971, John Willey and Sons Inc., New York.

21. Kittinger E., "Relaxation of sound velocity in vitreous selenium", 1978, J. Non-Cryst. Solids, **27**, 421-425.

22. Lakshmikumar S.T., Padaki V.C., Krishnapur P.P., Subramanayam S.V., Mallya R.M. and Gopal E.S.R., "Ultrasonic velocities and thermal expansion coefficients of amorphous $Se_{80}Te_{20}$ and $Se_{90}Te_{10}$ alloys near glass transitions", 1982, J. Mater. Sci., **17**, 183-192.

23. Kartha P.E.S., Padaki V.C., Lakshmikumar S.T. and Gopal E.S.R., "Behaviour of ultrasonic velocities in amorphous $Se_{90}Ge_{10}$ and $Se_{85}Ge_{15}$ alloys near their glass transition", 1981, Pramana, **17**, 33-38.

24. Kostial P., Malik L. and Both L., "New Aspect of Ultrasonic detection of some significant structural parameters of amorphous Se-Te alloys", 1983, phys. stat. sol., **80**, K167-K170.

25. Kasap S.O. and Juhasz C., "Kinematical transformations in amorphous selenium alloys used in xerography", 1986, J. Mater. Sci., **21**, 1329-1340.

26. Carini G.Jr., Cutroni M., Federico M. and Galli M., "Elastic constants of $Se_{1-x}Te_x$ solid amorphous alloys-the role of tellurium", 1984, J. Non-Cryst. Solids, **64**, 317-324.

27. Robinette S., "The influence of thermal treatment on the acoustics properties of an amorphous Se-36.4 at.% As

alloy", 1979, J. Non-Cryst. Solids, **33**, 279-284.

28. Ordu R., Riou C., and Vacher J., "New instrument for continuous and simultaneous recording of changes in ultrasonic attenuation and velocity", 1978, Rev. Sci. Instrum., **49**, 238-241.

29. Nagata K., Tagashira K., Taki S. and Takemura T., "Ultrasonic study of high pressure phase in polyethylene", 1980, Jpn. J. Appl. Phys., **19**, 985-990.

30. Ramaseshu Y. and Kalyansundaram P., "A technique for accurate measurement of 'ultrasonic transit time' using a single transducer", 1984, J. Phys. E: Sci. Instrum., **17**, 551-552.

31. Whitehead D.G. and Palmer S.B., "A high speed ultrasonic sing-around system", 1979, IEEE Trans. Instrum. Meas., **IM-28**, 220-223.

32. Aindow J.D. and Chivers R.C., "A narrow-band sing-around ultrasonic velocity measurement system", 1982, J. Phys. E: Sci. Instrum., **15**, 1027-1030.

33. Ramachandraiah P. and Suryanarayana M., "An ultrasonic sing-around system for thin solid samples", 1987, J. Phys. E: Sci. Instrum., **20**, 85-87.

34. Carini G. Jr. and Mento F., "A digital electronic instrument for measuring sound velocity", 1979, J. Phys. E: Sci. Instrum., **12**, 259-260.

35. Taki S., Furuta Y., and Takemura T., "New instrument for rapid measurement of changes in ultrasonic velocity", 1981, Rev. Sci. Instrum., **52**, 1388-1391.

36. Beyer R.T. and Letcher S.V., Physical Ultrasonics, 1969, Academic Press, New York.

37. Arridge R.G.C., Mechanics of Polymers, 1975, Clarendon Press, Oxford.

38. Holliday L., Structures and Properties of Oriented Polymers, 1975, Edited by I.M. Ward, John Wiley and Sons, New York.

39. Cheng W.M., Miller G.A., Manson J.A., Hertzberg R.W. Sperling L.H., "Mechanical behaviour of poly(methyl methacrylate)", 1990, J. Mater. Sci., **25**, 1931-1938.

40. Askeland D.R., The Science and Engineering of Materilas, 1984, Brooks/Cole Engineering Division, Monterey.

41. Soga N., Kunugi M. and Ota R., "Elastic properties of Se and As_2Se_3 glasses under pressure and temperature", 1973, J. Phys. Chem. Solids., **34**, 2143-2148.

42. Hilderbrandt J., "Thermal fatigue of Composites", 1990, M.Sc. Thesis, University of Saskatchewan.

43. Shackelford J.F., Introduction to Material Science for Engineers, 1985, Macmillan Publishing Company, New York.

44. Zawada L.P., Wetherhold R.C., "Thermal fatigue of ceramic fiber/glass matrix composites", 1989, Ceram. Eng. Sci. Proc., **10**, 1320-1326.

45. Christopher W.F. and Fox D.W., Polycarbonates, 1962, Reinhold Publishing Corporation, New York.

46. Cowie J.M.G., Polymers: Chemistry and Physics of Modern Materials, 1973, Intext Educational Publishers, New York.

48. Kasap S.O. and Yannacopoulos S., "Kinetics of structural relaxations in the glassy semiconductor a-Se", 1989, J. Mater. Res., **4**, 893-905.

47. Wacker I, Yannacopoulos S., Kasap S.O., Unpublished work, 1990.

49. Macho E., Algena A., and Colmenero J., "Simultaneous evaluation of viscosity and retardation time in glassy polymers by a parallel-plate technique", 1988, J. Appl. Phys., **64**, 642-646.

50. Yannacopoulos S. and Kasap S.O., "Thermomicrohardness analysis (TμHA) of glassy materials", 1990, Theoretical and Applied fracture mechanics, **13**, 53-58.

51. Etienne S., Guenin G. and Perez I., "Etudes par ultrasons des coefficients d'e'lasticite'du se'le'nium vitreux vers T_g", 1979, J. Appl. Phys., **12**, 2189-2202.

52. Padaki V.C., Lakshmikumar S.T., Jayannavar A.M., and Gopal E.S.R., "Ultrasonic velocity measurements in amorphous Se-P system from 300 to 4.5 K", 1981, Acustica, **49**, 342-345.

53. Mizutani K., "Temperature dependence of fracture toughness of poly(methyl methacrylate)", 1987, J. Mater. Sci. Lett., **6**, 915-916.

54. Kung T., Li J.C.M., "Recovery processes in amorphous polymers", 1987, J. Mater. Sci., **22**, 3620-3630.

55. Ania F., Martinez-Salazar J., Balta Calleja F.J., "Physical ageing and glass transition in amorphous polymers as revealed by microhardness", 1989, J. Mater. Sci., **24**, 2934-2938.

56. Kawagoe M., Nunomoto S., "Effect of preexisting crazes on the dynamic viscoelasticity of poly(methyl methacrylate)", 1990, J. Mater. Sci., **25**, 743-748.

57. Williams D.J., Polymer Science and Engineering, 1971, Prentice-Hall, Inc., New Jersey.

58. Katasumi Y., Yun M.S., Ozaki M., Kim S.H., Inuishi Y. and Kyokane J., "Electrical transport and breakdown of Poly-p-Phenylenesulfide", Jpn. J. Appl. Phys., **22**, 1510-1514.

APPENDIX A

NON-PIEZOELECTRIC TYPES OF ULTRASONIC TRANSDUCERS

A) MAGNETOSTRICTIVE OSCILLATORS

These devices make use of a phenomenon called *magnetostriction*. Ultrasonic waves are generated due to change in length of a bar of ferromagnetic/ferrimagnetic material on being subjected to a varying magnetic field. Conversely, a mechanical stress applied to a rod or a bar causes a change in intensity of magnetisation. For most applications the upper frequency limit is of the order of 100-300 kHz and are mainly used for generating high intensity ultrasonic energy[1].

B) MECHANICAL GENERATORS & RECEIVERS

These include whistles, sirens which are used as generators, and radiometers and Rayleigh discs acting as receivers. They are used to obtain high amplitude, often high intensity vibrations at low sonic frequencies[13]. The upper frequency limit of mechanical transducers is about 100 kHz[1].

C) ELECTROMAGNETIC TRANSDUCERS

These transducers operate in a fashion similar to the loudspeaker, except instead of generating audio frequencies they generate ultrasonic frequencies. These transducers are used at the lower end of the ultrasonic frequency range for higher power generation and at frequencies upto 50 kHz. They are also used as receivers at megacycle frequencies.

D) ELECTROSTATIC TRANSDUCERS

When a steady potential difference is applied across two parallel metal plates, a force of attraction is experienced between them. On superimposing an alternating voltage of lower amplitude than this steady potential difference, the force of attraction varies sinusoidally at the same frequency as that of the applied voltage. Now if one of the plates is freely supported, the other vibrates at that frequency. These transducers are used only for low power applications. The upper frequency limits are in the upper Kilocycle range for transmitting and in the lower Megacycle range for receiving.

APPENDIX B

BRIEF DESCRIPTION OF POLYMERS

A *polymer* is a large molecule constructed from many small structural units called monomers, covalently bonded in any conceivable pattern[46]. Polymers can be linear, branched or cross linked[57]. If the repeat units are arranged in a single-stranded structure as shown in Fig. B.1(a), the polymer is referred as a linear polymer. If a linear chain has side-chain appendages, as in Fig. B.1(b) the polymer is referred to as a branched polymer. If the units are joined in a three-dimensional array as depicted in Fig. B.1(c) (in two dimensions), the polymer is said to be cross linked.

B.1 THE GLASS TRANSITION

Solids can also exist in an amorphous state, where the molecular arrangement of the atoms is random. Common example of this state of supercooled liquid is inorganic glass. Amorphous materials do not melt at a fixed melting point with the absorption of latent heat but, rather soften over quite a large range of temperature centred about a mean value called the *glass transition temperature*[37]. These materials are also called as *glassy or vitreous* materials and they exist in a viscoelastic state[57].

The temperature at which T_g is observed depends largely on the chemical nature of the polymer chain and for most

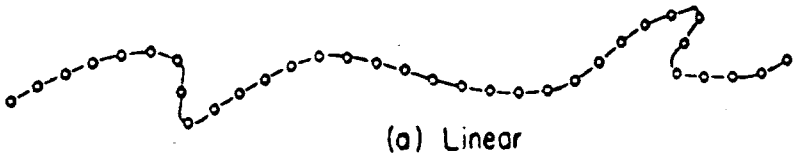

(a) Linear

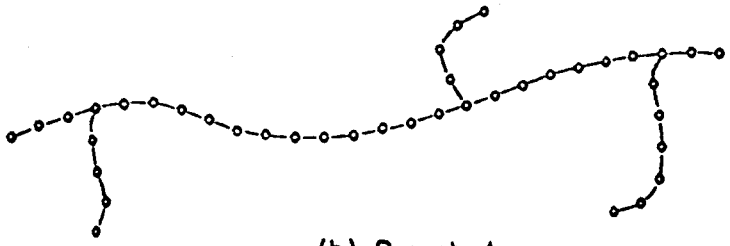

(b) Branched

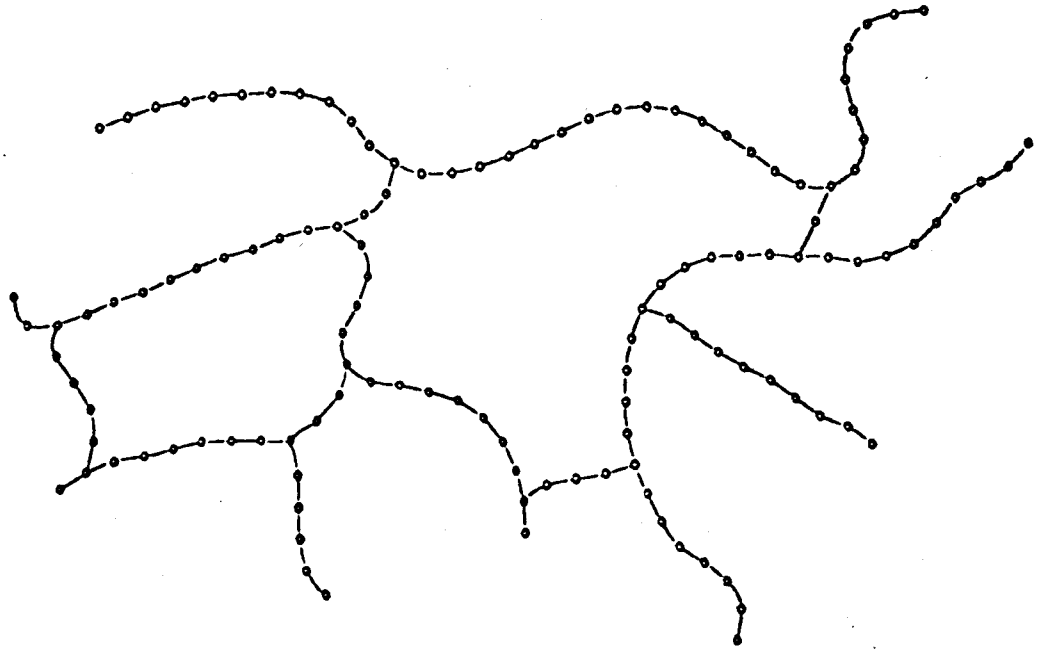

(c) Crosslinked

Fig. B.1 Basic polymer systems[57].

common synthetic polymers lies between 170 and 500 K[57]. The transition from a glass to a rubber-like state is accompanied by marked changes in the specific volume, the modulus, the heat capacity, the refractive index, and other physical properties of the polymer. The change in a physical property can be used to locate T_g. If a curve is plotted of the specific volume of a polymer as a function of temperature it will be generally of the form shown in Fig. B.2(a). The specific volume changes linearly with temperature upto a transition region where a change of slope occurs after which the curve continues linearly but at a steeper gradient. T_g is usually defined as the point at which tangents of the two curves intersect. If the polymer had been crystallisable the curve of specific volume against temperature would have shown a discontinuity at the melting point as seen in Fig. B.2(b).

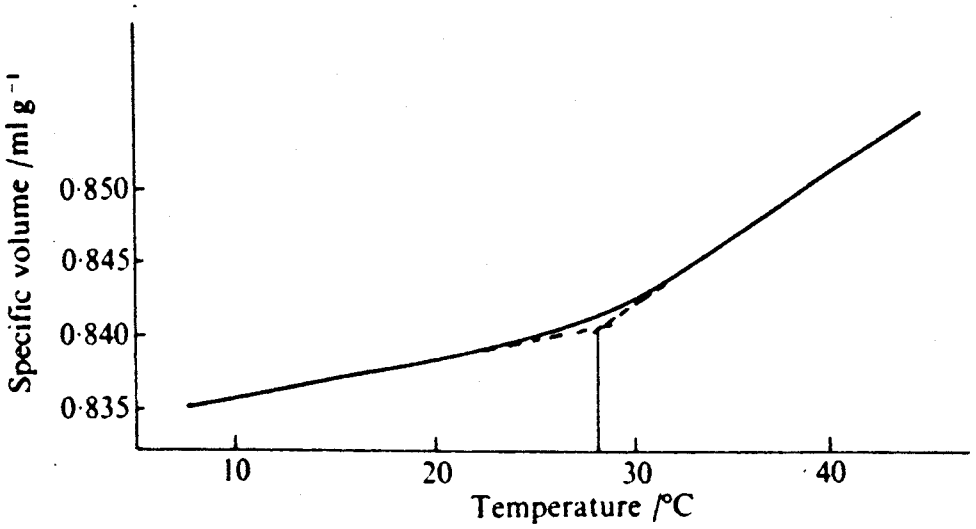

(a)

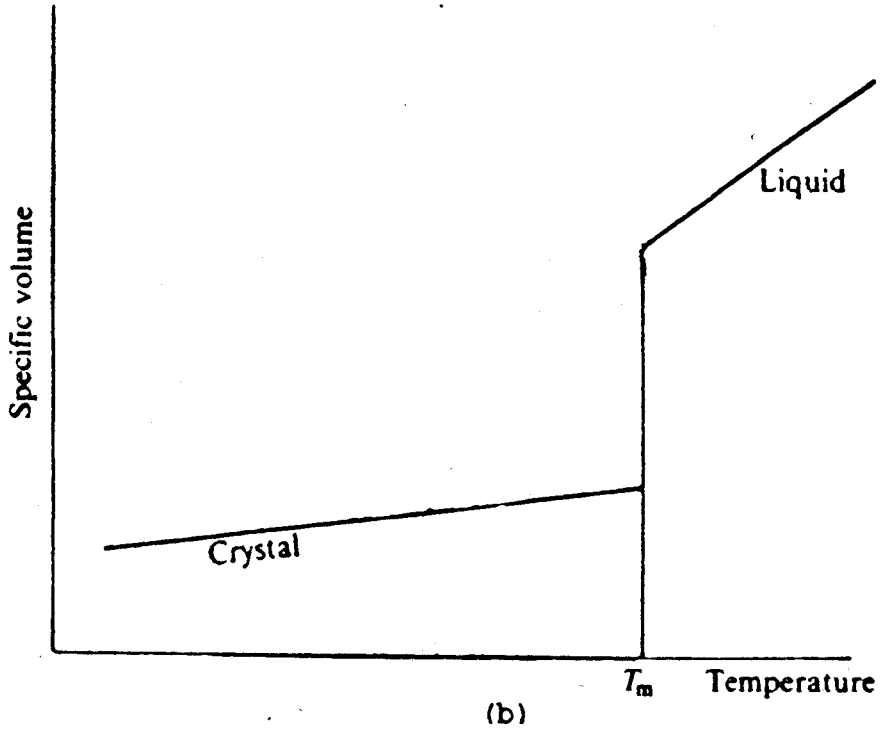

(b)

Fig. B.2 (a) Specific volume of a typical amorphous material as a function of temperature in the neighbourhood of glass transition. (b) Specific volume of a non-amorphous material as a function of temperature[37].